SHRIMP U–Pb zircon evidence for age, provenance, and tectonic history of early Paleozoic Ganderian rocks, east-central Maine, USA

Allan Ludman[1*], John Aleinikoff[2], Henry N. Berry IV[3], and John T. Hopeck[4]

1. School of Earth and Environmental Sciences, Queens College (CUNY), Flushing, New York 11367, USA
2. United States Geological Survey, MS 973, Denver, Colorado 80225, USA
3. Maine Geological Survey, 93 State House Station, Augusta, Maine 04333, USA
4 Maine Department of Environmental Protection, 17 State House Station, Augusta, Maine 04333, USA
*Corresponding author <allan.ludman@qc.cuny.edu>

Date received: 27 November 2017 ¶ Date accepted: 01 October 2018

ABSTRACT

SHRIMP U–Pb zircon ages from Ganderia in eastern Maine clarify the ages and provenance of basement units in the Miramichi and St. Croix terranes and of cover rocks in the Fredericton trough and Central Maine/Aroostook-Matapedia basin (CMAM). These new data constrain timing of orogenic events and help understand the origin of the cover rock depocenters.

Detrital zircon data generally confirm suggested ages of the formations sampled. Zircon grains with ages of ca. 430 Ma in both depocenters, only slightly older than their host rocks, were probably derived from the earliest volcanic eruptions in the Eastport-Mascarene belt. Their presence indicates that unnamed CMAM sandstone units may be as young as Pridoli and their absence from the Appleton Ridge and Digdeguash formations suggests that these formations are older than initial Eastport-Mascarene volcanism. Detrital and volcanic zircon ages confirm a Late Cambrian to Middle Ordovician age for the Miramichi succession and date Miramichi volcanism at 469.3 ± 4.6 Ma. In the St. Croix terrane, zircon grain with an age of 477.4 ± 3.7 Ma from an ashfall at the base of the Kendall Mountain Formation and age spectra and fossils from overlying quartz arenite suggest that the formation may span Floian to Sandbian time. The main source of CMAM and Fredericton sediment was recycled Ganderian basement from terranes emergent after Late Ordovician orogenesis, supplemented by Silurian tephra. Zircon barcodes and lithofacies and tectonic models suggest little, if any, input from Laurentia or Avalonia.

Zircon- and fossil-based ages indicate coeval Upper Ordovician deformation in the St. Croix (ca. 453 to 442 Ma) and Miramichi (ca. 453 to 446 Ma) terranes. Salinic folding in the southeastern Fredericton trough is bracketed between the 421.9 ± 2.4 Ma age of the Pocomoonshine gabbro-diorite and 430 Ma detrital zircons in the Flume Ridge Formation. Zircon ages, lithofacies analysis, and paleontological evidence support the origin of the Fredericton trough as a Salinic foredeep. The CMAM basin cannot have been an Acadian foreland basin, as sedimentation began millions of years before Acadian subduction.

RÉSUMÉ

Le système de datation U-Pb sur zircon au moyen du SHRIMP de Ganderia dans l'est du Maine clarifie la datation et la provenance d'unités souterraines des terranes de Miramichi et St. Croix et des rochers de la dépression de Frédéricton au bassin du centre du Maine et d'Aroostook-Matapédia (CMAM). Ces nouvelles données limitent l'échelonnement des phénomènes orogéniques et facilitent la compréhension de l'origine des zones de dépôt du rocher.

Les données sur le zircon détritique confirment généralement la datation suggérée des formations échantillonnées. Les grains de zircon datant d'environ 430 Ma dans les deux zones de dépôt, à peine plus anciens que leurs roches hôtes, provenaient probablement des premières éruptions volcaniques de la région d'Eastport-Mascarene. Leur présence indique que les unités sans noms de grès du CMAM pourraient être aussi jeunes que Pridoli et leur absence des formations d'Appleton Ridge et Digdeguash suggère que ces formations sont plus anciennes que le volcanisme d'origine d'Eastport-Mascarene. La datation du zircon détritique et volcanique confirme l'âge avancé du Cambrien au milieu de l'âge du Ordovicien pour la succession de Miramichi et évalue l'âge du volcanisme de Miramichi à 469,3 ± 4,6 Ma. Dans la terranne de St. Croix, le grain de zircon datant de 477,4 ± 3,7 Ma à partir d'une chute de cendre à la base de la formation de la Kendall Mountain et d'un spectre d'âge et de fossiles aérnite de quartz superposé suggère que la formation traverse la période de Floian à Sandbian. La source principale de sédiment du CMAM et de Frédéricton provenait de recyclage souterrain de Ganderian à

doi:10.4138/atlgeol.2018.012

partir des terrannes émergentes à la suite de l'orogenèse tardive d'Ordovician, complétés par le tephra Silurien. Les codes à barres et lithofaciès de zircon et les modèles tectoniques suggèrent peu, voir aucune donnée de Laurentia ou d'Avalonia.

La datation selon le zircon et le fossile indique le même âge que la déformation de l'Ordovicien supérieur dans les terrannes de St. Croix (environ de 453 à 442 Ma) et Miramichi (environ de 453 à 446 Ma). Le pli salinique au sud-est de la dépression de Frédéricton se trouve dans une fourchette d'âge entre l'âge du gabbro-diorite de Pocomoonshine 421,9 ± 2,4 Ma et 430 Ma de zircons détritiques dans la Formation de Flume Ridge. La datation du zircon, les analyses de lithofaciès et les preuves paléontologiques soutiennent l'origine de la dépression de Frédéricton en tant qu'avant-fosse salinique. Le bassin du CMAM ne peut pas avoir été un bassin d'avant-pays acadien puisque la sédimentation a commencé des millions d'années avant la subduction acadienne.

[*Traduit par la redaction*]

INTRODUCTION

This study was undertaken to address problematic stratigraphic and tectonic interpretations in east-central and eastern Maine that could not be resolved by mapping and lithofacies analysis. The goals of this study are to use ages of detrital, volcanic, and plutonic zircon to (1) constrain the stratigraphic ages of mostly unfossiliferous sandstone units from the Fredericton trough and Central Maine/Aroostook-Matapedia (CMAM) depocenters (Fig. 1); (2) determine whether the sediment in these basins was derived from sources external to Ganderia, i.e., Laurentia and/or Avalonia (Fig. 2); and (3) date Cambrian-Ordovician strata in the Miramichi and St. Croix terranes. It was anticipated that detrital zircon age spectra might provide a distinctive Ganderian "signature" useful for distinguishing the terrane in southern New England. New age data are reported for Silurian sedimentary rocks of the CMAM basin and Fredericton trough, and pre-Silurian sedimentary and volcanic rocks from the St. Croix and Miramichi Ganderian "basement" terranes.

Tectonic framework

A complex tectonic evolution spanning the entire Appalachian Wilson cycle has been interpreted in the northern Appalachian orogen (Table 1), punctuated by several orogenic events as the microcontinental plates Ganderia, Avalonia, and Meguma (Fig. 2) were rifted from Gondwana and progressively accreted to Laurentia (ancestral North America). Today, Ganderia is a major terrane in the orogen that reaches its maximum width where it underlies most of Maine and New Brunswick (Fig. 2). It is floored by Late Neoproterozoic to Early Cambrian crust that detached from Gondwana in the Early Cambrian, at which time it was separated by the Iapetus Ocean from Laurentia. Subduction of Iapetan lithosphere beneath the leading edge of Ganderia created the Popelogan arc and associated Tetagouche back-arc basin of the Miramichi terrane (Fig. 1), separating the leading (northwestern in current geography) and trailing components of Ganderia. These components were reunited during the Penobscot orogeny, and the Popelogan arc collided with Laurentia in the Late Ordovician, closing the main body of Iapetus. Closure of a back-arc basin at the trailing edge of Ganderia (St. Croix terrane) during the Salinic orogeny completed the accretion of Ganderia to Laurentia.

Emergent highlands composed of Ganderian basement rocks supplied sediment to the adjacent Fredericton and CMAM depocenters from the Late Ordovician through Late Silurian (Ludman *et al.* 2017). These sedimentary rocks were subsequently folded during the Salinic orogeny, and again during Early Devonian (Acadian) accretion of Avalonia (Fyffe *et al.* 2011). This paper focuses mostly on rocks deposited between the Penobscot and Acadian orogenies, but also examines some of the Miramichi and St. Croix source rocks whose ages have previously been uncertain.

Geologic setting

Precambrian to mid-Ordovician Ganderian arc and back-arc rocks are exposed in Maine and New Brunswick as small inliers and extensive northeast-trending belts separated by thick Late Ordovician to Silurian or Devonian turbiditic rocks (Fig. 1). The Middle Ordovician and older rocks will be referred to in this paper as "basement" and Late Ordovician and younger rocks as "cover". The thick turbidite successions that today isolate the older belts at the surface and obscure their subsurface relationships are generally ascribed to the Fredericton trough and the Central Maine and Aroostook-Matapedia basins, recognized by Ludman *et al.* (2017) as a single Central Maine/Aroostook-Matapedia (CMAM) depocenter (Fig. 1).

Age and relationship among cover sandstone units have been problematic for many years because of sparse bedrock exposures and similar lithologies and bedding styles, lack of distinctive marker horizons, and extremely rare fossil age control. Lithofacies and paleocurrent analyses indicate deposition in two distinct sedimentary regimes: a Late Ordovician to Late Silurian phase in which several emergent pre-Silurian belts shed sediment locally into the adjacent basins (Ludman *et al.* 2017), and a Late Silurian to Middle Devonian regime in which sandstones deposited in a NW-migrating Acadian foreland basin swamped the original source areas with sediment from a single eastern source (Bradley *et al.* 2000; Bradley and O'Sullivan 2016).

The study area outlined in Figure 3 spans much of eastern and east-central Maine, a region blanketed by thick glacial deposits and characterized by less than 1% bedrock exposure. Most basement and cover rocks experienced lower

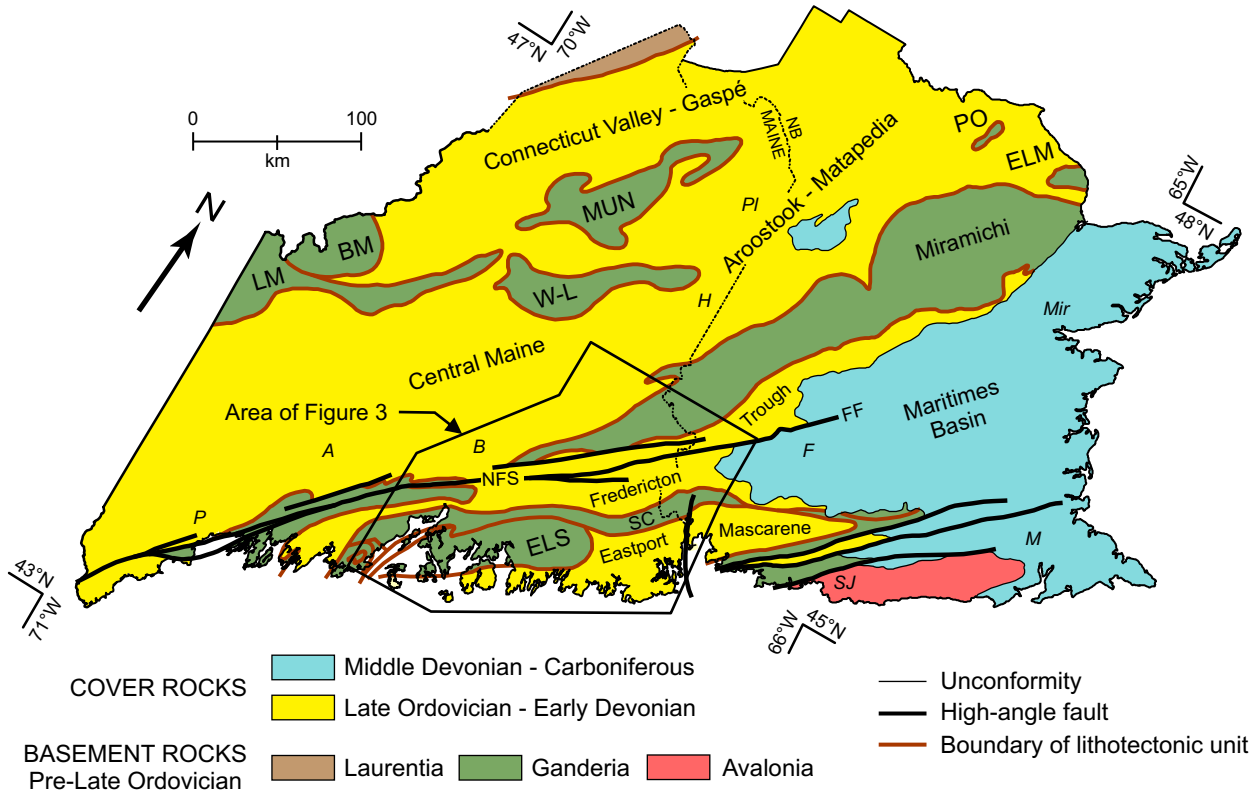

Figure 1. General distribution of Late Ordovician–Early Devonian cover rocks and tracts of exposed basement in Maine and New Brunswick (NB). Contacts have been projected through (removed) plutons to clarify general basement-cover relationships. Selected basement tracts: Lobster Mountain (LM), Boundary Mountains (BM), Weeksboro – Lunksoos Lake (W-L), Popelogan (PO), Elmtree (ELM), Ellsworth (ELS), and St. Croix (SC). Towns: Augusta (*A*), Bangor (*B*), Houlton (*H*), Portland (*P*), and Presque Isle (*PI*), Maine; Fredericton (*F*), Miramichi (*Mir*), Moncton (*M*), and Saint John (*SJ*), New Brunswick. Faults: Norumbega Fault System (NFS) and Fredericton Fault (FF). (Modified from Hibbard *et al.* 2006; Fyffe *et al.* 2011; Ludman *et al.* 2017; and Mohammadi *et al.* 2017.)

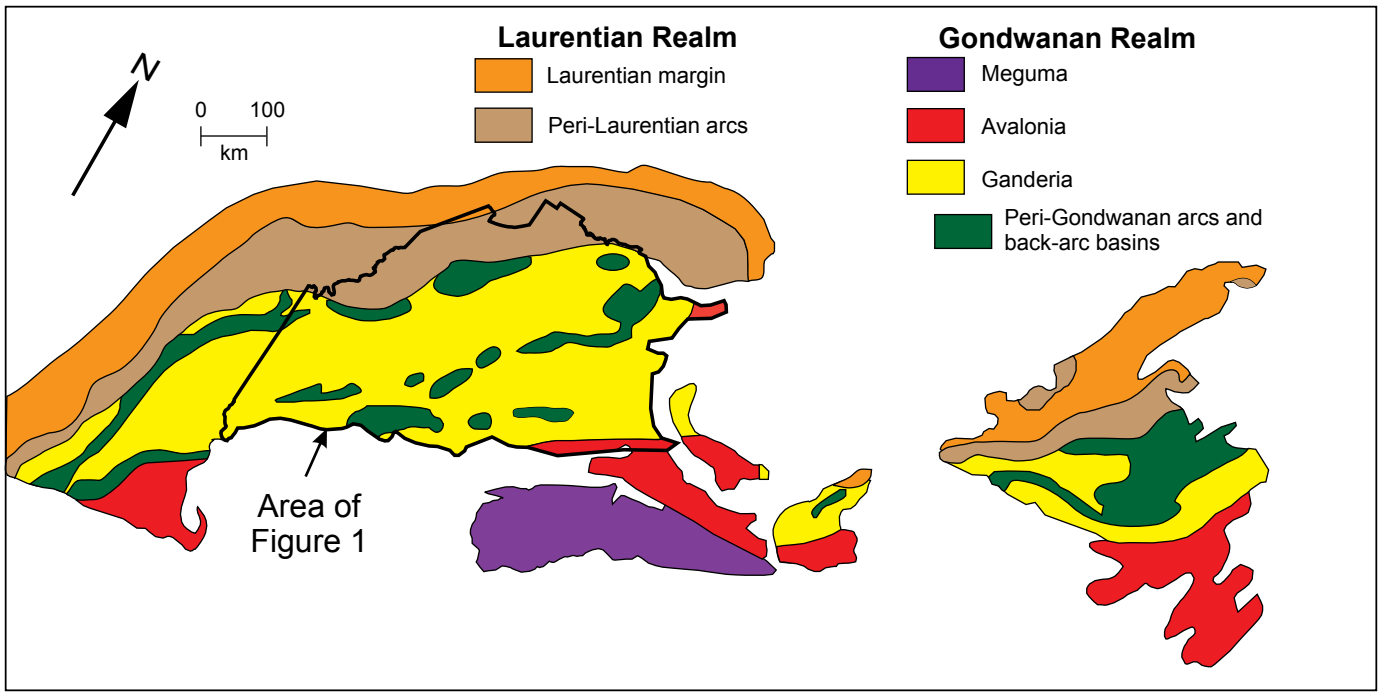

Figure 2. Tectonic framework of the northern Appalachians of New England and Canada (after Hibbard *et al.* 2006).

Table 1. Tectonic evolution of the northern Appalachian study area (after Hibbard *et al.* 2006; Hatcher 2010; Fyffe *et al.* 2011; van Staal *et al.* 2016; Wilson *et al.* 2017). Shading indicates the ages of basement (brown) and cover (yellow) rocks examined in this study.

	AGE	OROGENY	TECTONIC EVENTS
APPALACHIAN CYCLE	Permian	Alleghanian	Gondwana accreted to previously amalgamated plates forming supercontinent Pangea
	Late Devonian	"Neoacadian"	Meguma accreted to previously amalgamated plates
	Early Devonian	Acadian	Avalon accreted to previously amalgamated plates
	Late Silurian	Salinic	Accretion of Ganderia to Laurentia completed by closure of remnant back-arc basin at trailing edge of Ganderia
	Silurian		Continued Ganderia-Laurentia convergence by closure of Tetagouche back-arc basin (Miramichi terrane)
	Late Ordovician		Leading edge of Ganderia (Popelogan arc) collides with Laurentia
	Ordovician		Continued Ganderia-Laurentia convergence
	Cambrian-Ordovician	Penobscot	Ganderian components (Miramichi, Annidale,) reunited near trailing edge of the Ganderian plate
	Cambrian - Early Ordovician		Ganderia rifted from Gondwana, drifts toward Laurentia, and is fragmented by extension during Iapetan subduction that produces island arcs and back-arc basins
	Latest Neoproterozoic		Rifting of Rodinia, opening of Iapetus Ocean
	Neoproterozoic (~1Ga)	Grenville	Assembly of supercontinent Rodinia

greenschist (chlorite zone) regional metamorphic conditions with more intense metamorphism in contact aureoles surrounding numerous felsic and mafic plutons. Well-preserved primary sedimentary features indicate that most of the cover rocks were deposited as low-, intermediate-, and high-energy turbidites.

Despite the low-grade metamorphism, both basement and cover rocks experienced complex multiphase deformation including recumbent folding and thrusting, upright folding, high-angle reverse faulting, and several episodes of late dextral strike-slip and steep normal and reverse dip-slip faulting (Ludman *et al.* 1993; Tucker *et al.* 2001; Ludman 2017). Complex faulting typically obscures critical relationships between the cover rocks and their basement terrrane sources (Osberg *et al.* 1989; Tucker *et al.* 2001; Fyffe *et al.* 2011; Ludman 2017; Ludman *et al.* 2017).

Figure 3. (next page) Generalized bedrock map of central and eastern Maine showing localities of samples analyzed in this study. Dashed rectangles show locations of detailed maps in Figure 14. Numbers indicate cover units. Sample prefixes indicating sampled units are used throughout this paper. AR: Appleton Ridge; BL: Baskahegan Lake; BM: Bowers Mountain; FR: Flume Ridge; HC: Hutchins Corner; KM: Kendall Mountain; MA: Madrid; MH: Mayflower Hill; OS: Olamon Stream; PM: Pocomoonshine gabbro-diorite; VG: Vassalboro Group, undifferentiated. Selected plutons: Bottle Lake Complex (Bot), Lucerne (Lu), Deblois (Deb). *Towns*: Bangor (B), Danforth (D), Ellsworth (El), Eastport (EP), Greenfield (G), Lincoln (L), Princeton (P), Rockland (R), Skowhegan (S), Waterville (W). Geology modified from Osberg *et al.* (1985), Tucker *et al.* (2001), and Ludman *et al.* (2017).

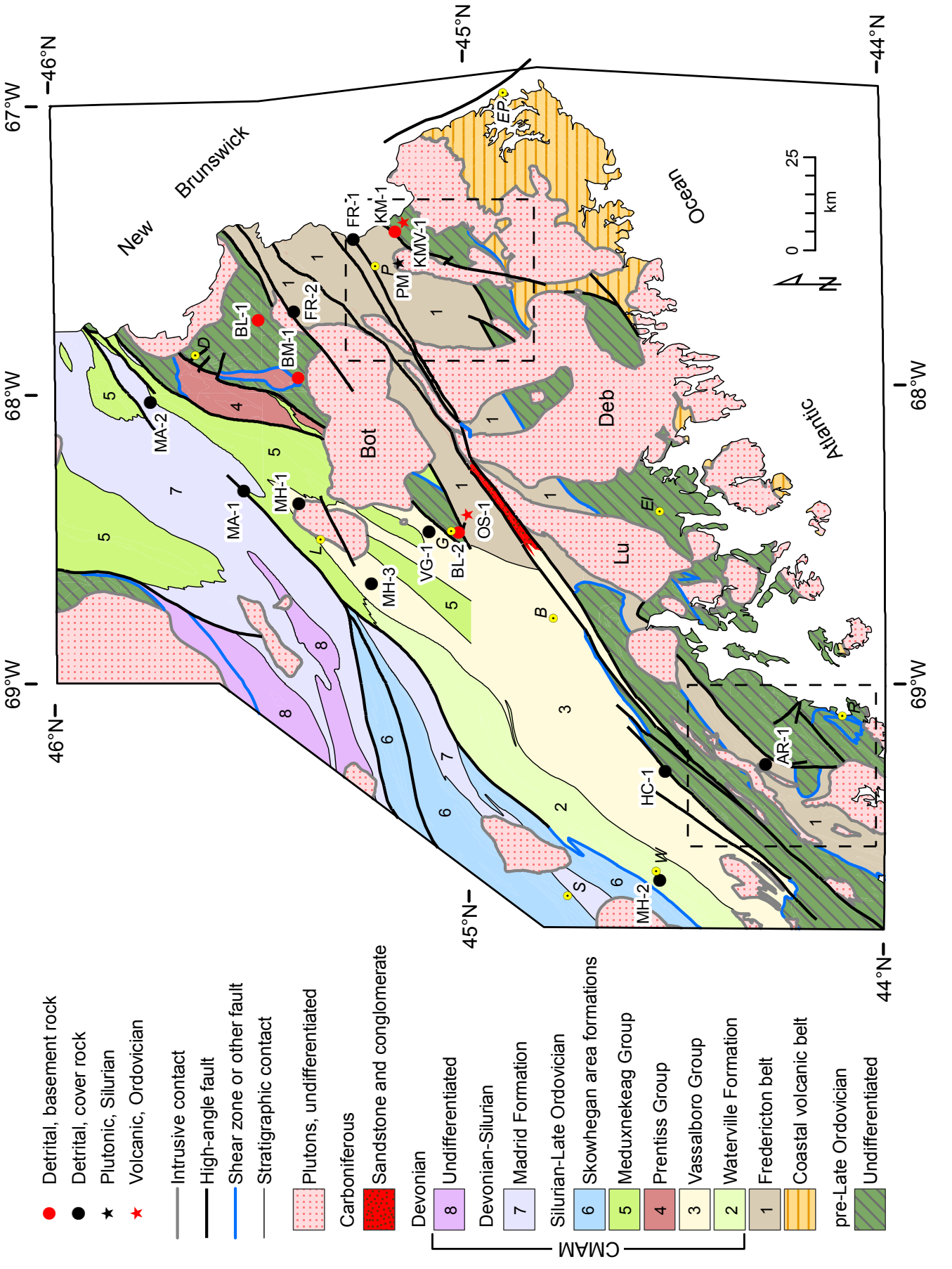

Previous work

Stratigraphy

Stratigraphic interpretations of Cambrian to Middle Ordovician basement and overlying cover successions in Maine and adjacent New Brunswick have evolved over several decades, and revisions continue today (e.g., Marvinney *et al.* 2010; Ludman 2013; Bradley and O'Sullivan 2016; Ludman *et al.* 2017). The area covered in this paper (Fig. 3) was for many years known only from reconnaissance mapping. It was surrounded by well-established stratigraphic successions in western, central, and northeastern Maine, but its relationships with the rocks of southern Maine and southwestern New Brunswick were uncertain on the two most recent Maine bedrock maps (Doyle and Hussey 1967; Osberg *et al.* 1985). More than 30 years of fieldwork since the 1985 Maine bedrock map was published have resolved long-standing correlation problems and provided a lithofacies framework for the detrital zircon studies reported here (summarized by Ludman *et al.* 2017; Ludman 2013), including:

(1) The Central Maine and Aroostook-Matapedia successions accumulated in a single depocenter – the CMAM basin – sourced from emergent highlands to the west (Boundary Mountains, Lobster Mountain, Weeksboro–Lunksoos Lake) and to the east (Miramichi), and by NE-to- SW axial currents.

(2) The Fredericton trough was a two-sided basin that received sediment from post-Middle Ordovician Miramichi and St. Croix highlands to the west and east, respectively. No similar highland is present in southwestern Maine, and relationships between Fredericton and Central Maine strata there are uncertain.

(3) Silurian lithofacies patterns adjacent to the Cambrian-Ordovician Weeksboro-Lunksoos Lake and Munsungun belts indicate that these areas also supplied post-Late Ordovician sediment to the CMAM basin.

(4) Sedimentation in the Fredericton trough ended in the late Silurian with onset of Salinic deformation but continued in CMAM through the Early Devonian.

(5) Acadian, Alleghanian, and post-Alleghanian folding and faulting have distorted original basin geometries and drastically telescoped the basin sediments.

Recent geologic mapping has refined the stratigraphy in the Fredericton trough in New Brunswick from that described by Ruitenberg and Ludman (1978), and provided fossil age control for some of the units (see Table 2; summarized in Dokken *et al.* 2018; Fyffe 1991, 1995; Fyffe and Riva 2001; Fyffe *et al.* 2011). Distinctive units along the northwest flank of the Fredericton trough in New Brunswick apparently are not present in Maine, perhaps due to facies changes, removal by faulting, or a combination of the two.

The basement tracts in the study area were clearly emergent and served as major *internal* Ganderian sediment sources for the cover rock basins following accretion of Ganderia to Laurentia (Ludman *et al.* 2017). It was hoped that detrital zircon age spectra might identify input from sources *external* to Ganderia – Laurentia and/or the approaching Avalonian plate. Our current interpretation of regional correlation is summarized in Table 2. Because of the complexity of this table, only Period and Series chronostratigraphic divisions are shown.

Detrital zircon studies

Previous detrital zircon studies in Maine and New Brunswick have helped to constrain depositional ages and determine provenance of rocks related to this study. Bradley and O'Sullivan (2016) reported detrital zircon age spectra from several proximal units on the west flank of the CMAM basin in western Maine. Discrepancies between ages of the youngest zircon grains and stratigraphic ages inferred from regional correlations suggest that some units may be as much as 15 m.y. younger than previously thought. McWilliams *et al.* (2010) demonstrated that the Connecticut Valley-Gaspé trough, containing the northwesternmost cover succession (Fig. 1), was derived from highlands flanking the basin. Studies in southwestern Maine, adjacent New Hampshire, and Massachusetts identified both Laurentian and Ganderian sources for rocks correlated with CMAM and Fredericton successions in an area where there is no basement block separating the two basins (Sorota 2013). Hussey *et al.* (2016) cited paleocurrent indicators as evidence for an eastern (peri-Gondwanan) source for rocks in southwestern Maine and southeastern New Hampshire correlated with the Fredericton trough succession.

Some detrital zircon work has been done in southwestern New Brunswick on stratigraphic units continuous with those sampled in this study. Fyffe *et al.* (2009) compared detrital zircon age spectra from pre-Silurian terranes in southern New Brunswick and coastal Maine to assess their tectonic settings and refine their provenance and accretionary histories. Pre-Silurian units related directly to this project include the Baskahegan Lake Formation, oldest unit in the Miramichi terrane, also reported here, and the Calais Formation in the lower part of the St. Croix terrane. Current work in New Brunswick has focused on rocks of the Fredericton trough in an attempt to clarify the tectonic setting and provenance of its thick turbidite succession (Dokken *et al.* 2018).

Detrital zircon studies designed to distinguish terranes and reconstruct relationships among peri-Gondwanan fragments resulting from the breakup of Rodinia are described in the Discussion section, below.

Sampling strategy

Figure 3 shows the locations of the one plutonic, two volcanic, and 14 detrital zircon samples analyzed in this study. Sampling was designed to supplement previous detrital zircon age data described above for the CMAM and Fredericton cover rocks, as well as the Miramichi and St. Croix source areas. Where prior data were available for a formation, sites were chosen to broaden geographic and stratigraphic

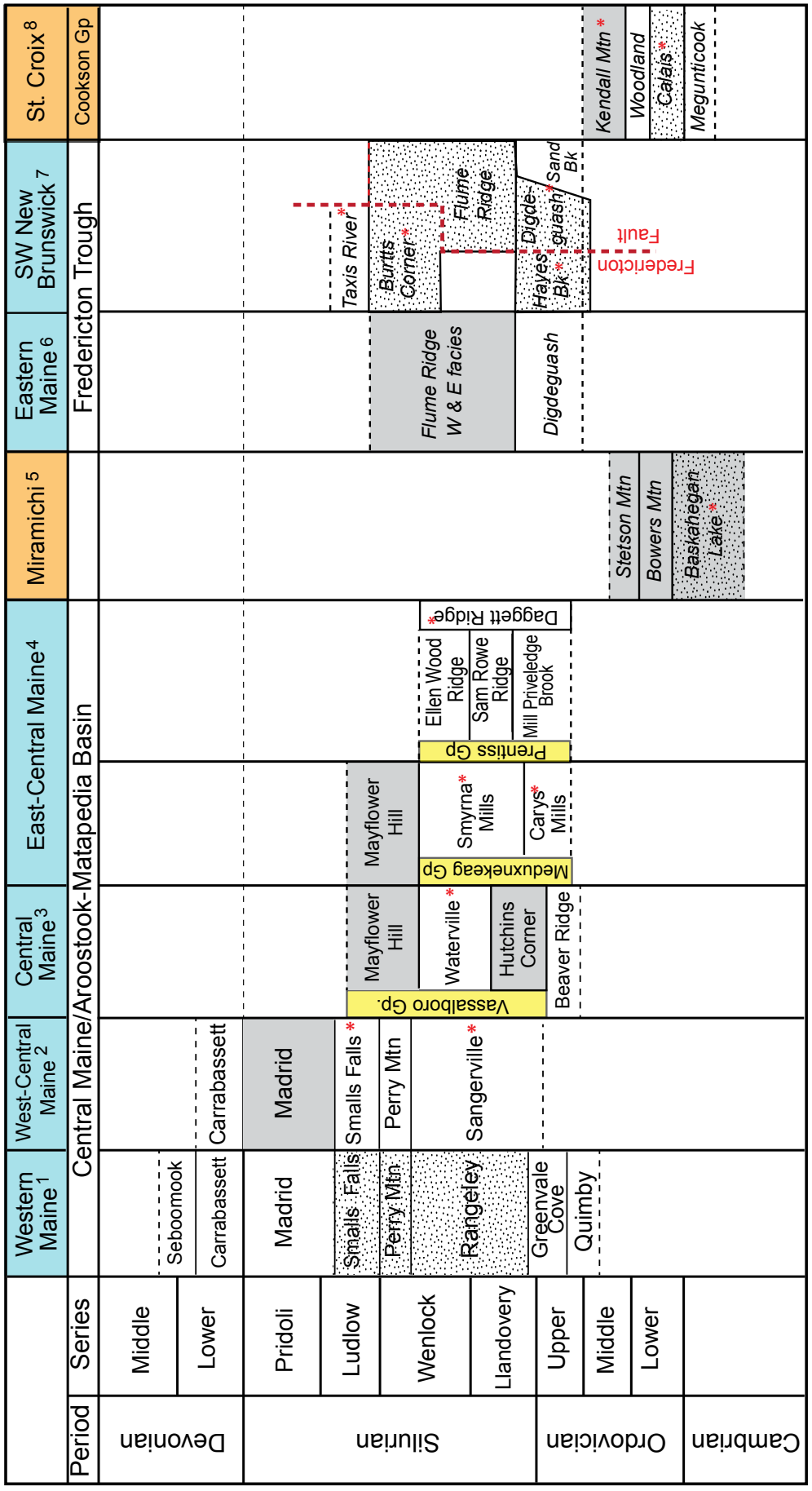

Table 2. Correlation of stratigraphic units discussed in this paper (after Cohen *et al.* 2013, 2017 modification). Shading indicates formations sampled in this study. Asterisks show units with fossil age control. Stipples indicate detrital zircon data from other studies (sources of zircon data follow, *in italics*). Sources of information: 1: Moench and Pankiwskyj (1988), *Bradley and O'Sullivan (2016)*; 2. Ludman (1976); Pankiwskyj *et al.* (1976); 3: Osberg *et al.* (1985); Osberg (1988); Marvinney *et al.* (2010); 4: Ludman *et al.* (2017); 5: Ludman and Barry (2003); 6: Ruitenberg and Ludman (1978); Ludman *et al.* (2017); 7: Fyffe (1991), (1995); *Fyffe et al. (2009); Dokken et al. (2018)*; 8: modified from Ludman and Hill (1990); Ludman (1991).

coverage in an attempt to detect possible changes in sediment source for that unit. Wherever possible, formations were sampled in areas where their stratigraphic positions are well established, at or close to where they were defined, and in the rare places where there is fossil age control. Formation abbreviations for dated samples are explained in Figure 3 and are used throughout the text, tables and appendices B, C, and D.

Plutonic zircon

The Pocomoonshine gabbro-diorite intruded folded strata of the Fredericton trough, and thus provides a minimum age for both deposition in that depocenter and onset of Salinic deformation in eastern Maine and New Brunswick (West *et al.* 1992). A $^{40}Ar/^{39}Ar$ hornblende cooling age of 422.7 ± 3 Ma (West *et al.* 1992) has been the regional standard for defining the onset of Salinic deformation in Maine and New Brunswick, and a sample from near the northern margin of the Pocomoonshine gabbro-diorite was collected to compare the U–Pb zircon crystallization age of the pluton with the previously determined hornblende cooling age.

Volcanic zircon

Samples were collected from the thick volcanic Olamon Stream Formation at the top of the Miramichi succession (OS-1) and from a tuff horizon (KMV-1) at the base of the Kendall Mountain Formation, youngest unit in the St. Croix terrane, to determine their eruptive ages, clarify stratigraphic ranges of underlying units, and constrain the timing of the Ordovician tectonism. A cryptocrystalline tuff from the Smyrna Mills Formation was also collected but proved to have insufficient zirconium to attempt zircon separation and dating.

Detrital zircon

Ten samples of cover rock were collected for detrital zircon dating; the stratigraphic problems addressed by these samples are detailed below. Eight of these samples are interpreted to have been deposited in the initial Late Ordovician – Middle Silurian sedimentary regime in the CMAM basin [(Mayflower Hill (MH) and Hutchins Corner (HC) formations; Vassalboro Group (VG)], and Fredericton trough [(Flume Ridge (FR) and Appleton Ridge (AR)], and two in the subsequent Late Silurian to Early Devonian regime in CMAM [(Madrid Formation (MA)].

Four additional sedimentary rock samples were collected from basement terranes; three from the Miramichi Baskahegan Lake (BL-1, BL-2) and Bowers Mountain (BM) formations and one from the Kendall Mountain (KM-1) Formation. Nine of the fourteen detrital zircon sample sites are from chlorite-grade rocks, two from higher grades of regional metamorphism (HC-1 at biotite grade, AR-1 at andalusite + staurolite grade), and three from contact aureoles with biotite-cordierite assemblages (MH-1, BM-1, and KM-1).

U–Pb geochronology

Zircon was extracted from 5–10 kg samples collected at outcrops shown in Figure 3. Standard mineral separation procedures included crushing and pulverizing, followed by processing over a Wilfley table, through a magnetic separator, and in heavy liquids to obtain a heavy mineral concentrate composed mostly of zircon. Detrital zircon was sprinkled onto double-sided tape to minimize sampling bias, whereas igneous zircon from three samples was hand-picked under a binocular microscope. Zircon grains were mounted in epoxy, ground to about half thickness, and sequentially polished using 6 μm and 1 μm diamond suspension. All polished grains were imaged in reflected and transmitted light on a petrographic microscope, and in cathodoluminescence (CL) using the USGS-Denver JEOL5800LV scanning electron microscope (SEM).

Zircon was dated by the U–Pb method using the USGS/Stanford sensitive high-resolution ion microprobe-reverse geometry (SHRIMP-RG) at Stanford University following the methods described in Williams (1998). For all analyses, the primary beam was about 20–25 μm in diameter. For igneous zircon, the magnet was cycled through the appropriate mass stations five or six times, whereas for detrital zircon the magnet was cycled four times to maximize the number of grains analyzed (between 60 and 70 grains per sample). Measured $^{206}Pb/^{238}U$ ratios for zircon analyses were normalized to the value for standard R33 (ca. 419 Ma; Black *et al.* 2004).

SHRIMP data for zircon were reduced using Squid 2 (Ludwig 2009) and plotted using Isoplot 3 (Ludwig 2003). Nested concordia plots for detrital zircon ages from 14 cover rock and basement sandstones are shown in Figure 4. U–Pb data for detrital zircon are screened such that ages that are greater than 10% discordant (Fig. 5) are excluded from the relative probability plots that display age distributions. For the entire detrital zircon data set of 916 analyses, nine analyses were excluded. These include: #26, 40 for BL-2; #17 for MH-1; #22, 37, 51, 63 for VG-1; and # 26, 47 for MA-1. For relative probability plots, we used $^{206}Pb/^{238}U$ data for ages <1300 Ma, and $^{207}Pb/^{206}Pb$ data for ages >1300 Ma. Ages of igneous rocks are calculated as concordia ages (Ludwig 1980, 2003) and reported with 2-sigma uncertainties. Concentrations of U and Th are believed to be accurate to about ± 20%, and are used only for comparing analyses.

RESULTS

Nested concordia plots for detrital zircon ages from the 14 cover and basement sandstones are shown in Figure 4, and Figure 5 contains complete detrital zircon age spectra for the sampled rocks. Two general conclusions can be drawn from Figure 5: (1) The presence of Silurian zircon grains solely in the cover rocks and the much older ages of the youngest basement rock zircon grains confirm that the two suites have significantly different ages, and (2) zircon

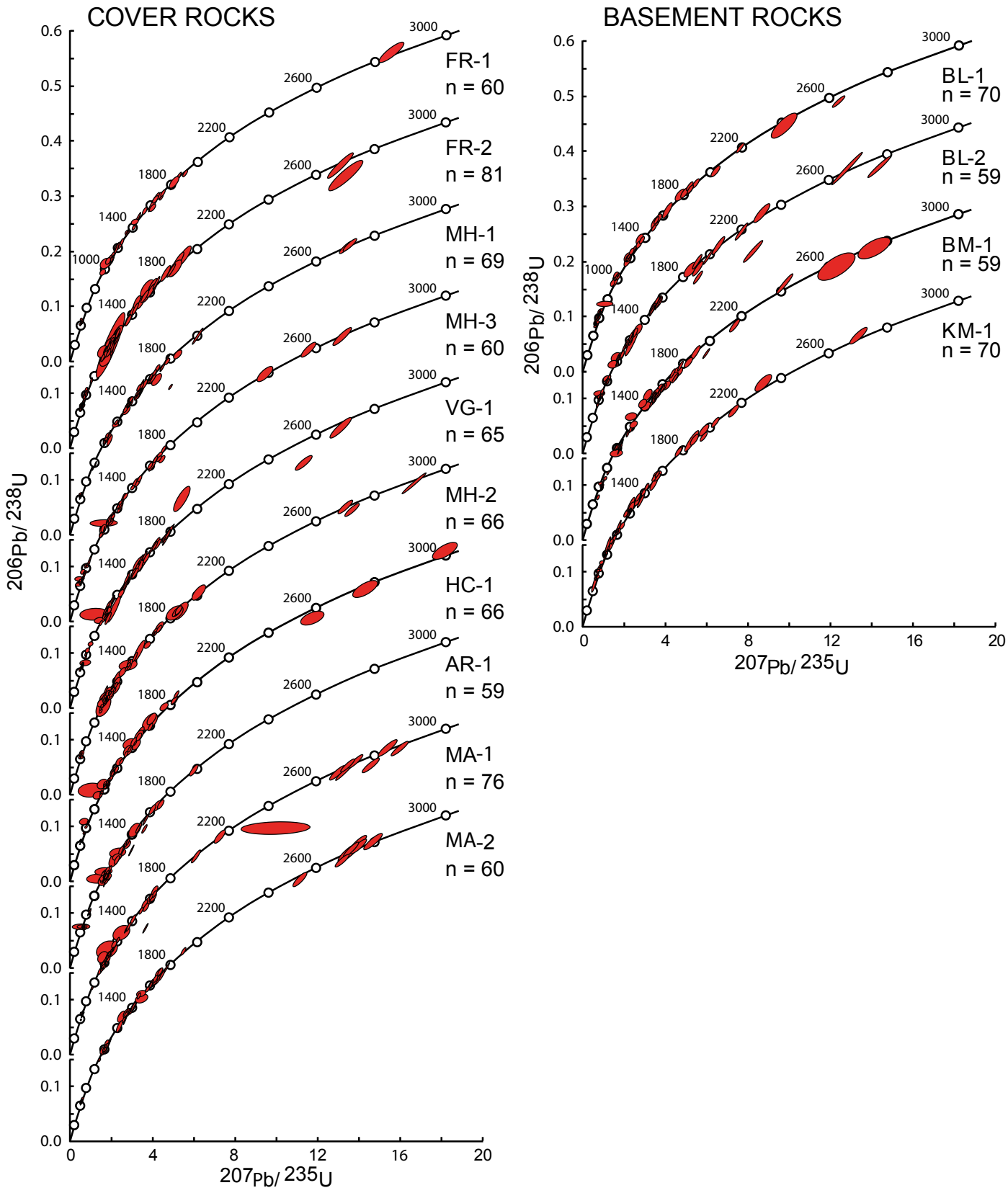

Figure 4. Nested concordia plots for detrital zircon from cover and basement rocks. Formation labels as in Figure 3.

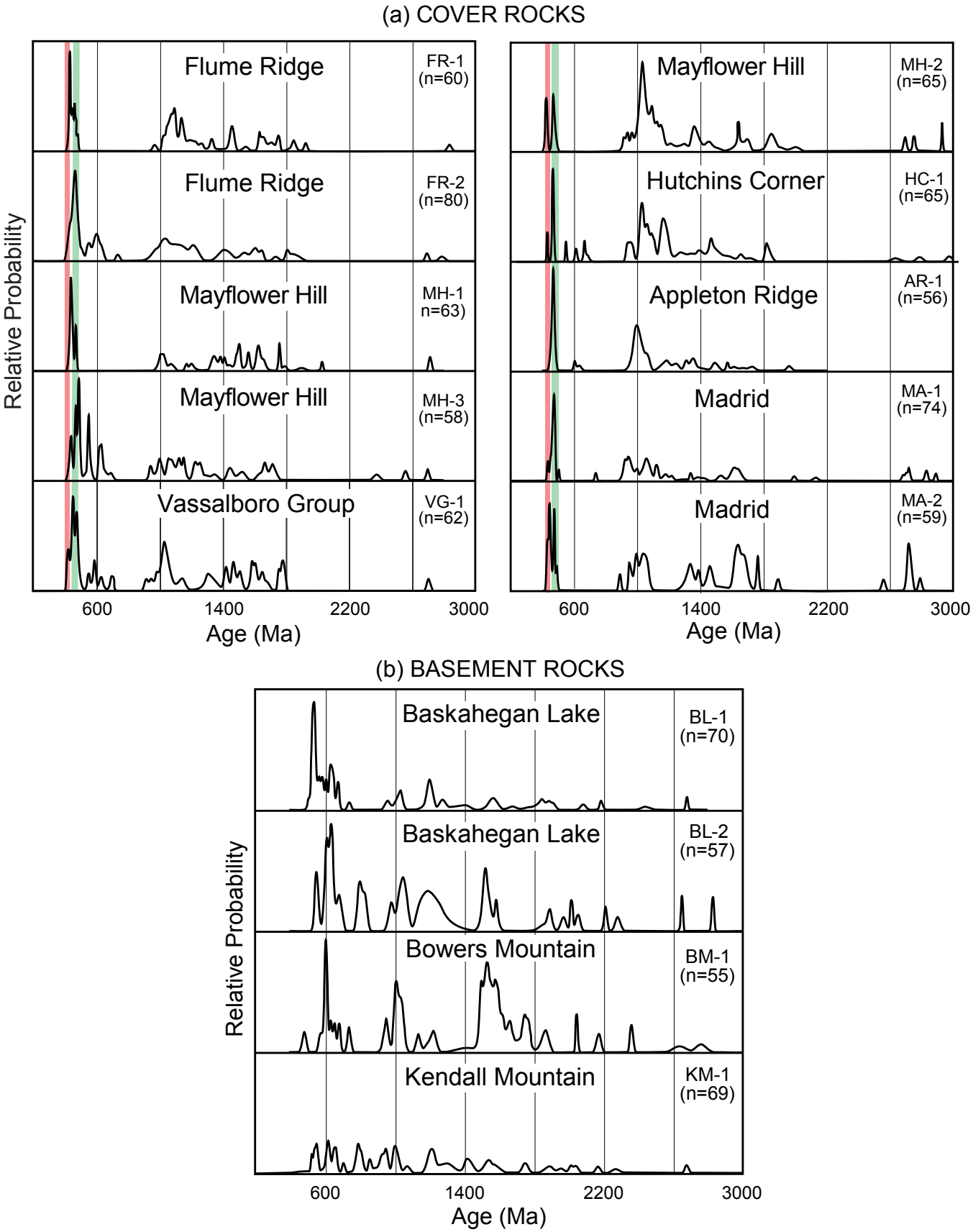

Figure 5. Complete detrital zircon age spectra for formations sampled in this study. In (a), green shading indicates span of Ganderian volcanism (after Wilson *et al.* 2015) and pink shading indicates Eastport-Mascarene volcanism. Sample identification as in Figure 3.

populations between 2.0 and 2.5 Ga in the basement rocks are absent from the cover rocks, suggesting a source not tapped by the younger strata.

Additional results addressing specific stratigraphic problems of the basement and cover successions are described below, combining detrital zircon, paleontological, and field evidence. The crystallization age of the Pocomoonshine gabbro-diorite is presented first as it constrains both stratigraphic ages of the Fredericton cover succession and the timing of Late Silurian (Salinic) tectonism. Boundaries between stratigraphic stages cited throughout this paper are from the International Chronostratigraphic Chart (Cohen *et al.* 2013; 2017 modification).

The age of the youngest detrital zircon grains in a rock is, ideally, a maximum deposition age for the host formation. Conditions in this study are far from ideal, partly because of uncertainties about the stratigraphic positions of some samples within their formations, ages based on poorly preserved fossils, and limits to which a single detrital zircon- or fossil-based age can be applied to a formation thousands of metres thick. Appendix A compares current chronostratigraphic nomenclature with that used in reporting Maine fossil ages in the 1950s through 1980s.The significance of each dated sample is given in Appendix B, and all analytical data are reported in Appendices C and D.

Analytical issues are also problematic, as analytical error for most samples (Appendices C and D) typically spans one or more Silurian and/or Ordovician stages. Finally, the youngest zircon age in some samples comes from only one or two zircon grains and, although interesting, these are statistically unreliable. Despite these obstacles, the data do provide new insights into the ages and ranges of the sampled formations. In addition, volcanic zircon from the Miramichi and St. Croix basement terranes provide eruptive ages that help resolve stratigraphic problems described below.

Age of the Pocomoonshine gabbro-diorite

Zircon from the northern part of the Pocomoonshine gabbro-diorite (Fig. 6a) was extracted from a sample of fine-grained gabbro (Fig. 6b). These grains are subhedral to anhedral, and display fine oscillatory zoning (Fig. 6c) indicative of an igneous origin. U–Pb isotopic data of 18 analyses are concordant and result in a concordia age of 421.9 ± 2.4 Ma (Fig. 6d). This age overlaps within uncertainty with the 422.7 ± 3 Ma $^{40}Ar/^{39}Ar$ hornblende cooling age (West *et al.* 1992), confirming that the Pocomoonshine gabbro-diorite was emplaced during the Late Silurian. The overlap also indicates that the pluton cooled rapidly and was emplaced at a shallow crustal level.

Ages and relationships of basement units

Miramichi terrane

The Miramichi terrane extends southwestward for more than 300 km from northern New Brunswick into Maine where it narrows and terminates abruptly at the surface in the Greenfield area (Fig. 1; Ludman 2018). The Bottle Lake pluton divides the terrane in Maine into northern (Danforth) and southern (Greenfield) segments (Fig. 3). The two segments have similar stratigraphies, with the turbiditic Baskahegan Lake Formation at the base of each, overlain by a dominantly pelitic, partially euxinic, unit and capped by a thick volcanic section. The upper parts of these sections are sufficiently dissimilar to require different nomenclature (Fig. 7).

The Baskahegan Lake Formation comprises turbiditic quartzofeldspathic and quartzose sandstone with varying amounts of interbedded slate. The base of the overlying Bowers Mountain Formation in the Danforth segment is mostly black sulfidic shale with quartz arenite that pass upward into interbedded gray shale and siltstone. The equivalent Greenfield Formation in the Greenfield segment contains some black shale but also has numerous manganese-rich mudstone/siltstone horizons and a distinctive manganiferous iron formation. A thick succession of dacitic, rhyodacitic, and andesitic tuffs and flows form the tops of both segments. The Stetson Mountain volcanic rocks (Danforth segment) are typically fine grained ashfall tuffs with subordinate crystal tuffs and sparse coarser-grained ashflow tuffs, whereas the equivalent Olamon Stream volcanics (Greenfield segment) are coarser (including a few agglomerates), and have more flows and crystal or lithic tuffs.

Correlation with fossil-bearing units outside the study area suggests a Cambrian to Middle Ordovician age range for the Miramichi succession in Maine. The lower limit is based on correlation of the Baskahegan Lake Formation with the Grand Pitch Formation in the Weeksboro–Lunksoos Lake terrane (Fig. 1), which contains the Early to Middle Cambrian trace fossil *Oldhamia* (Neuman 1984). Ichnofossils in New Brunswick (Pickerill and Fyffe 1999) indicate that the Baskahegan Lake Formation extends into the Early Ordovician but is older than the overlying late Tremadocian Bright Eye Brook Formation (Fyffe *et al.* 1983). The upper age limit of the Miramichi succession in Maine is set by poorly constrained "Lower to Middle Ordovician" graptolites in the Stetson Mountain Formation (Larrabee *et al.* 1965). Until this study there had been no direct evidence for the age of the Bowers Mountain Formation, nor radiometric age control for the volcanic section in Maine.

Igneous zircon was collected from a felsic lava in the Olamon Stream Formation (OS-1) to directly date this formation and, indirectly, the correlative Stetson Mountain Formation. Detrital zircon from sandstone near the base of the Bowers Mountain Formation (BM-1) and from Baskahegan Lake sandstones in both segments (BL-1, BL-2) was dated in an attempt to constrain the ages and ranges of these formations.

Olamon Stream Formation: The first radiometric age of Miramichi volcanism in Maine is provided by zircon from the Olamon Stream Formation (OS-1). The sample, originally thought to be in place, proved to be part of a train of extremely coarse glacial debris derived from outcrops of

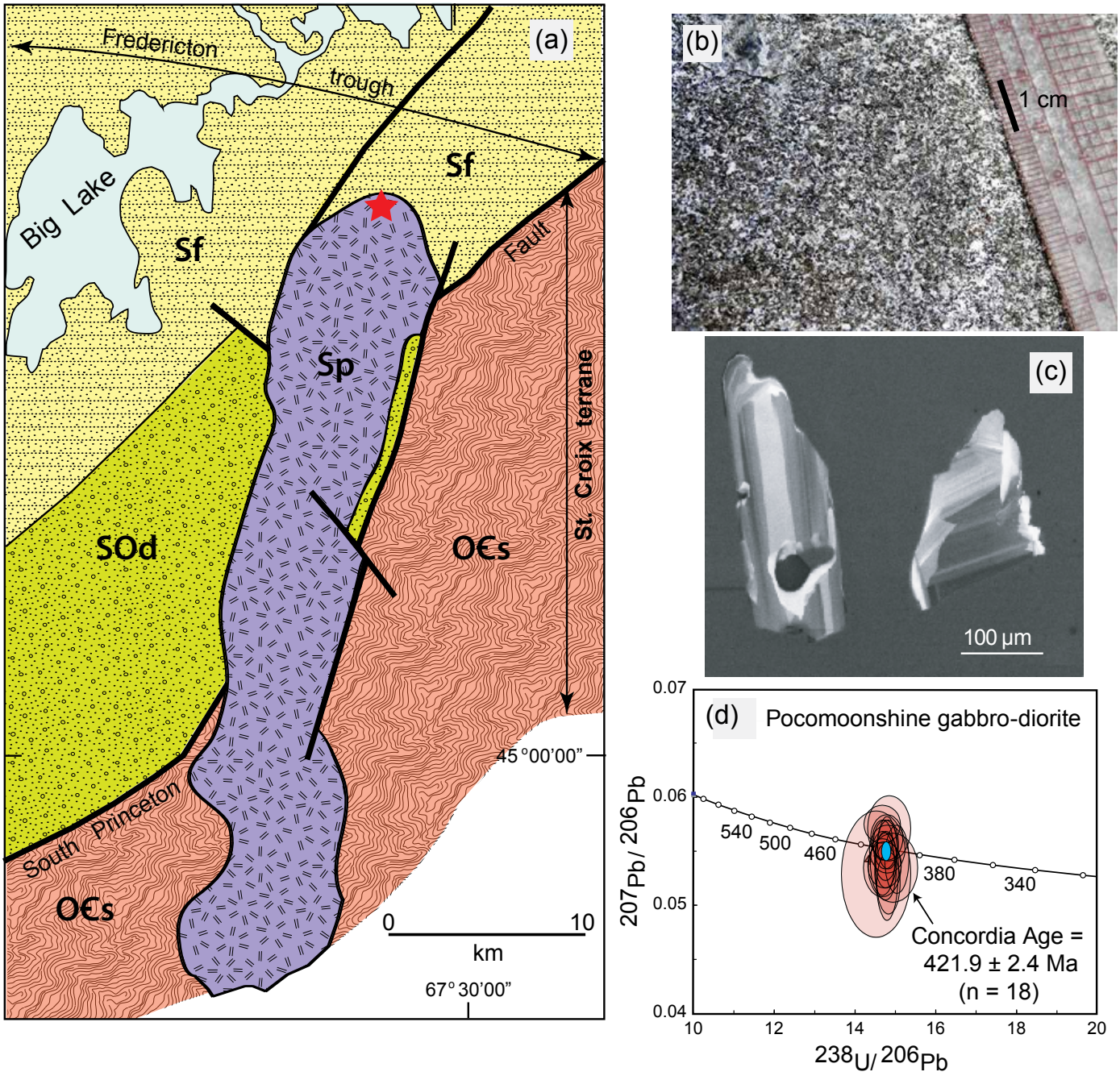

Figure 6. Age of the Pocomoonshine gabbro-diorite. (a) Intrusive relationships showing Pocomoonshine gabbro-diorite sealing the Fredericton trough/St. Croix boundary (after Osberg *et al.* 1985). Star shows location of dated sample. Sp = Pocomoonshine gabbro-diorite; Fredericton trough: Sf = Flume Ridge; SOd = Digdeguash; St. Croix terrane: O€s = Cookson Group. Thin lines = stratigraphic and intrusive contacts. Thick lines = faults. (b) Fine grained gabbro sample dated. (c) Cathodoluminescence image of typical zircons. (d) Concordia diagram showing distribution of measured ages.

identical rock about a kilometre to the north of the sampling site. The rock is a crystal-rich felsic lava flow containing abundant 2–8 mm quartz and feldspar phenocrysts in a buff-weathering, very fine-grained matrix (Fig. 8a). Zircon from the Olamon Stream felsic lava is fairly coarse (~100–200 µm), euhedral, and displays fine, concentric oscillatory zoning (Fig. 8b), suggesting an igneous origin. A few grains contain partially resorbed cores; two analyses of cores yielded ages of about 660 and 550 Ma, thought to represent inheritance of Neoproterozoic xenocrystic zircon from an unknown source.

U–Pb isotopic data of 15 analyses yield a concordia age of 469.3 ± 4.6 Ma (Fig. 8c), at the boundary between the Lower and Middle Ordovician (Floian–Dapingian), and is interpreted as the eruption age of the felsic lava. This age for the youngest formation in the Miramichi succession

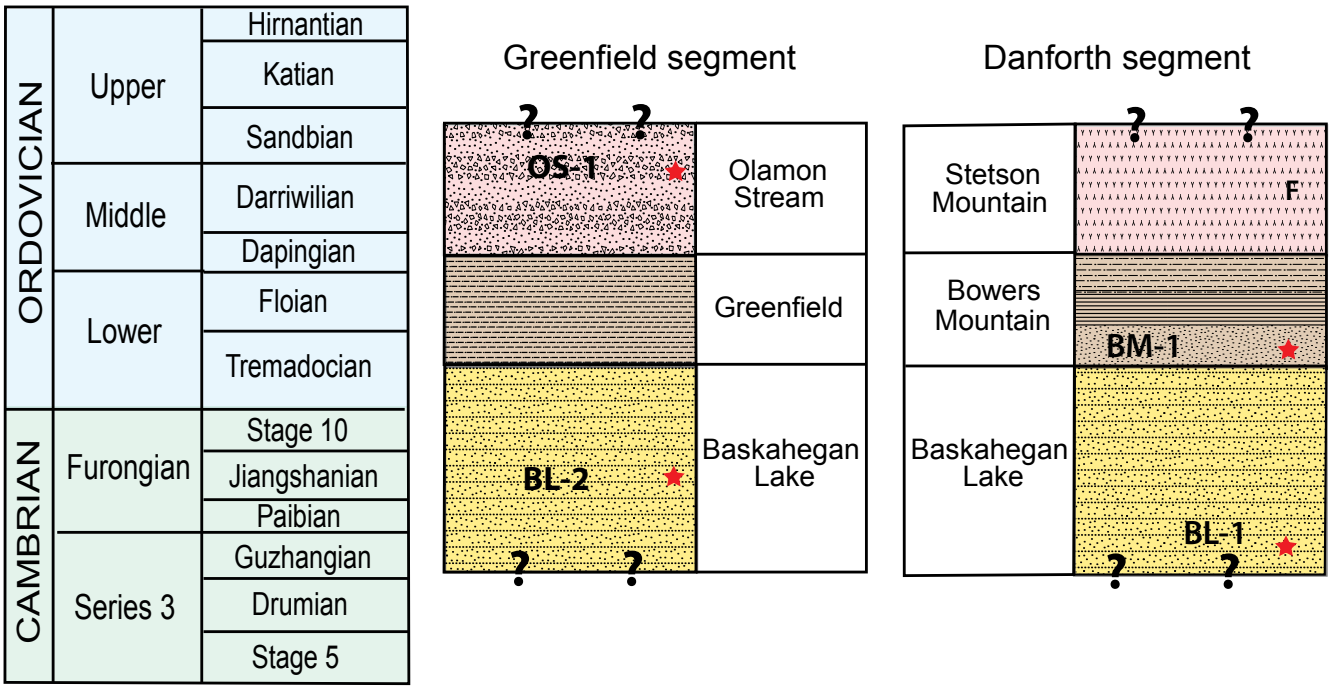

Figure 7. Stratigraphy of the Greenfield and Danforth segments of the Miramichi terrane in Maine. Stars = zircon samples. F = fossils. Positions of samples and fossils within formations uncertain except for BM-1.

also constrains the range of the underlying units and is the maximum age for subsequent Ordovician deformation (see Discussion below).

Bowers Mountain and Baskahegan Lake formations: Figure 9 is an expanded excerpt from Figure 5a, highlighting the Late Neoproterozoic to Early Cambrian ages of the youngest detrital zircon grains in the four basement units sampled. The absence of Silurian zircon clearly distinguishes all four units from the younger cover rocks. The latest Neoproterozoic to earliest Cambrian age of the youngest zircons in the Baskahegan Lake Formation is consistent with its Cambrian-Early Ordovician age described above, and with zircon ages from the formation in New Brunswick (Fyffe *et al.* 2009). Unfortunately, the youngest zircon ages in the Bowers Mountain and Kendall Mountain formations are not statistically robust enough to establish a youngest age population as they were found in only one grain each (Fig. 9).

St. Croix terrane

Stratigraphic ages of units in the St. Croix terrane shown in Table 2 are based on fossils in the lower and uppermost formations of the succession. Tremadocian graptolites at Cookson Island indicate an Early Ordovician age for the upper part of the Calais Formation, above a thick basal pillow basalt member. Graptolites in black shale interbedded with quartz arenite in the Kendall Mountain Formation suggest a Late Ordovician (Caradoc) age (Fyffe and Riva 1990) but there is no age control for the intervening Woodland Formation.

The age and stratigraphic affinity of the Kendall Mountain Formation have been debated. Fyffe *et al.* (2009) proposed that this formation lies conformably below the Digdeguash Formation, but Ludman (1990) mapped a terrane-bounding fault between the two formations and interpreted the Kendall Mountain as the youngest formation in the St. Croix terrane. This study attempted to resolve this issue by (1) acquiring a detrital zircon age spectrum for the Kendall Mountain (KM-1) to compare with those of the Digdeguash (Fyffe *et al.* 2009; Dokken *et al.* 2018) and basement units, and (2) dating a tuff horizon (KMV-1) just above the contact with the underlying Woodland Formation.

Kendall Mountain Formation: Zircon was extracted from a white, cryptocrystalline felsic rock (KMV-1) interpreted as an ashfall tuff interbedded with thinly laminated black shale and siltstone near the base of the Kendall Mountain Formation (Figs. 10a–b) in the St. Croix terrane. These grains are fine (~50–100 μm in length), euhedral, and display fine, concentric oscillatory zoning, indicative of an igneous origin (Fig. 10c).

U–Pb isotopic data for 16 grains yield a concordia age of 477.4 ± 3.7 Ma (Fig. 10d). This age is interpreted as the time of eruption of the felsic tuff and thus dates the base of the Kendall Mountain Formation as Lower Ordovician (Floian–Tremadocian). It is considerably older than the Late Ordovician (Caradoc) fossil-based age for the formation but is compatible with detrital zircon ages from overlying quartz arenites (see below).

Contributions of zircon ages to basement stratigraphy: Figure 11 shows the relationships between detrital and volcanic zircon ages obtained in this study with the stratigraphic ages of their host rocks. In the Miramichi terrane, ages of the

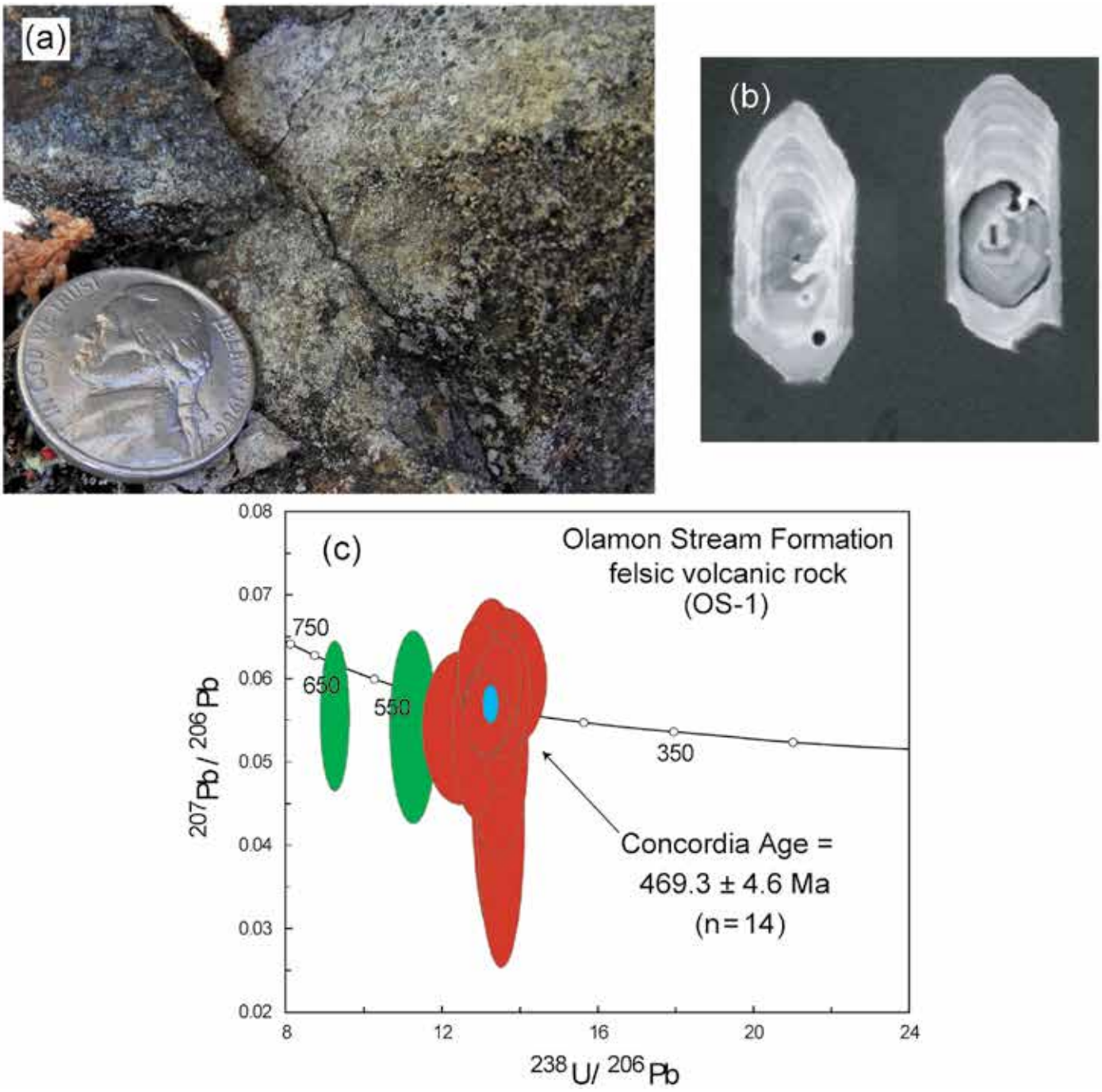

Figure 8. Age of the Olamon Stream lava. (a) Close-up showing microporphyritic lava. (b) Typical zircons dated. Note inherited core on grain to right. (c) Concordia diagram showing distribution of measured ages. Red ellipses are igneous analyses, green are inherited zircons.

youngest zircons in the Baskahegan Lake Formation are statistically significant and consistent with its proposed Cambrian to Early Ordovician age. They set maximum Late Neoproterozoic and Early Cambrian depositional ages for the Miramichi succession in the Greenfield and Danforth segments, respectively but constrain the age of the formation only slightly. The age of the youngest Bowers Mountain detrital zircons could potentially have limited the upper range of the Baskahegan Lake Formation but the single 485 Ma age is statistically insignificant. The 469.3 ± 4.6 Ma age for the Olamon Stream lava dates one horizon within the thick Miramichi volcanic pile. It also limits the age of the Bowers Mountain Formation to the Early Ordovician, between that eruptive age and the Cambrian–Early Ordovician ichnofossils in the underlying Baskahegan Lake Formation (Pickerill and Fyffe 1999).

In the St. Croix terrane, ages of volcanic and detrital zircons in the Kendall Mountain Formation improve

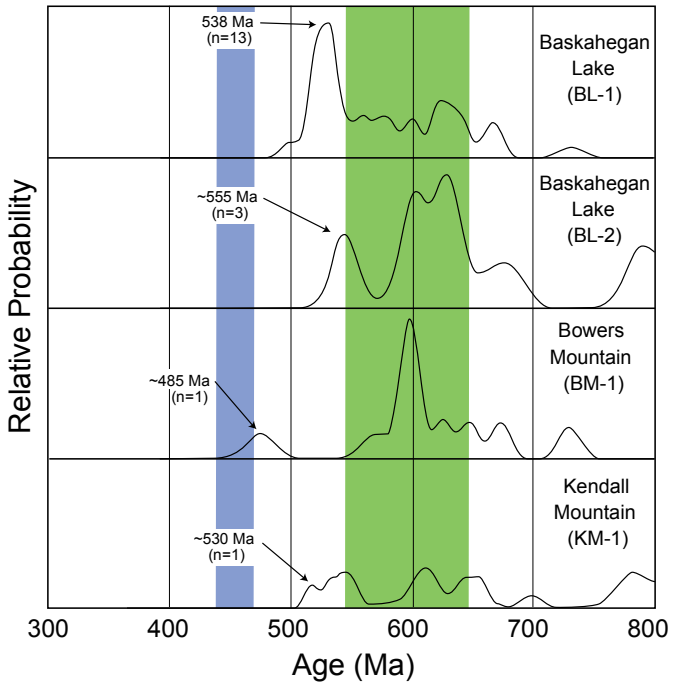

Figure 9. Excerpt of relative probability plot for basement samples showing details of youngest zircon populations. Blue = Span of Ganderian volcanism; Green = Avalonian.

understanding of Cookson Group stratigraphy in three ways. First, the 477.4 ± 3.7 Ma age of the volcanic horizon just above the base of the formation narrows the range of the underlying Woodland Formation to a narrow span in the Tremadocian, bracketed between the Kendall Mountain volcanic horizon and the Tremadocian fossils in the Calais Formation (Cumming 1967; Fyffe and Riva 1990). Second, if the fossil-based Caradocian age of the Kendall Mountain is correct, the range of the formation would span much of the Ordovician Period, from Tremadocian through Caradocian (Fig. 11, right column). Finally, the detrital zircon age spectrum for Kendall Mountain quartz arenite (KM-1) differs significantly from that of the adjacent Digdeguash Formation (Dokken *et al.* 2018) from which it is separated by a terrane-bounding fault (Ludman 1990; Mohammadi *et al.* 2017), but is similar to those of the Miramichi basement units, confirming the basement rock status of the Kendall Mountain.

Ages and relationships of cover rocks

The youngest zircon populations in all but one of the sandstones from the Fredericton trough and CMAM localities shown in Figure 3 are between ca. 434 and 422 Ma — Middle (Wenlock) to Upper (Ludlow) Silurian (Fig. 12). The exception is the Appleton Ridge Formation whose youngest zircon population is ca. 469 ± 3 Ma. Although the ages of the youngest zircon grains are suggestive, they are represented for most samples by only one or two grains, too few to be useful in providing reliable maximum ages of individual units (Dickinson and Gehrels 2009).

The suggested presence of ca.422 to 434 Ma detrital zircon

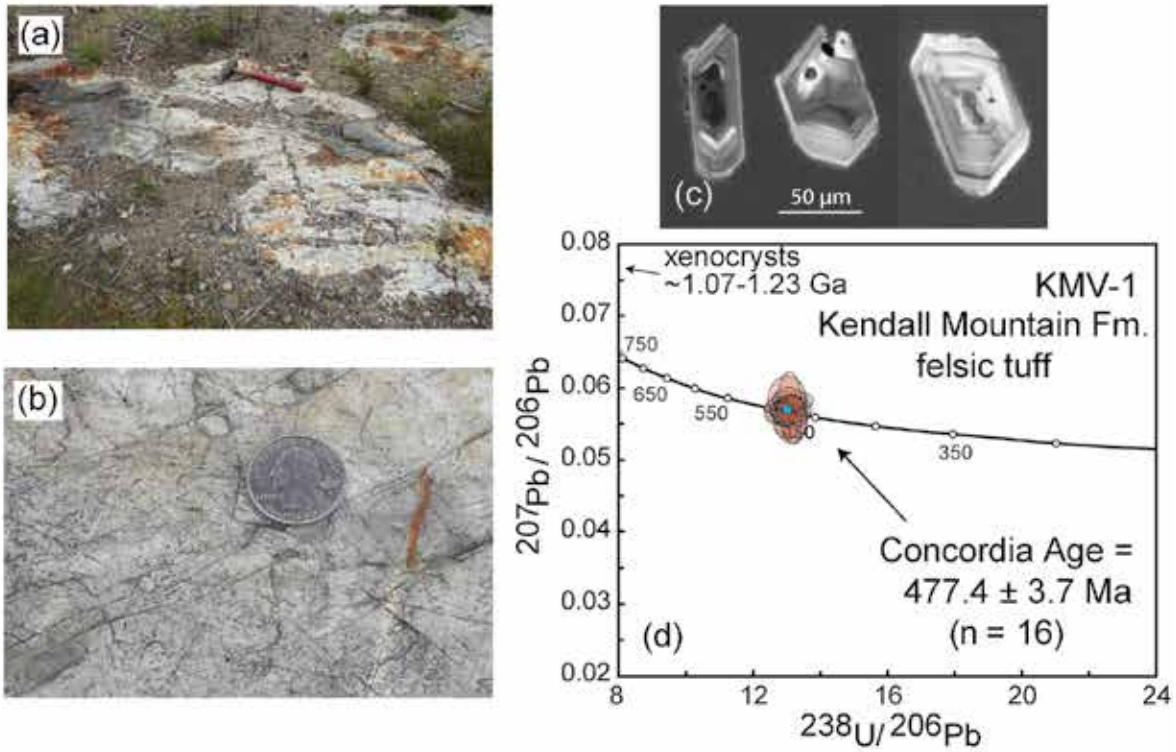

Figure 10. Age of Kendall Mountain volcanic horizon. (a) KMV outcrop showing subhorizontal black shale and white-weathering tuff. (b) Close-up of the dated tuff. (c) Typical zircon from tuff horizon. (d) Concordia diagram showing individual zircon analyses with 2-sigma uncertainties and calculated concordia age.

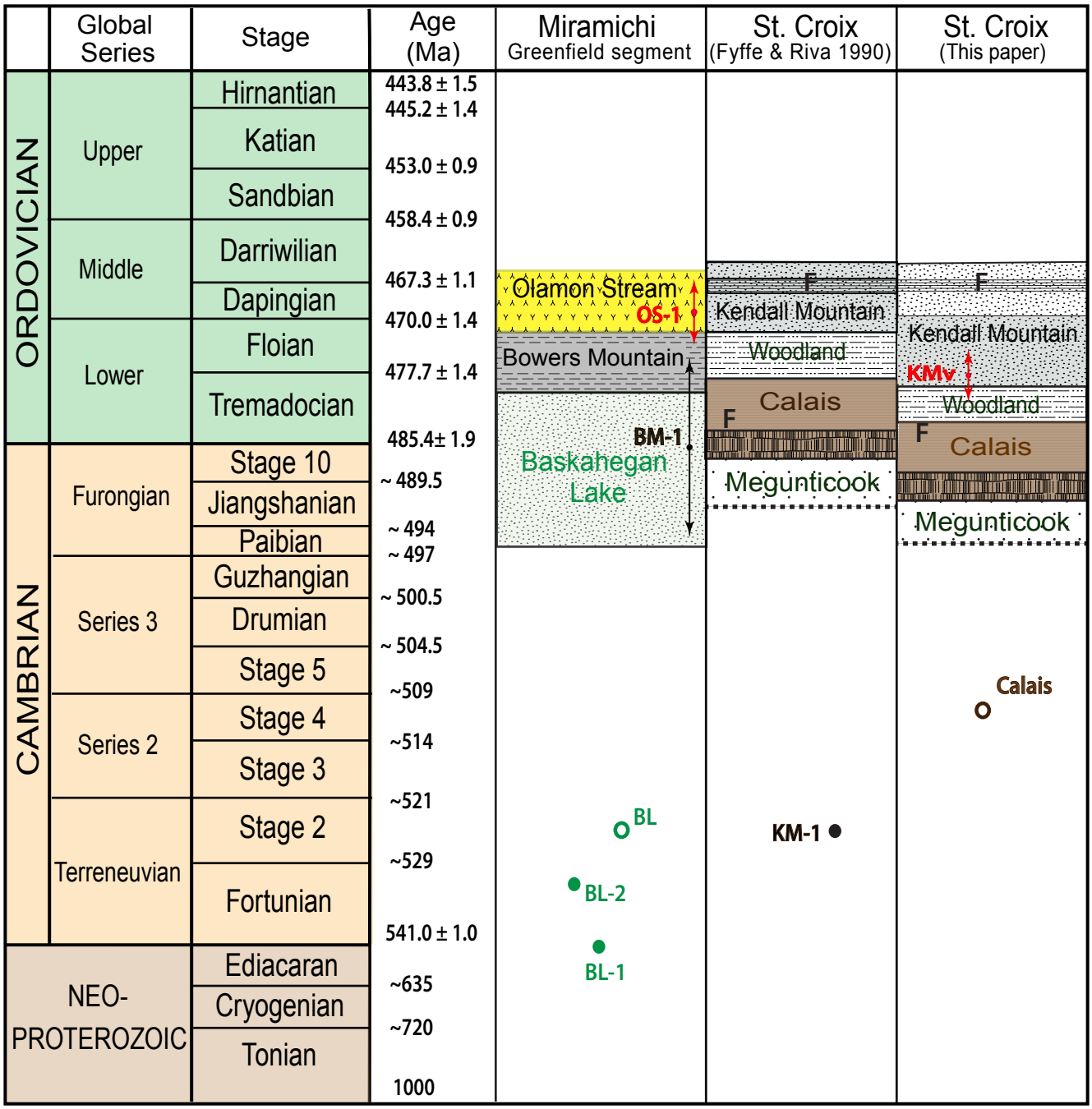

Figure 11. Isotopic and paleontological evidence for ages of Miramichi and St. Croix basement successions. Filled circles = ages of youngest zircon from this study; Open circles = data from Fyffe *et al.* (2009); Red stars = eruptive ages with error bars.

grains in formations known or inferred to be Silurian mirrors data reported from western Maine (Bradley and O'Sullivan 2016), and southwestern Maine, southeastern New Hampshire, and Massachusetts (Wintsch *et al.* 2007; Sorota 2013). These Middle to Late Silurian ages overlap the putative ages of several of their host rocks and have raised questions about the accuracy of the stratigraphic assignments and/or the measured ages.

In many instances, it is unlikely that there was enough time for those zircon grains to crystallize in an igneous rock and then be exhumed, weathered, eroded, deposited in units thousands of metres thick, and lithified before well-dated deformation (in the Fredericton trough) or deposition of overlying Late Silurian to Early Devonian strata (in CMAM). The most likely explanation for these zircon grains is direct derivation from tephra eruptions. The timing and broad geographic distribution of zircons of this age is compatible with Silurian "supervolcano" eruptions in coastal Maine that produced volumes of tephra comparable to those of the largest measured eruptions (Seaman and Hamdi 2018). The suggested Wenlockian timing corresponds with tephra eruptions of the Dennys Formation in the Eastport–Mascarene

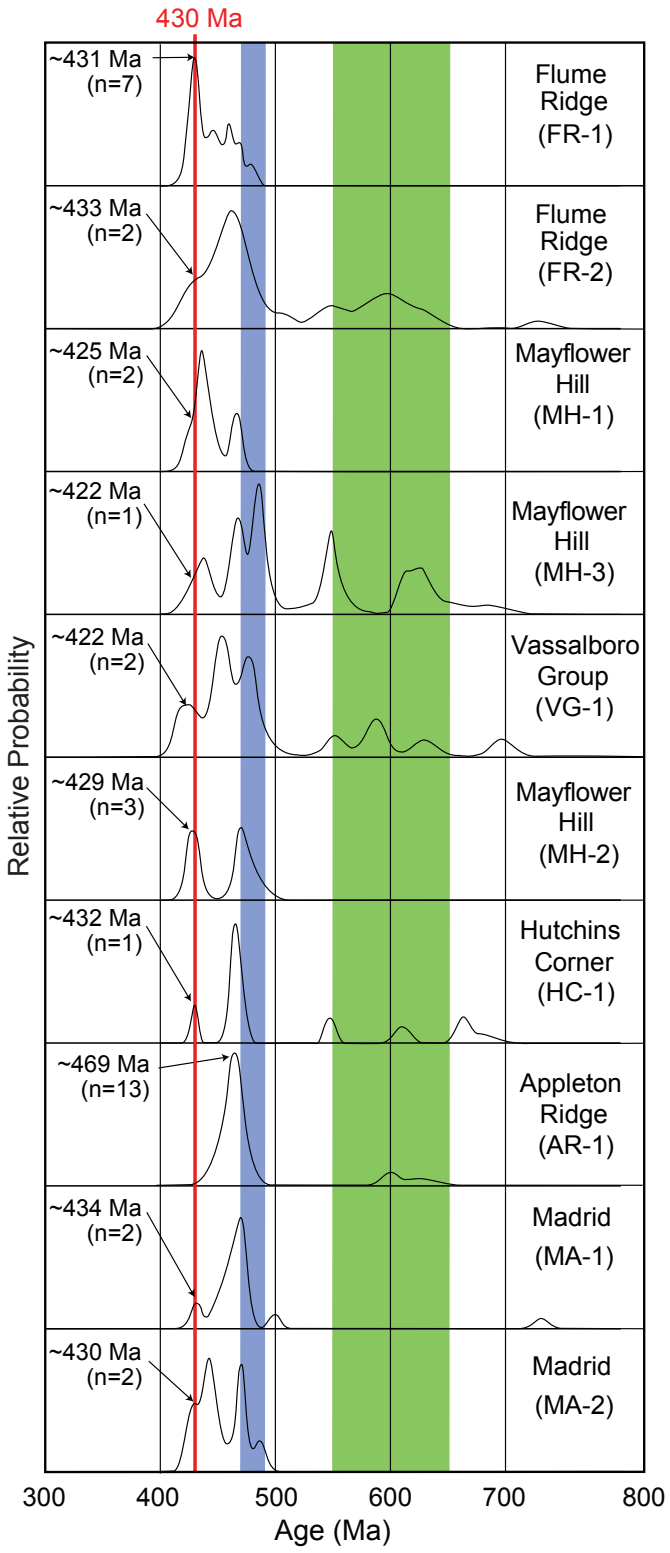

Figure 12. Excerpt from relative probability plots showing youngest detrital zircon from cover rocks. Blue = Span of Ganderian volcanism; Green = Avalonian.

arc (Gates and Moench 1981; see Fig. 1), although this would imply a slightly older eruption than those dated by Seaman and Hamdi (2018).

Fredericton trough

Figure 13 shows the current interpretation of Fredericton trough stratigraphy in eastern Maine and New Brunswick. The Flume Ridge Formation underlies more than 75% of the Fredericton Trough in Maine and is divided into western and eastern facies. The western facies, close to the Miramichi terrane, is characterized by coarser grains, more abundant lithic fragments and pelite, thicker beds, and lower carbonate content than the eastern facies exposed in the central and eastern parts of the trough. Fossils have not been found in Maine but provide good age control for units in the western part of the Fredericton trough in New Brunswick (Fig. 13) and for at least part of the Digdeguash Formation on the east flank of the basin (Dokken *et al.* 2018).

Zircon from calcareous wackes of the Flume Ridge eastern (FR-1) and western (FR-2) facies were dated for comparison with data from New Brunswick (Dokken *et al.* 2018) and to broaden the geographic distribution of zircon ages from this widespread formation. The Digdeguash Formation was not sampled in this study; however, zircons from the mid-coastal Appleton Ridge Formation (AR-1) were dated to test its proposed equivalence with the Digdeguash (e.g., Hussey *et al.* 2010; Berry *et al.* 2016).

Flume Ridge Formation: The age of the Flume Ridge Formation had previously been bracketed between early Silurian graptolites (Upper Rhudannian; ca. 440 Ma) in the underlying Digdeguash Formation (Fyffe and Riva 2001) and the 421.9 ±2.4 Ma Pocomoonshine gabbro-diorite that intrudes folded Flume Ridge and Digdeguash strata. The youngest zircon grains in FR-1 and FR-2 are ca. 430 Ma, providing a maximum age for deposition of the formation and narrowing its range to 430–421.9 ± 2.4 Ma (Wenlock to Pridoli).

Digdeguash Formation: The Digdeguash Formation lies conformably and gradationally below the Flume Ridge in eastern Maine (Ludman 1990). Rhuddanian graptolites from an uncertain stratigraphic level indicate an early Llandoverian age for part of the Digdeguash (Fyffe and Riva 2001) but the 430 Ma youngest Flume Ridge zircons suggest that it may be as young as Wenlockian. The lower range of the Digdeguash is unknown, but is limited by its youngest detrital zircons, a small population around 490 Ma (late Cambrian; Dokken *et al.* 2018).

Age of the Appleton Ridge Formation and relationship to the Digdeguash Formation: The Fredericton cover succession is truncated to the southwest by the ca. 384 Ma Deblois pluton (Ludman *et al.* 1999) and ca. 380 Ma Lucerne pluton (Wones and Ayuso 1993) (Fig. 3). Large roof pendants in these plutons mapped as Bucksport Formation are very similar to the Flume Ridge Formation, and Appleton Ridge lithology and bedding southwest of these plutons are similar to those of the Digdeguash Formation (Fig. 14). The Bucksport and Appleton Ridge formations thus appear to extend the Flume Ridge–Digdeguash succession of the Fredericton trough to the west shore of Penobscot Bay (Fig. 14).

The age of the Appleton Ridge Formation is uncertain,

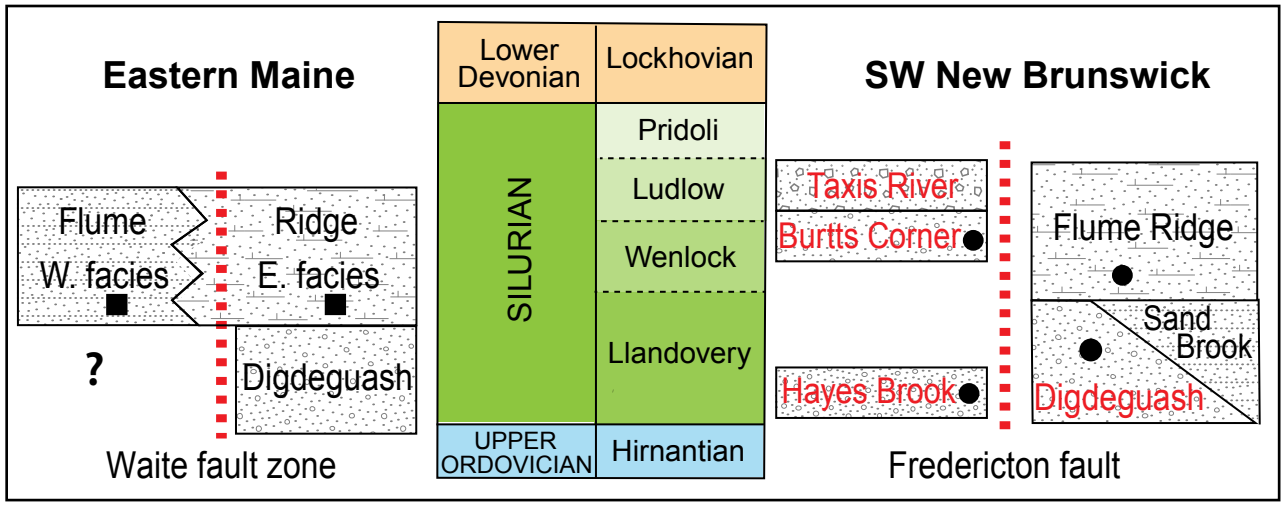

Figure 13. Stratigraphy of the Fredericton trough in eastern Maine and southwestern New Brunswick. Red color indicates formations for which there is fossil age control. Filled squares: units sampled in this study; filled circles: units sampled by Dokken *et al.* (2018). After Ludman *et al.* (2017) and Dokken *et al.* (2018).

listed on recent maps as Silurian–Ordovician(?) (West 2006; Pollock 2012). Results of this study (Fig. 12, AR-1) constrain this age range to Middle Ordovician–latest Silurian, that is, between the prominent youngest detrital zircon peak at 469 Ma on Figure 12 (the Floian–Dapingian boundary) and the age of 422 ±2 Ma (Pridoli) from the North Union tonalite gneiss (Tucker *et al.* 2001) that intruded the Appleton Ridge Formation. It is noteworthy that Pollock (2012) interpreted the Appleton Ridge as being younger than the Bucksport Formation.

Detrital zircon age spectra for the Appleton Ridge and Digdeguash formations are similar in some ways but differ in others (Fig. 15). The most significant difference is a prominent zircon population in the Appleton Ridge Formation at around 1 Ga (Fig. 15), suggesting a source that apparently did not contribute to the Digdeguash Formation. Both have zircon populations at around 465 Ma and 600 Ma, suggesting common sources – most likely Miramichi volcanic rocks and peri-Gondwanan sources, respectively – but in different proportions. Additional data are needed to determine whether these differences demonstrate that the Appleton Ridge and Digdeguash formations are not equivalent or that the differences are the result of bias in the zircon grains dated.

Central Maine/Aroostook-Matapedia basin

Samples were collected from several unfossiliferous sandstone units in the CMAM basin (Fig. 3). Osberg (1988) concluded that the stratigraphic succession in the axial part of the basin near Waterville (*W* in Fig. 3) is a "sandwich" in which the thin-bedded, dominantly pelitic Waterville Formation is overlain (Mayflower Hill) and underlain (Hutchins Corner) by similar thick-bedded, variably calcareous sandstone units (Table 2). The Waterville Formation contains middle Silurian (Wenlock) graptolites (Ruedemann, cited in Perkins and Smith 1925) and early Silurian (Llandovery) trace fossils (Orr and Pickerill 1995).

Where sandstone is demonstrably younger than the Waterville Formation, Marvinney *et al.* (2010) recommended that the name Mayflower Hill Formation be used, following Osberg's (1968) original name. Three samples met this condition and are assigned to the Mayflower Hill Formation. Two lie in the same outcrop belt, demonstrably above a Waterville Formation equivalent (Smyrna Mills Formation) — MH-1 east of Lincoln (*L* on Fig. 3), and MH-3 at Howland dam southwest of Lincoln. MH-2 was collected 5 m above basal black phyllite at the contact with the underlying Waterville Formation near the eponymous Mayflower Hill in Waterville (*W*) (Stop 5 of Ludman and Osberg 1987). Osberg (1988) named the sandstone below the Waterville Formation the Hutchins Corner Formation, and HC-1 was collected from rocks interpreted as the Hutchins Corner Formation from Freedom village, Maine, at the east edge of the belt.

Where the position of a sandstone unit relative to the Waterville Formation is uncertain, or where the Waterville is absent, as in the broad swath of sandstone between Waterville and the Miramichi terrane (Fig. 3), Marvinney *et al.* (2010) recommended using the less specific term Vassalboro Group for the unit (Table 2). One sample meets this criterion and is designated as Vassalboro Group, undifferentiated (VG-1) in this paper and Appendices A and B.

Two samples of rocks mapped as the Madrid Formation (MA-1, MA-2) were collected in the northern part of our study area to explore possible differences between detrital zircon age spectra from the early and late stages of CMAM sedimentation. Their assignment to the Madrid is highly probable but they are separated by other units from known Madrid belts to the west on which the stratigraphic succession is based (Osberg *et al.* 1985).

The small number of zircon grains that yield the youngest

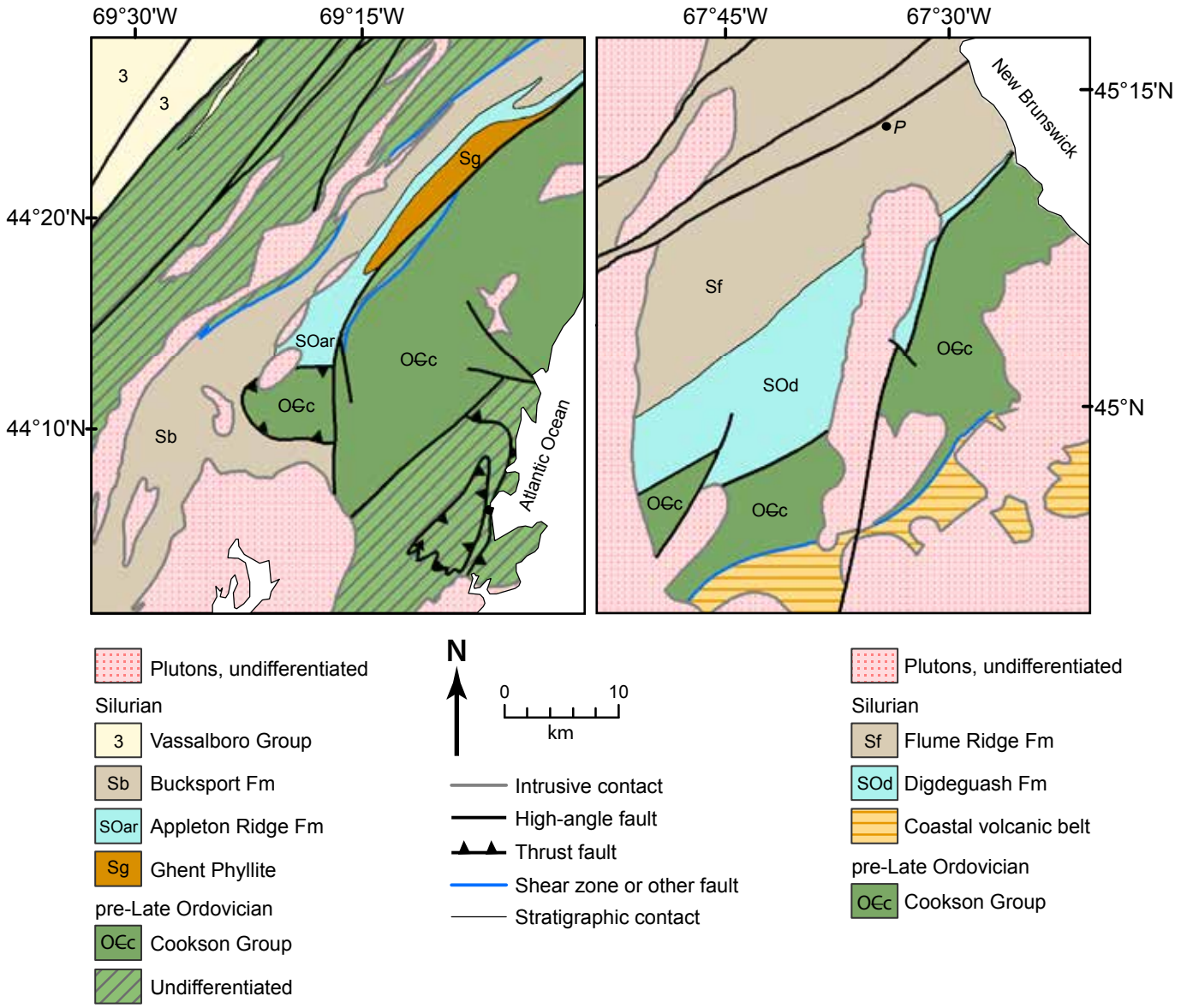

Figure 14. Comparison of stratigraphic relationships at the east side of the Fredericton belt. The lithologic sequence of Bucksport-Appleton Ridge-Cookson Group in south-central Maine (left) is similar to that of Flume Ridge-Digdeguash-Cookson Group in eastern Maine (right). Geology adapted from Osberg *et al.* (1985); Tucker *et al.* (2001); Ludman and Berry (2003); West (2006); Pollock (2012); and Berry *et al.* (2016.)

ages is insufficient for determining definite maximum ages in most CMAM samples without further analyses, but their general temporal distribution is suggestive, as shown in Figure 16. Even though the 1σ errors reported in Appendices C and D span the short middle and late stages of the Silurian (see Appendix A), it is likely that the Madrid, Mayflower Hill, Hutchins Corner, and undifferentiated Vassalboro Group samples are, indeed, Silurian. If additional dates in the future corroborate those obtained in this study, all the sampled CMAM rocks would be younger than the Waterville Formation fossils. This result might be problematic in particular for the Hutchins Corner sample (HC-1) which is currently interpreted to be stratigraphically below the Waterville (Osberg 1988). If further detrital zircon work confirms it to be Wenlock, then its relation to the Llandovery fossil age of the Waterville will need to be revisited.

DISCUSSION

Provenance

The provenance of stratigraphic units examined in this study, by definition the *birthplace* or *origin of the deposited material,* has two components: the *immediate* source(s) from which the sediment containing zircon was eroded, transported, and deposited in CMAM or the Fredericton trough, and the *ultimate* source where the zircons crystallized,

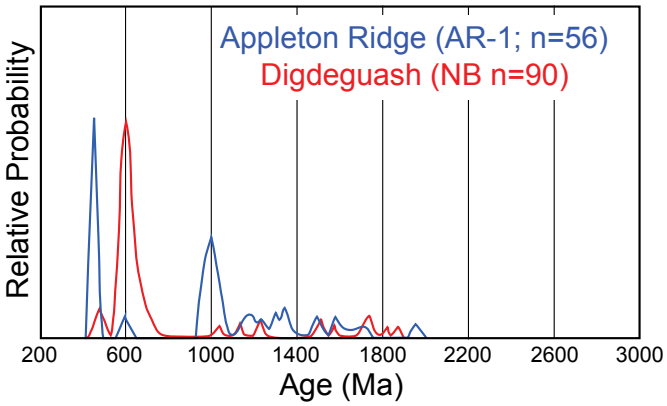

Figure 15. Comparison of Digdeguash (Dokken *et al.* 2018) and Appleton Ridge (this study) detrital zircon age spectra.

e.g., Amazonia, West Africa, Avalonia. While plutonic and volcanic zircons directly date the times of their crystallization, detrital zircons from a single sandstone may have been recycled from multiple sources whose ages span billions of years. Interpreting the immediate provenance of the rocks in this study is further complicated by the fact that some zircon grains may not have been recycled, but rather deposited directly from pyroclastic volcanic eruptions.

Interpretation of the immediate source of detrital zircons must take into account not only their age spectra but, wherever possible, sedimentologic and lithofacies evidence for the sediment source. There is strong evidence for the immediate source of the cover rock sediment in CMAM (Ludman *et al.* 2017) and the Fredericton trough (Fyffe 1995), but lacking that evidence for the basement rocks, it is only possible to speculate about their ultimate provenance by comparing their detrital zircon barcodes with those of potential source terranes.

Immediate source of CMAM and Fredericton trough sediment

Several lines of evidence indicate that most CMAM and Fredericton sediment was recycled from Ganderian sources with little input from external terranes. First, the Miramichi and several other Ganderian basement terranes in Maine were emergent highlands by the late Ordovician (Hirnantian) immediately after accretion of the main body of Ganderia to Laurentia, and were clearly sources of sediment for both CMAM (Bradley and Hanson 2002; Bradley and O'Sullivan 2016; Hopeck 1998; Pankiwskyj *et al.* 1976) and the Fredericton trough (Fyffe 1995; Ludman *et al.* 2017).

Second, although the leading edge of Ganderia had docked with Laurentia by the late Ordovician (van Staal *et al.* 2009), there would have been significant obstructions during the early Silurian to eastward transport of Laurentian sediment to the two depocenters. To reach CMAM, Laurentian sediment would have had to traverse the deep-water Connecticut Valley-Gaspé trough (Tremblay and Pinet 2005, 2016) and bypass the exhumed Boundary Mountains, Munsungun, and Weeksboro-Lunksoos Lake basement terranes. To reach the Fredericton trough, the sediment would have had to traverse the entire deep-water CMAM and then bypass the Miramichi terrane (Ludman *et al.* 2017). Tightly folded rocks of CMAM today span a width of 160 km, but the undeformed depocenter was at least three to five times wider (Bradley *et al.* 2000) and would have been a formidable barrier to transport of Laurentian sediment.

It would also have been difficult for detritus to reach the Fredericton trough or CMAM from a peri-Gondwanan source southeast of Ganderia (most likely Avalonia). Starting at about 430 Ma, that sediment would have had to traverse the Eastport-Mascarene arc-trench system created by subduction of oceanic lithosphere that separated Avalonia from composite Laurentia + Ganderia (Llamas and Hepburn 2013).

In the absence of external sources, Ganderian basement terranes were most likely the primary sources of CMAM and Fredericton sediment. Hopeck (1998) demonstrated that exhumed Miramichi basement contributed sediment to CMAM in Maine by Hirnantian times, just a few kilometres from the New Brunswick border. It would therefore have been available as a source for the Fredericton trough immediately to the southeast as proposed by Fyffe (1995).

The updated geologic map of eastern and east-central Maine (Fig. 3) shows that samples FR-1, FR-2, and AR-1 were deposited in the Fredericton trough. Significant zircon populations in these rocks between ca. 475 and 455 Ma and ca. 422 and 435 Ma are interpreted to have been derived from two volcanic episodes. The older group corresponds to eruptions in the Popelogan arc and Tetagouche back-arc basin early in the evolution of Ganderia as described above (Wilson *et al.* 2015). Their recycling into the cover rocks is evidenced by abundant Miramichi volcanic clasts in both CMAM (Hopeck, 1998; Ludman *et al.* 2017) and the Fredericton trough (Fyffe 1995), and the 469.3 ± 4.6 Ma age of the Olamon Stream lava reported here.

The younger group was interpreted above as having come directly (i.e., not recycled) from Silurian pyroclastic eruptions in the Eastport-Mascarene volcanic arc. This continental arc formed by melting of, and deposition on, Ganderian lithosphere during westward subduction of a seaway separating Avalonia from composite Laurentia + Ganderia (Llamas and Hepburn 2013). Thus, although they are the product of the Acadian orogenic cycle, these zircons, like those of the older group, are Ganderian.

An alternate explanation for the Fredericton trough

Dokken *et al.* (2018) reached different conclusions about the Fredericton trough, most importantly that (a) the Miramichi terrane was not exhumed until Wenlock times; (b) there is no peri-Gondwanan debris in the northern part of the Fredericton trough; and (c) Laurentian sediment is abundant in all units in the northern part of the Fredericton trough and overwhelmed peri-Gondwanan sediment in the

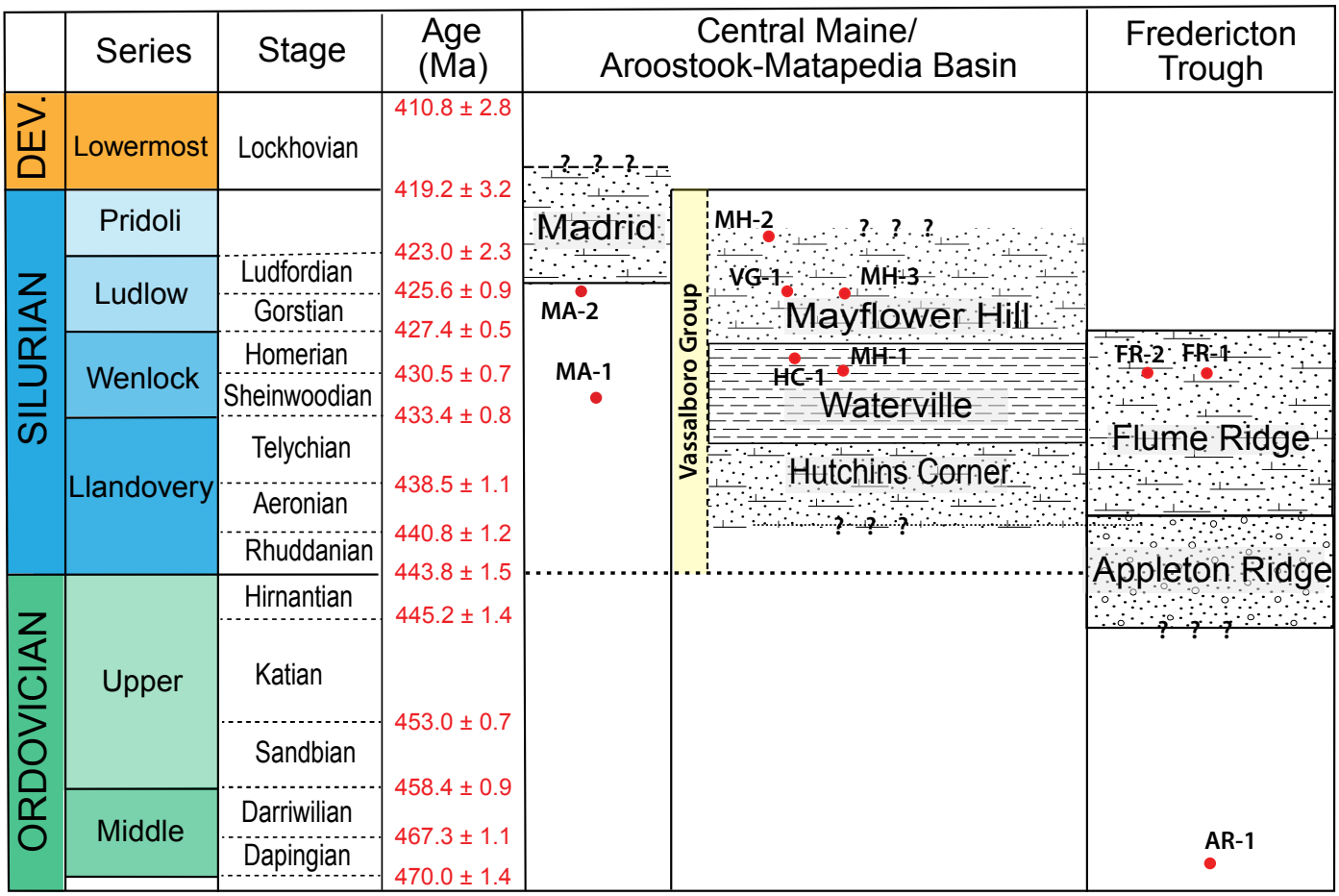

Figure 16. Ages of youngest cover rock zircons compared with previously interpreted stratigraphic ages of the formations from which they were collected.

southern part by the middle Silurian.

Evidence cited above contradicts these assertions and in addition:

(a) Dokken *et al.* (2018) reasoned that the Miramichi terrane could not have been a sediment source because it was undergoing deep crustal, high-grade metamorphism during late Ordovician to early Silurian subduction (van Staal *et al.* 2008) and was not exhumed until Wenlock time. The timing and intensity of Miramichi metamorphism in northern New Brunswick are not in question, but neither can be applied to the full > 350 km extent of the terrane. The entire Maine portion of the Miramichi terrane experienced no greater than lowest greenschist conditions during all late Ordovician through Devonian deformation events. Thus, while the northernmost Miramichi terrane was being subducted to deep crustal levels (van Staal *et al.* 2008), the southern part, from at least the Maine-New Brunswick border to Greenfield, was at very shallow crustal levels, and, as shown above, had been exhumed well before the Wenlock

(b) Dokken *et al.* (2018) reported that peri-Gondwanan detritus is absent from the Rhudannian Hayes Brook Formation and arrived later in the younger Burtts Corner and Flume Ridge formations, signaling exhumation of the Miramichi terrane. However, they attributed the dominant 465-480 Ma zircon populations in all three formations to distant peri-Laurentian arcs rather than to local Ganderian (i.e., peri-Gondwanan) Popelogan and Tetagouche eruptions. For reasons given above, a Laurentian or peri-Laurentian source is unlikely.

(c) As explained above, it is unlikely that Laurentian sediment contributed significantly to the Fredericton trough at any time in its history.

Immediate source of basement rocks

Basement rock barcodes contain zircon populations at ca. 800 Ma (BL-2, KM-1) and ca. 2.0 to 2.5 Ga (BL-2, BM-1, KM-1) that are absent from or rare in the cover rocks (Fig. 5). These suggest a source or sources not tapped by the younger strata, but without the sedimentologic evidence that clarified the source of the cover rock sediment, it is impossible to distinguish between the immediate and ultimate provenance of these basement zircon populations.

Ultimate source/tectonic fingerprint of the Ganderian detrital zircons

Detrital zircon age spectra have become an important

tool for identifying terranes formed during the breakup of Rodinia and reconstructing where in Rodinia those fragments originated. Most northern Appalachian studies focus on distinguishing Laurentia from Ganderia, Avalonia, and Meguma, the other Rodinian fragments with which it was reunited during the Paleozoic (Dorais *et al.* 2014; McWilliams *et al.* 2010; Wintsch *et al.* 2007). Others seek to determine whether Ganderia broke off directly from Gondwana or from Amazonia (van Staal *et al.* 2012; Fyffe *et al.* 2009). Interpretations are based on matching local and regional detrital zircon age spectra with ages of tectonic, plutonic, and volcanic zircon-producing events unique to individual fragments (e.g., Nance *et al.* 2008).

Figure 17 compares the Ganderian signature obtained from basement and cover rocks in this study with the compilation by Nance *et al.* (2008) of events in the eastern Laurentian, Amazonian, and West African cratons. The continuous range of zircon ages between 600 Ma and 1.8 Ga from the study area is most similar to the compilation of Amazonian events (Nance *et al.* 2008), supporting the earlier conclusions of van Staal *et al.* (2012) and Fyffe *et al.* (2009). However, the viability of a West African connection has been raised by recently reported detrital zircon ages from the Mauritanide orogen (Bradley 2018) indicating similarities with Amazonian events.

Timing of orogenic events in eastern Maine

Late Ordovician

Although the ages reported here from the Miramichi and St. Croix terranes improve understanding of stratigraphy and provenance of the basement rocks, they contribute little to refining the ages of Ordovician orogenic events. Deformation of the St. Croix terrane occurred between ca. 453 and 442 Ma, bracketed between middle Caradocian fossils in the Kendall Mountain Formation (Fyffe and Riva 1990) and Upper Rhudannian fossils in the Digdeguash Formation (ages after Cohen *et al.* 2013).

Deformation of the Miramichi terrane in Maine occurred at about the same time (between ca. 453 and 445 Ma), bracketed between deposition of "Llanvirnian to Caradocian" black shale in the Stetson Mountain Formation (Larrabee *et al.* 1965) and Hirnantian limestone of the Carys Mills Formation (Rickards and Riva 1981). The 469.3 ± 4.6 Ma zircon age of the Olamon Stream lava suggests a range for eruption of the upper volcanic component of the Miramichi suite (ca. 469–453 Ma) but does not refine the timing of Late Ordovician deformation.

Silurian

The U–Pb zircon age for the post-Salinic Pocomoonshine gabbro-diorite (421.9 ± 2.4 Ma) overlaps the 423 ± 3 Ma $^{40}Ar/^{39}Ar$ hornblende cooling age of West *et al.* (1992) and is the minimum age of the Salinic event. This is consistent with the ca. 450–430 Ma span proposed for the Salinic event in New Brunswick (Wilson *et al.* 2015), but the presence of ca. 431 and 433 Ma zircon grains suggests that the Salinic might have lasted somewhat longer in eastern Maine. The overlap of the zircon crystallization and hornblende cooling ages shows that the pluton cooled rapidly at shallow crustal levels.

Transition from Late Ordovician to Silurian tectonism

Detrital zircon ages of the cover rocks provide insight into conditions between Late Ordovician and Silurian (Salinic) tectonism. An enormous volume of turbidites was deposited during this interval in the area between western Maine and central New Brunswick (Ludman *et al.* 2017). Detrital and plutonic zircon ages suggest that the transition from post-Middle Ordovician sedimentation to Salinic deformation in the later part of that time span is best described as "busy", with several events in a short time span: (1) crystallization of ca. 430 Ma zircon during Eastport-Mascarene volcanism; (2) incorporation of the zircon in the kilometres-thick Flume Ridge Formation; (3) lithification of a thick pile of Flume Ridge + Sand Brook + Digdeguash turbidites; (4) intense isoclinal folding; and (5) post-folding emplacement of the Pocomoonshine gabbro-diorite at (421.9 ± 2.4 Ma).

Origin of the Fredericton trough and CMAM

Several tectonic settings have been proposed for the CMAM basin and Fredericton trough. Bradley and Hanson (2002) described CMAM as an Acadian foreland basin, but Bradley and O'Sullivan (2016) expressed uncertainty as to whether sediments were deposited on oceanic or continental crust. Tucker *et al.* (2001) envisaged an extensional setting for CMAM, describing cover rock basins as graben and the pre-Middle Ordovician source areas as horsts. Tremblay and Pinet (2005) also proposed an extensional origin for the Connecticut Valley-Gaspé trough, northwesternmost Ganderian cover rock basin (Fig. 1), and suggested a similar origin for CMAM (which they called the Merrimack basin).

The Fredericton trough has been described variably as a remnant of oceanic crust following Late Ordovician accretion (Park and Whitehead 2003), a post-"Taconian" (= post-Late Ordovician) successor basin (Williams 1979), and a Salinic fore-arc basin or foredeep associated with westward subduction that closed a back-arc basin on the outboard margin of Ganderia (Fyffe *et al.* 2011; Wilson *et al.* 2015).

Recent tectonic models concluded that all oceanic crust in the study area had been consumed by Late Silurian-Early Devonian accretion of Ganderia to Laurentia (e.g., Fyffe *et al.* 2011; Wilson *et al.* 2015). These models proposed two stages of subduction: Late Ordovician closing of the Iapetus ocean followed by Salinic closing of a back-arc basin associated with the Tetagouche volcanic arc in New Brunswick. Timing of initial sedimentation in the two depocenters and their size and geometry provide a means to test these hypotheses.

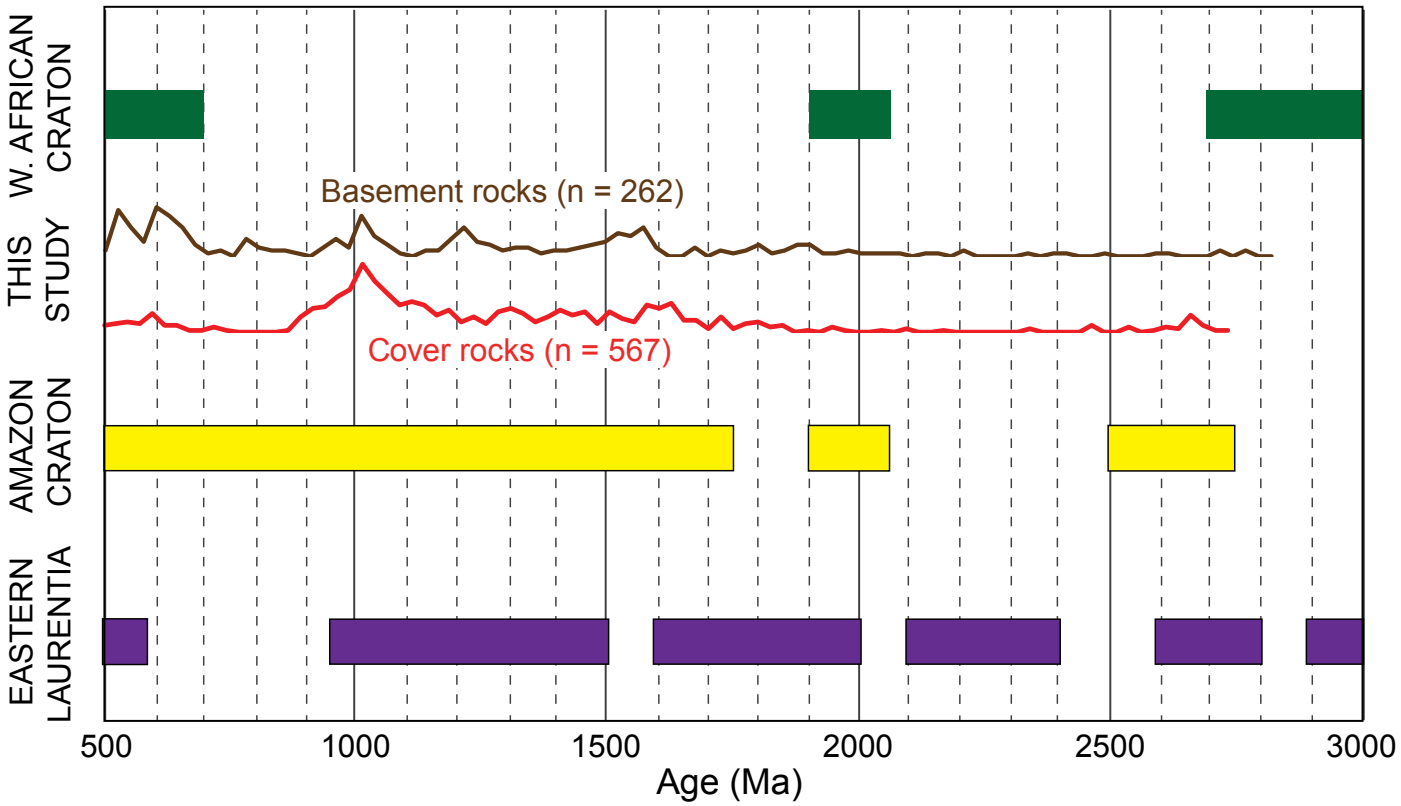

Figure 17. Detrital zircon age distribution in basement and cover rocks compared with timing of zircon-producing events in eastern Laurentia, Amazonia, and the West African craton. Modified after Nance *et al.* (2008).

Fredericton trough

Fossil and geochronologic evidence indicate that turbidite sedimentation in the Fredericton trough began shortly after Late Ordovician deformation, by the Rhudannian or earlier, and continued until Salinic deformation and emplacement of the Pocomoonshine gabbro-diorite at ca. 422 Ma. In the eastern part of the study area, the Fredericton trough was separated from CMAM during Silurian time by a Miramichi highland that shed sediment into both basins (Ludman *et al.* 2017). This timing is compatible with the Salinic foredeep model cited above, with subsidence of the Fredericton trough caused by tectonic loading associated with thrust sheets of the Brunswick subduction complex (Fyffe *et al.* 2011; Wilson *et al.* 2015). This model is also supported by estimated pre-deformation width and lateral extent of the Fredericton trough comparable with those of modern foredeep basins (Allen and Homewood 1986; DeCelles 2012). In addition, estimates of Fredericton trough sedimentation rates are comparable to those of modern deep marine depocenters based on published thicknesses of Fredericton trough formations, decompacted following curves of Kominz *et al.* (2011) and the time frame discussed above.

Central Maine/Aroostook-Matapedia basin

Sedimentation began in CMAM at approximately the same time as in the Fredericton trough (Ludman *et al.* 2017), but its origin is less certain and its evolution was more complex, with two distinct phases of sedimentation. The initial phase of deep-water turbidite sedimentation began on both west and east flanks of the basin by late Ordovician time, as evidenced by the Quimby Formation in western Maine (Bradley and O'Sullivan 2016) and Carys Mills (Hirnantian), Daggett Ridge, and Mill Priviledge Brook formations in eastern Maine (Ludman *et al.* 2017). The eastern flank of the CMAM basin in mid-coastal Maine is unknown due to truncation by faulting (Tucker *et al.* 2001).

Initial CMAM sedimentation thus preceded the onset of Acadian subduction and deformation by millions of years, so the CMAM basin could not have originated as an Acadian foreland basin as is commonly proposed (e.g., Bradley and O'Sullivan 2016; Hatcher 2010). Tremblay and Pinet (2005, 2016) suggested that the northwesternmost Ganderian cover rock basin, the Connecticut Valley-Gaspé trough (Fig. 1), probably formed by intraplate extension and proposed a similar origin for the western part of the CMAM basin ("Merrimack trough" in their paper).

The size of the CMAM basin is also problematical for a foreland basin. Although its current ~160 km deformed width is comparable to that of modern deep marine foreland basins such as the Hidaka Trough (northern Japan; Noda *et al.* 2013) and the Western Taiwan foreland basin (Yu and Chou 2001), CMAM experienced intense Acadian shortening. Bradley *et al.* (2000) estimated that its current

outcrop width is only 30% of its undeformed extent but did not consider (1) an episode of recumbent folding, (2) two generations of thrusting now recognized in the basin (Tucker *et al.* 2001), (3) blind thrusts imaged in seismic reflection profiling (Doll *et al.* 1996), nor (4) thrusting of the east flank of the basin over its Miramichi source (Ludman *et al.* 2017). The degree of crustal shortening was probably greater than 70% and CMAM was possibly as much as 800–1 000 km wide, far wider than modern marine foreland basins.

The second sedimentary regime began in the Late Silurian and continued through the Early Devonian (Bradley *et al.* 2000), adding approximately 9 km of sediment to the CMAM basin after sedimentation had ceased in the Fredericton trough (Bradley and O'Sullivan 2016). Cogent paleocurrent, paleontological, and geochronological evidence show that the CMAM basin had become an Acadian foredeep during this time span, and that its sediment was sourced uniformly from an Acadian forebulge to the southeast (Bradley *et al.* 2000).

Recognition of Ganderia in southern New England

Detrital zircon barcodes have been used to distinguish intensely metamorphosed Laurentian, Ganderian, and Avalonian terranes in southern New England, where the northern Appalachian orogen is telescoped to a fraction of its width in the study area (Fig. 2) (e.g., Dorais *et al.* 2014; Walsh *et al.* 2007; Wintsch *et al.* 2007). If our interpretation of provenance is correct, the basement rock barcodes (Fig. 5b) represent an unadulterated Ganderian signature that should be useful in identifying the terrane where its presence and/or extent are uncertain. Cover rock barcodes (Fig. 5a) should also be useful, despite their modification by addition of Silurian volcanic zircons.

CONCLUSIONS AND FUTURE DIRECTIONS

Constraints on ages and correlation of stratified rocks

1. Ages of volcanic zircon date for the first time the uppermost (volcanic) formation in the Miramichi basement succession in Maine (469.3 ± 4.6 Ma), and a tuff horizon near the base of the Kendall Mountain Formation of the St. Croix basement succession (477.4 ± 3.7 Ma). These ages constrain times of deposition of unfossiliferous sandstone units in the CMAM and Fredericton cover successions.

2. The presence of Silurian detrital zircon that is only slightly older than the ages of the host cover rocks suggests derivation from Silurian volcanism, probably of the Eastport-Mascarene volcanic belt.

3. The Appleton Ridge Formation apparently lacks the Silurian detrital zircon component present in the other cover rocks, suggesting that it was deposited prior to that volcanism.

4. Proposed correlation of the Appleton Ridge and Digdeguash formations remains unresolved. Both units were intruded by ca. 422 Ma plutons, lack Silurian detrital zircon, and have similar populations of early Paleozoic detrital zircon. However, possible differences in provenance and difficulty in assessing different proportions of zircon age populations because of the limited number of analyzed grains preclude a definite statement about their correlation.

Provenance of stratified rocks

1. Detrital zircon age spectra combined with tectonic and lithofacies models indicate that recycled Ganderian basement was the dominant source material for the cover rocks.

2. Populations of zircon found in the basement rocks but not in the cover successions, suggest early Paleozoic sediment sources that were not tapped by the cover rocks.

3. Comparison of detrital zircon age distribution with ages of zircon-producing events from Rodinian cratonic fragments suggests that Ganderia was derived from Amazonia.

Tectonic implications

1. Salinic deformation in eastern Maine and southwestern New Brunswick is bracketed between the 421.9 ± 2.4 Ma U–Pb zircon crystallization age of the Pocomoonshine gabbro-diorite and the ca. 431 Ma age of the youngest zircons in the Flume Ridge Formation that it intrudes. The overlap of the crystallization age with a 423 ±3 Ma hornblende cooling age (West *et al.* 1992) shows that the pluton cooled rapidly at shallow crustal depths.

2. Proposed evolution of the Fredericton trough as a Salinic foredeep is supported by detrital zircon ages and comparison of pre-deformation basin dimensions and estimated sedimentation rates with those of modern analogues.

3. Initial sedimentation in the Central Maine/Aroostook-Matapedia basin pre-dated onset of Acadian subduction, proving that the basin did not originate as an Acadian foreland basin. A second phase of sedimentation *was* Acadian, with a northwest-migrating forebulge shedding sediment diachronously into a CMAM foredeep.

Future directions

1. Expanded detrital zircon dating: Ages of the youngest zircon grains present in most samples are based on too few grains to be statistically meaningful. Additional dating of grains separated during this study by LA-ICPMS is planned to address this issue. Also, in view of the analytical error associated with SHRIMP analysis *vis a vis* the short time span of Silurian stages, more precise TIMS dating of screened grains would provide precision comparable to that associated with the most recent chronostratigaphic charts and better constrain the maximum ages of the formations sampled.

Detrital zircon studies have answered some questions and raised new ones on the west (Bradley and O'Sullivan 2016) and east (this study) flanks of the CMAM basin but similar work is needed in the axial and western intermediate facies,

particularly from sites that yielded the rare fossils which provide ages for formations in those facies.

2. Better fossil age control: The low regional metamorphic intensity in and north of the study area suggests that a search for acritarchs and spores may be fruitful. A pilot feasibility study is under way involving units from the Miramichi, Fredericton, and CMAM successions.

3. More information about the origin of the CMAM basin: Researchers in New Brunswick have deciphered a complex tectonic/stratigraphic history from detailed mapping and geochemical studies of the Popelogan-Tetagouche arc/back-arc basin system (e.g., Wilson *et al.* 2015; van Staal *et al.* 2016). There is a pressing need for modern interdisciplinary work of this type in northern Maine, where the Weeksboro-Lunksoos and Munsungun arc terranes are more broadly exposed than the Popelogan (Osberg *et al.* 1985), and were emergent source areas within the CMAM basin.

ACKNOWLEDGMENTS

Several individuals have contributed substantially to this project. Gary Aldaz and Jimi Rabin were eager and energetic field assistants during mapping in the Bowers Mountain and Bottle Lake quadrangles and provided the muscle that collected some of the Miramichi samples. We thank Chris Gerbi for generously donating zircon separates from the Appleton Ridge Formation. We are indebted to Dwight Bradley, Chris Hepburn, and John Waldron who generously shared unpublished detrital zircon data and preliminary manuscripts and offered suggestions that guided interpretations presented above. We may not always agree on those interpretations but these collegial discussions enriched our understanding of regional relationships. Discussions with Wally Bothner, Bob Wintsch, and the late Arthur Hussey about their work in southwestern Maine helped place our results in a broader regional context. Comments on early versions of this paper by Sandra Barr, Bill Devlin, Chris Hepburn, Justin Strauss, Greg Walsh, Bob Wintsch, and two anonymous reviewers significantly improved both the scientific conclusions and readability of the manuscript. The Maine Geological Survey, guided by State Geologist Robert Marvinney, provided logistic and moral support, and Amber Whittaker drafted the updated geologic maps in Figures 3 and 14. We are grateful to Renee Pillers of the U.S.G.S. for help with difficult mineral separa-tions, image preparation, and SHRIMP-RG analysis.

REFERENCES

Allen, P. and Homewood, P. *(Editors)*. 1986. Foreland Basins. International Association of Sedimentologists, Special Publication No. 8, Blackwell Scientific Publications, 453 pp.

Berry, H., West, D., and Burke, W. 2016. Bedrock relationships along the Sennebec Pond fault: A structural puzzle, a stratigraphic enigma, and a tectonic riddle. *In* Guidebook for field trips along the Maine coast from Maquoit Bay to Muscongus Bay. *Edited by* H. Berry and D. West. New England Intercollegiate Geologic Conference, pp. 43–70.

Black, L., Kamo, S., Allen, C., Davis, D., Aleinikoff, J., Valley, J., Mundil, R., Campell, I., Korsuch, R., Williams, I., and Foudoulis, C. 2004. Improved $^{206}Pb/^{238}U$ microprobe geochronology by the monitoring of a trace-element-related matrix effect; SHRIMP, ID–TIMS, ELA–ICP–MS and oxygen isotope documentation for a series of zircon standards. Chemical Geology, 205(1–2), pp. 115–140. https://doi.org/10.1016/j.chemgeo.2004.01.003

Bradley, D. 2018. Mesoproterozoic detrital zircons from Neoproterozoic strata in West Africa and implications for Appalachian terranes. *In* 53nd Northeastern Annual Section Meeting, Burlington, Vermont, March 18–20, 2018. Geological Society of America Abstracts with Programs, 50, No. 2. https://doi.org/10.1130/abs/2018NE-310858

Bradley, D. and Hanson, L. 2002. Paleocurrent analysis of a deformed Devonian foreland basin in the Northern Appalachians, Maine, USA. Sedimentary Geology, 148, pp. 425–447. https://doi.org/10.1016/S0037-0738(01)00161-0

Bradley, D. and O'Sullivan, P. 2016. Detrital zircon geochronology of pre- and syncollisional strata, Acadian orogen, Maine Appalachians. Basin Research (2016), pp. 1–20. https://doi.org/10.1111/bre.12188

Bradley, D., Tucker, R., Lux, D., Harris, A., and McGregor, D. 2000. Migration of the Acadian orogen and foreland basin across the Northern Appalachians of Maine and adjacent areas. United States Geological Survey Professional Paper 1624, 51 pp. https://doi.org/10.3133/pp1624

Cohen, K., Finney, S., Gibbard, P., and Fan, J.-X. 2013. The ICS International Chronostratigraphic Chart (updated 2017). Episodes 36, pp. 199–204.

Cumming, L. 1967. Geology of the Passamaquoddy Bay region, Charlotte County, New Brunswick. Geological Survey of Canada, Paper 65-29, 36 pp. https://doi.org/10.4095/100976

DeCelles, P. 2012. Foreland basin systems revisited: Variations in response to tectonic settings. *In* Tectonics of Sedimentary Basins: Recent Advances. *Edited by* C. Busby and A. Pérez. Blackwell Publishing, Ltd., pp. 405–426. https://doi.org/10.1002/9781444347166.ch20

Dickinson, W. and Gehrels, G. 2009. Use of U–Pb ages of detrital zircons to infer maximum depositional ages of strata: A test against a Colorado Plateau Mesozoic database. Earth and Planetary Science Letters, 288, pp. 115–125. https://doi.org/10.1016/j.epsl.2009.09.013

Dokken, R., Waldron, J., and Dufrane, A. 2018. Detrital zircon geochronology of the Fredericton Trough, New Brunswick, Canada: Constraints on the Silurian closure of remnant Iapetus Ocean. American Journal of Science, 318, pp. 684 – 725. https://doi.org/10.2475/06.2018.03

Doll, W., Domoracki, J. Costain, J. Coruh, C, Ludman, A., and Hopeck, J. 1996. Seismic reflection evidence for the evolution of a transcurrent fault system: Norumbega fault zone, Maine. Geology, 24, pp. 251–254. https://doi.

org/10.1130/0091-7613(1996)024<0251:SREFTE>2.3.CO;2

Dorais, M., Wintsch, R., Kunk, M., Aleinikoff, J., Burton, W., Underdown, C., and Kerwin, C. 2014. P-T-t conditions, Nd and Pb isotopic compositions, and detrital zircon geochronology of the Massabesic Gneiss complex, New Hampshire: Isotopic and metamorphic evidence for the identification of Gander basement, central New England. American Journal of Science, 312, pp. 1049–1097. https://doi.org/10.2475/10.2012.01

Doyle, R. and Hussey, A. 1967. Preliminary Geologic Map of Maine. Maine Geological Survey, Augusta, Maine, scale 1:500 000.

Fyffe, L. 1991. Geology of the Flume Ridge-Kedron Stream map areas, New Brunswick. *In* Project Summaries for 1991, Sixteenth Annual Review of Activities. *Edited by* S.A. Abbott. New Brunswick Department of Natural Resources and Energy, Mineral Resources, Information Circular 91-2, pp. 12–20.

Fyffe, L. 1995. Fredericton Belt. *In* Geology of the Appalachian-Caledonian Orogen in Canada and Greenland. *Edited by* H. Williams. Geological Survey of Canada, Geology of Canada, No. 6, pp. 351–354.

Fyffe, L. and Riva, J. 1990. Revised stratigraphy of the Cookson Group of southwestern New Brunswick and adjacent Maine. *In* New age determinations in the Atlantic provinces. *Edited by* R. Raeside and S. Barr. Atlantic Geology, 26, pp. 271–276.

Fyffe, L. and Riva, J. 2001. Regional significance of graptolites from the Digdeguash Formation of southwestern New Brunswick. *In* Current Research 2000. *Edited by* B.M.W. Carroll. New Brunswick Department of Natural Resources, Minerals and Energy Division, Mineral Resource Report 2001-4, pp. 47–54.

Fyffe, L., Barr, S., Johnson, S., McLeod, M., McNicoll, V., Valverde-Vaquero, P., van Staal, C., and White, C. 2009. Detrital zircon ages from Neoproterozoic and Early Paleozoic conglomerate and sandstone units of New Brunswick and coastal Maine: Implications for the tectonic evolution of Ganderia. Atlantic Geology, 45, pp. 110–144. https://doi.org/10.4138/atlgeol.2009.006

Fyffe, L., Forbes, W., and Riva, J. 1983. Graptolites from the Benton area of west-central New Brunswick and their regional significance. Maritime Sediments and Atlantic Geology, 19, pp. 117–125. https://doi.org/10.4138/1570

Fyffe, L., Johnson, S., and van Staal, C. 2011. A review of Proterozoic to Early Paleozoic lithotectonic terranes in the northeastern Appalachian orogen of New Brunswick, Canada, and their tectonic evolution during Penobscot, Taconic, Salinic, and Acadian orogenesis. Atlantic Geology, 47, pp. 211–248. https://doi.org/10.4138/atlgeol.2011.010

Gates, O. and Moench, R. 1981. Bimodal Silurian and Lower Devonian volcanic rock assemblages in the Machias-Eastport area, Maine. United States Geological Survey Professional Paper 1184, 32 pp. https://doi.org/10.3133/pp1184

Hatcher, R. 2010. The Appalachian orogeny: A brief summary. *In* From Rodinia to Pangea: The lithotectonic record of the Appalachian region. *Edited by* R. Tollo, M. Bartholomew, J. Hibbard, and P. Karabinos. Geological Society of America, Memoir 206, pp. 51–69.

Hibbard, J., van Staal, C., Rankin, D., and Williams, H., 2006. Lithotectonic map of the Appalachian orogen, Canada-United States of America. Geological Survey of Canada, Map 2096A, scale 1:1 500 000.

Hopeck, J. 1998. Stratigraphy and structural geology of the Wytopitlock and Springfield fifteen-minute quadrangles, eastern Maine; Unpublished PhD dissertation; City University of New York, New York, New York, 160 pp.

Hussey, A., Bothner, W., and Aleinikoff, J. 2010. The tectonostratigraphic framework and evolution of southwestern Maine and southeastern New Hampshire. *In* From Rodinia to Pangea: The lithotectonic record of the Appalachian region. *Edited by* R. Tollo, M. Bartholomew, J. Hibbard, and P. Karabinos. Geological Society of America, Memoir 206, pp. 205-230. https://doi.org/10.1130/2010.1206(10)

Hussey, A., Bothner, W., and Thompson, P. 2016. Bedrock geology of the Kittery 1:100 000 quadrangle, southwestern Maine and southeastern New Hampshire. Maine Geological Survey, Bulletin 45, 99 pp.

Kominz, M., Patterson, K., and Odette, D. 2011. Lithology dependence of porosity in slope and deep marine sediments. Journal of Sedimentary Research, 81, pp. 730–742. https://doi.org/10.2110/jsr.2011.60

Larrabee, D., Spencer, C., and Swift, D. 1965. Bedrock geology of the Grand Lake area, Aroostook, Hancock, Penobscot, and Washington counties, Maine. United States Geological Survey, Bulletin 1201-E, 38 pp, with map, scale 1:250 000.

Llamas, A. and Hepburn, J. 2013. Geochemistry of Silurian-Devonian volcanic rocks in the Coastal Volcanic Belt, Machias-Eastport area, Maine: Evidence for a pre-Acadian arc. Geological Society of America Bulletin, 125, pp. 1930–1942. https://doi.org/10.1130/B30776.1

Ludman, A. 1976. A fossil-based stratigraphy in the Merrimack Synclinorium, central Maine. *In* Contributions to New England Stratigraphy. *Edited by* L. Page. Geological Society of America, Memoir 148, pp. 65–78. https://doi.org/10.1130/MEM148-p65

Ludman, A. 1990. Bedrock geology of the Big Lake 15' quadrangle, Maine. Maine Geological Survey Open-File Report 90-26, 22 p., with map scale 1:62 500.

Ludman, A. 1991. Revised stratigraphy of the Cookson Group (St. Croix terrane), eastern Maine and southwestern New Brunswick. *In* Geology of the Coastal Lithotectonic Block and neighboring terranes, eastern Maine and southern New Brunswick. *Edited by* A. Ludman. New England Intercollegiate Geological Conference guidebook, pp. 114–132.

Ludman, A. 2013. Closing the gap: Relationships of the Waterville and Aroostook-Matapedia successions. *In* Guidebook for field trips in north-central Maine. *Edited by* L. Hanson. New England Intercollegiate Geological Confer-

ence, pp. 1–14.
Ludman, A. 2018. Preliminary bedrock geology of the Greenfield quadrangle, Maine. Maine Geological Survey, Open-File Map 18-13, scale 1:24 000.
Ludman, A. 2017. Multiple deformation of chlorite-grade Late Ordovician to Early Devonian strata in eastern Maine. *In* 52nd Northeastern Annual Section / 51st North-Central Annual Section Meeting, Pittsburgh, Pennsylvania March 19–21, 2017. Geological Society of America Abstracts with Programs, 49, 2. https://doi.org/10.1130/abs/2017NE-290457
Ludman A. and Berry, H. 2003. Bedrock geology of the Calais 1:100 000 quadrangle, Maine. Maine Geological Survey, Open-File Map 03-97, scale 1:100 000.
Ludman, A. and Hill, M. 1990. Bedrock geology of the Calais 15' quadrangle, Eastern Maine. Maine Geological Survey, Open-File Report 90-27, 32 pp., map scale 1:62 500.
Ludman, A. and Osberg, P. 1987. Structure and stratigraphy of the central Maine turbidite belt in the Skowhegan-Waterville region. *In* Northeastern section of the Geological Society of America, Centennial Field Guide, volume 5. *Edited by* D. Roy. Geological Society of America, pp. 279–283. https://doi.org/10.1130/0-8137-5405-4.279
Ludman, A., Hopeck, J., and Berry, H. 2017. Provenance and paleogeography of post-Middle Ordovician pre-Devonian sedimentary basins on the Gander composite terrane, eastern and east-central Maine: implications for Silurian tectonics in the northern Appalachians. Atlantic Geology, 53, p. 63–85. https://doi.org/10.4138/atlgeol.2017.003
Ludman, A., Hopeck, J., and Brock, P. 1993. Nature of the Acadian orogeny in eastern Maine. *In* The Acadian Orogeny: Recent Studies in New England, Maritime Canada, and the Autochthonous Foreland. *Edited by* D. Roy and J. Skehan. Geological Society of America Special Paper 275, pp. 67–84. https://doi.org/10.1130/SPE275-p67
Ludman, A., Lanzirotti, A., Lux, D., and Wang, C. 1999. Constraints on timing and displacement of multiple shearing in the Norumbega fault system, eastern Maine; *In* Norumbega fault system of the Northern Appalachians. *Edited by* A. Ludman and D. West, Jr. Geological Society of America Special Paper 331, pp. 179–194. https://doi.org/10.1130/0-8137-2331-0.179
Ludwig, K. R. 1980. Calculation of uncertainties of U–Pb isotope data: Earth and Planetary Science Letters, 46, pp. 212–220. https://doi.org/10.1016/0012-821X(80)90007-2
Ludwig, K.R. 2003. Isoplot/Ex version 3.00. A geochronological toolkit for Microsoft Excel. Berkeley Geochronology Center Special Publication, No. 4, Berkeley, California, 73 pp.
Ludwig, K.R. 2009. Squid 2, version 2.50, A user's manual. Berkeley Geochronology Center, Special Publication, No. 5, Berkeley, California, 110 pp.
Marvinney, R., West, D.P., Jr., Grover, T., and Berry, H. 2010. A stratigraphic review of the Vassalboro Group in a portion of central Maine; *In* Guidebook for field trips in coastal and interior Maine. *Edited by* C. Gerbi, M. Yates, A. Kelley, and D. Lux. New England Intercollegiate Geological Conference guidebook, pp. 61–76.
McWilliams, C., Walsh, G., and Wintsch, R. 2010. Silurian-Devonian age and tectonic setting of the Connecticut Valley-Gaspé trough in Vermont based on U–Pb SHRIMP analyses of detrital zircons. American Journal of Science, 310, pp. 325–363. https://doi.org/10.2475/05.2010.01
Moench, R. and Pankiwskyj, K. 1988. Geologic map of western interior Maine [with contributions by G. Boone, E. Boudette, A. Ludman, W. Newell, and T. Vehrs]. United States Geological Survey, Miscellaneous Investigations Map I-1692, scale 1:250 000.
Mohammadi, N., Fyffe, L., McFarlane, C., Thorne, K., Lentz, D., Charnley, B., Branscombe, L., and Butler, S. 2017. Geological relationships and laser ablation ICP-MS U–Pb geochronology of the Saint George Batholith, southwestern New Brunswick, Canada: implications for its tectonomagmatic evolution. Atlantic Geology, 57, pp. 207–240. https://doi.org/10.4138/atlgeol.2017.008
Nance, D., Murphy, B., Strachan R., Keppie, D., Gutiérrez -Alonso, G., Fernández-Suárez, J., Quesada, C., Linnemann, U., D'Lemos, R., and Pisarevsky, S. 2008. Neoproterozoic–early Palaeozoic tectonostratigaphy and palaeogeography of the peri-Gondwanan terranes: Amazonian v. West African connections. In The boundaries of the West African craton. Edited by N. Ennih and J-P Liégeois. Geological Society of London, Special Publications 297, pp. 345–383.
Neuman, R. 1984. Geology and paleobiology of islands in the Ordovician Iapetus Ocean–Review and implications. Geological Society of America Bulletin, 95, pp. 1188–1201. https://doi.org/10.1130/0016-7606(1984)95<1188:GAPOII>2.0.CO;2
Noda, A., TuZino, T., Joshima, M., and Goto, S. 2013. Mass-transport-dominated sedimentation in a foreland basin, the Hidaka Trough, northern Japan. Geochemistry, Geophysics, Geosystems, 14, pp. 2638–2660. https://doi.org/10.1002/ggge.20169
Orr, P. and Pickerill, R. 1995. Trace fossils from Early Silurian flysch of the Waterville Formation, Maine, USA. Northeastern Geology and Environmental Sciences, 17, pp. 394–414.
Osberg, P. 1968. Stratigraphy, structural geology, and metamorphism of the Waterville-Vassalboro area, Maine. Maine Geological Survey Bulletin 20, 64 pp., with map, scale 1:62 500.
Osberg, P. 1988. Geologic relations within the shale-wacke sequence in south-central Maine. Maine Geological Survey, Studies in Maine Geology, 1, pp. 51–73.
Osberg, P., Hussey, A., II, and Boone, G. 1985. Bedrock Geologic Map of Maine. Maine Geological Survey, scale 1:500 000.
Osberg, P., Tull, J., Robinson, P., Hon, R., and Butler, J. 1989. The Acadian orogen. *In* The Appalachian-Ouachita Orogen in the United States. *Edited* by R. Hatcher, W. Thomas, and G. Viele. Geological Society of America, The Geology of North America, F2, pp. 179–232.
Pankiwskyj, K., Ludman, A., Griffin, J., and Berry, W. 1976.

Stratigraphic relationships on the southeast limb of the Merrimack Synclinorium in central and west-central Maine. *In* Studies in New England Geology. *Edited by* A. Brownlow and P. Lyons. Geological Society of America Memoir, 146, pp. 263–280.

Park, A. and Whitehead, J. 2003. Structural transect through Silurian turbidites of the Fredericton Belt southwest of Fredericton, New Brunswick: the role of the Fredericton Fault in late Iapetus convergence. Atlantic Geology, 39, p. 227–237. https://doi.org/10.4138/1183

Perkins, E. and Smith, E. 1925. Contributions to the geology of Maine, No. 1. A geological section from the Kennebec River to Penobscot Bay. American Journal of Science, 9, pp. 204–225. https://doi.org/10.2475/ajs.s5-9.51.204

Pickerill, R. and Fyffe, L. 1999. The stratigraphic significance of trace fossils from the Lower Paleozoic Baskahegan Lake Formation near Woodstock, west-central New Brunswick. Atlantic Geology, 35, pp. 205–214. https://doi.org/10.4138/2035

Pollock, S. 2012. Bedrock geology of the Belfast quadrangle, Maine. Maine Geological Survey, Open-File Map 12-37, scale 1:24 000.

Rickards, R. and Riva, J. 1981. *Glyptograptus? Persculptus* (Salter), its tectonic deformation, and its stratigraphic significance for the Carys Mills Formation of N.E. Maine, U.S.A. Geological Journal, 16, pp. 219–235. https://doi.org/10.1002/gj.3350160402

Ruitenberg, A. and Ludman A. 1978. Stratigraphy and tectonic setting of Early Paleozoic rocks in the Wirral-Big Lake area, southwestern New Brunswick and southeastern Maine. Canadian Journal of Earth Sciences, 15, pp. 22–32.

Seaman, S. and Hamdi, S. 2018. Crustal structure and Late Paleozoic supervolcano-scale eruptions in Maine, USA. *In* 53nd Northeastern Annual Section Meeting, Burlington, Vermont, March 18–20, 2018. Geological Society of America Abstracts with Programs, 50, No. 2. https://doi.org/10.1130/abs/2018NE-311335

Sorota, K. 2013. Age and origin of the Merrimack terrane, southeastern New England: a detrital zircon U–Pb geochronology study. Unpublished M.S. thesis, Boston College, Boston, Massachusetts,153 pp.

Stacey, J.S. and Kramers, J.D. 1975. Approximation of terrestrial lead isotope evolution by a two-stage model. Earth and Planetary Science Letters, 26, pp. 207–221. https://doi.org/10.1016/0012-821X(75)90088-6

Steiger, R.H. and Jäger, E. 1977. Subcommission on geochronology: Convention on the use of decay constants in geo- and cosmochronology. Earth and Planetary Science Letters 36(3), pp. 359–362. https://doi.org/10.1016/0012-821X(77)90060-7

Tremblay, A. and Pinet, N. 2005. Diachronous supracrustal extension in an intraplate setting and the origin of the Connecticut Valley-Gaspé and Merrimack troughs, northern Appalachians. Geological Magazine, 142, pp. 7–22. https://doi.org/10.1017/S001675680400038X

Tremblay, A. and Pinet, N. 2016. Late Neoproterozoic to Permian tectonic evolution of the Quebec Appalachians, Canada. Earth-Science Reviews, 160, pp. 131–170. https://doi.org/10.1016/j.earscirev.2016.06.015

Tucker, R., Osberg, P., and Berry H. 2001. The geology of a part of Acadia and the nature of the Acadian orogeny across central and eastern Maine. American Journal of Science, 301, pp. 205–260. https://doi.org/10.2475/ajs.301.3.205

van Staal, C., Barr, S., and Murphy, B. 2012. Provenance and tectonic evolution of Ganderia: Constraints on the evolution of the Iapetus and Rheic oceans. Geology, 40, pp. 987–990. https://doi.org/10.1130/G33302.1

van Staal, C., Currie, K., Rowbotham, G., Goodfellow, W., and Rogers, N. 2008. Pressure-temperature paths and exhumation of Late Ordovician-Early Silurian blueschists and associated metamorphic nappes of the Salinic Brunswick subduction complex, northern Appalachians. Geological Society of America Bulletin, 120, pp. 1455–1477. https://doi.org/10.1130/B26324.1

van Staal, C., Whalen, J., Valverde-Vaquero, P., Zagorevski, A., and Rogers, N. 2009. Pre- Carboniferous, episodic accretion-related, orogenesis along the Laurentian margin of the Northern Appalachians. *In* Ancient orogens and modern analogues. *Edited by B.* Murphy, D. Keppie, and A. Hynes. Geological Society of London, Special Publications, 327, pp. 271–316. https://doi.org/10.1144/SP327.13

van Staal, C., Wilson, R., Kamo, S., McClelland, W, and McNicoll, V. 2016. Evolution of the Early to Middle Ordovician Popelogan arc in New Brunswick, Canada, and adjacent Maine, USA: Record of arc-trench migration and multiple phases of rifting. Geological Society of America Bulletin, 128, pp. 122–146.

Walsh, G., Aleinikoff, J., and Wintsch, R. 2007. Origin of the Lyme Dome and implications for the timing of multiple Alleghanian deformational and intrusive events in southern Connecticut. American Journal of Science, 307, pp. 168–215. https://doi.org/10.2475/01.2007.06

West, D. 2006. Bedrock geology of the Washington quadrangle, Maine. Maine Geological Survey, Open-File Map 06-79, scale 1:24 000.

West, D., Ludman, A., and Lux, D. 1992. Silurian age for the Pocomoonshine gabbro-diorite, southeastern Maine, and its tectonic implications. American Journal of Science, 292, pp. 253–273. https://doi.org/10.2475/ajs.292.4.253

Williams, H. 1979. Appalachian orogen in Canada. Canadian Journal of Earth Sciences, 1979, 16, 792-807. https://doi.org/10.1139/e79-070

Williams, I. 1998. Chapter 1, U–Th–Pb geochronology by ion microprobe. *In* Applications of microanalytical techniques to understanding mineralizing processes. *Edited by* M. McKibben, W. Shanks, III, and W. Ridley. Reviews in Economic Geology, 7, pp. 1–35.

Wilson, R., van Staal, C., and McClelland, W. 2015. Synaccretionary sedimentary and volcanic rocks in the Ordovician Tetagouche backarc basin, New Brunswick, Canada: evidence for a transition from foredeep to forearc basin sedimentation. American Journal of Science, 315,

pp. 958–1001. https://doi.org/10.2475/10.2015.03

Wintsch, R., Aleinikoff, J., Walsh, G., Bothner, W., Hussey, A.M., II, and Fanning, C. 2007. SHRIMP U–Pb evidence for a Late Silurian age of metasedimentary rocks in the Merrimack and Putnam-Nashoba terranes, eastern New England; American Journal of Science, 307, pp. 119–167. https://doi.org/10.2475/01.2007.05

Wones, D. and Ayuso, R. 1993. Geologic map of the Lucerne Granite, Hancock and Penobscot Counties, Maine. United States Geological Survey Miscellaneous Investigations Series Map I-2360, Scale 1:250 000.

Yu, H. and Chou, Y. 2001. Characteristics and development of the flexural forebulge and basal unconformity of western Taiwan foreland basin. Tectonophysics, 333, 277–291. https://doi.org/10.1016/S0040-1951(00)00279-1

Editorial responsibility: Sandra M. Barr

Appendix A. Comparison of current chronostratigraphic nomenclature (after Cohen *et al.* 2013, 2017 modification) with British series names used in reports of fossil control of stratigraphic units in Maine in 1950s through 1970s.

Period	Global Series	Global Stage	U.K. Series
Devonian	Lower Devonian	Pragian	
		410.8±2.8	
		Lockhovian	
419.2±3.2			
Silurian	Pridoli		
	423.0±2.3		
	Ludlow	Ludfordian	
		425.6±0.9	
	427.4±0.5	Gorstian	
	Wenlock	Homerian	
		430.5±0.7	
	433.4±0.8	Sheinwoodian	
	Llandovery	Telychian	
		438.5±1.1	
		Aeronian	
		440.8±1.2	
443.8±1.5		Rhuddanian	
Ordovician	Upper	Hirnantian	Ashgill
		445.2±1.4	
		Katian	
		453.0±0.9	Caradoc
	458.4±0.9	Sandbian	
	Middle	Darriwilian	Llandeilo
			Llanvirn
		467.3±1.1	
	470.0±1.4	Dapingian	Arenig
	Lower	Floian	
		477.7±1.4	
485.4±1.9		Tremadocian	Tremadoc
Cambrian	Furongian		

Appendix B. Summary of dated zircon samples.

Sample number	Unit	Zircon Type	Lithology	Terrane/ depocenter	Age (Ma)	Significance
PLUTONIC ROCKS						
PM	Pocomoonshine gabbro-diorite	Plutonic	Fine grained gabbro	St. Croix/ Fredericton trough	421.9 ± 2.4[1]	Stitches Fredericton trough and St. Croix terrane. Provides minimum age of Salinic folding
BASEMENT ROCKS						
BL-1	Baskahegan Lake Fm.	Detrital	Wacke	Miramichi	538 (13)[2]	Lower member of oldest unit in Miramichi terrane-Danforth segment
BL-2	Baskahegan Lake Fm.	Detrital	Wacke	Miramichi	~555 (3)[2]	Oldest unit in Miramichi terrane Greenfield segment
BM-1	Bowers Mountain Fm.	Detrital	Quartz arenite	Miramichi	~485 (1)[2]	Near base of middle unit of Miramichi terrane Danforth segment
OS-1	Olamon Stream Fm.	Volcanic	Felsic lava	Miramichi	469.3 ± 4.6[1]	Eruptive age of youngest formation in Miramichi terrane, Greenfield segment
KM-1	Kendall Mountain Fm.	Detrital	Quartz arenite	St. Croix	~530 (1)[2]	Youngest unit in St. Croix terrane
KMV-1	Kendall Mountain Fm.	Volcanic	Felsic tuff	St. Croix	477.4 ± 3.7[1]	Eruptive age at base of youngest unit in St. Croix terrane
COVER ROCKS						
FR-1	Flume Ridge Fm.	Detrital	Wacke	Fredericton trough	~431 (7)[2]	Flume Ridge Formation eastern facies
FR-2	Flume Ridge Fm.	Detrital	Wacke	Fredericton trough	~433 (2)[2]	Flume Ridge Formation western facies
AR-1	Appleton Ridge Fm.	Detrital	Wacke	Fredericton trough	~469 (13)[2]	Test proposed correlative with the Digdeguash Formation in eastern Maine and New Brunswick
MH-1	Mayflower Hill Fm.	Detrital	Wacke	CMAM	~422 (2)[2]	Lies above Smyrna Mills Formation (Waterville Formation correlative) in Lincoln area
MH-2	Mayflower Hill Fm.	Detrital	Wacke	CMAM	~429 (3)[2]	Near base of formation at Mayflower Hill in Waterville; overlies Waterville Formation. Stop 5 of Ludman and Osberg (1987)
MH-3	Mayflower Hill Fm.	Detrital	Wacke	CMAM	~422 (1)[2]	Compare age of sandstone in same outcrop belt as MH-1
VG-1	Vassalboro Gp.	Detrital	Wacke	CMAM	~422 (2)[2]	Constrain age of sandstone in area where Waterville Formation is absent
HC-1	Hutchins Corner Fm.	Detrital	Wacke	CMAM	~432 (1)[2]	Constrain age of sandstone thought to lie beneath Waterville Formation in Vassalboro Group
MA-1	Madrid Fm.	Detrital	Wacke	CMAM	~434 (2)[2]	Attributed to later sedimentary phase than other cover rocks.
MA-2	Madrid Fm.	Detrital	Wacke	CMAM	~430 (2)[2]	

Notes: [1] = crystallization/eruptive age; [2] = mean depositional age defined by youngest zircon population (n); CMAM = Central Maine/Aroostook-Matapedia

Appendix C. SHRIMP U-Th-Pb data for detrital zircons from sedimentary rocks of eastern and east-central Maine. Asterisks indicate grains with greater than 10% discordance; these are not included in relative probability plots. Location coordinates in UTM metres, (Zone 19, NAD27).

sample[1]	measured $^{204}Pb/^{206}Pb$	measured $^{207}Pb/^{206}Pb$	%common ^{206}Pb	U (ppm)	Th/U	Age (Ma) $^{206}Pb/^{238}U^{2}$	err[4]	Age (Ma) $^{207}Pb/^{206}Pb^{2,3}$	err[4]	$^{207}Pb/^{235}U^{5}$	err[4] (%)	$^{206}Pb/^{238}U^{5}$	err[4] (%)	err. corr.
PRE-SILURIAN ROCKS														
MIRAMICHI TERRANE														
	Baskahegan Lake Formation (BL) : BL-1 Lower member, Miramichi Danforth segment. Brookton quadrangle, UTM Location 0597548E/5039799N													
12A64-1.1	---	0.0597	0	64	0.47	668	9			0.9	3.3	0.109	1.5	0.4
12A64-2.1	0.000068	0.0599	0.121	408	0.59	544	4			0.7	1.7	0.088	0.8	0.5
12A64-3.1	0.000026	0.0577	0.047	198	0.75	542	5			0.7	2.1	0.088	1.0	0.4
12A64-4.1	0.000060	0.0984	0.096	85	0.63	1576	17	1578	25	3.7	1.8	0.277	1.2	0.7
12A64-5.1	0.000152	0.0999	0.244	255	0.46	1490	12	1582	16	3.5	1.3	0.260	0.9	0.7
12A64-6.1	0.000012	0.1295	0.019	104	0.75	1995	20	2089	15	6.5	1.4	0.363	1.1	0.8
12A64-7.1	0.000112	0.0587	0.201	128	0.94	571	6			0.7	2.9	0.093	1.1	0.4
12A64-8.1	0.000102	0.1171	0.157	235	0.88	1839	15	1891	13	5.3	1.2	0.330	0.9	0.8
12A64-9.1	---	0.0964	0	43	0.60	1544	22	1554	33	3.6	2.4	0.271	1.6	0.7
12A64-10.1	0.000031	0.1121	0.048	97	0.62	1809	19	1826	19	5	1.6	0.324	1.2	0.7
12A64-11.1	0.000009	0.0801	0.015	260	0.34	1206	10	1194	22	2.3	1.4	0.206	0.9	0.6
12A64-12.1	0.000123	0.0577	0.222	178	0.64	535	5			0.7	2.8	0.087	1.0	0.4
12A64-13.1	-0.000038	0.0615	-0.066	134	0.51	586	6			0.8	2.5	0.095	1.1	0.4
12A64-14.1	0.000016	0.0592	0.029	348	1.12	545	5			0.7	1.7	0.088	0.9	0.5
12A64-15.1	---	0.0897	0	117	0.37	1376	14	1419	23	2.9	1.6	0.238	1.1	0.7
12A64-16.1	0.001743	0.0932	3.013	368	0.59	746	11			1.2	13.7	0.123	1.6	0.1
12A64-17.1	0.000159	0.0900	0.260	105	0.42	1338	14	1376	30	2.8	2.0	0.231	1.2	0.6
12A64-18.1	0.000057	0.0612	0.102	410	0.21	641	5			0.9	1.6	0.105	0.8	0.5
12A64-19.1	0.000040	0.0615	0.072	377	1.37	610	5			0.8	1.6	0.099	0.9	0.5
12A64-20.1	0.000091	0.0818	0.152	79	0.59	1207	14	1210	37	2.3	2.3	0.206	1.3	0.6
12A64-21.1	-0.000034	0.0585	-0.061	156	0.59	568	6			0.8	2.4	0.092	1.0	0.4
12A64-22.1	0.000009	0.1373	0.013	298	0.41	2193	17	2191	9	7.7	1.0	0.405	0.9	0.9
12A64-23.1	-0.000025	0.1082	-0.039	65	0.58	1788	22	1774	29	4.8	2.1	0.320	1.4	0.7
12A64-24.1	0.000081	0.0866	0.133	50	0.55	1387	19	1325	40	2.8	2.6	0.240	1.5	0.6
12A64-25.1	0.000016	0.0805	0.026	160	0.73	1197	11	1203	24	2.3	1.6	0.204	1.0	0.6
12A64-26.1	0.000038	0.0579	0.069	282	0.16	542	5			0.7	1.9	0.088	0.9	0.5
12A64-27.1	-0.000046	0.0743	-0.078	66	0.49	1026	13	1066	45	1.8	2.6	0.173	1.4	0.5
12A64-28.1	---	0.0741	0	366	0.41	1039	8	1044	18	1.8	1.2	0.175	0.9	0.7
12A64-29.1	0.000018	0.0590	0.031	303	2.75	593	5			0.8	1.8	0.096	1.0	0.5
12A64-30.1	-0.000031	0.0592	-0.055	362	0.90	531	4			0.7	1.7	0.086	0.9	0.5
12A64-31.1	0.000052	0.0591	0.094	111	1.21	561	11			0.7	3.5	0.091	2.0	0.6
12A64-32.1	0.000023	0.0841	0.038	302	0.62	1287	15	1286	16	2.6	1.5	0.221	1.3	0.8
12A64-33.1	---	0.0587	0	133	0.90	524	6			0.7	2.5	0.085	1.1	0.4
12A64-34.1	---	0.0618	0	245	0.35	643	6			0.9	1.8	0.105	0.9	0.5
12A64-35.1	-0.000046	0.1584	-0.066	24	0.30	2376	41	2445	26	9.8	2.6	0.446	2.1	0.8
12A64-36.1	0.000049	0.0648	0.085	182	0.74	682	6			1	2.1	0.112	1.0	0.5
12A64-37.1	---	0.0804	0	308	0.38	1220	10	1206	16	2.3	1.2	0.208	0.9	0.7
12A64-38.1	0.000056	0.0620	0.099	250	0.92	651	6			0.9	1.9	0.106	0.9	0.5
12A64-39.1	0.000058	0.0824	0.097	119	0.87	1269	13	1235	28	2.4	1.8	0.218	1.1	0.6
12A64-40.1	0.000014	0.0578	0.026	418	1.54	533	4			0.7	1.6	0.086	0.9	0.5
12A64-41.1	0.000010	0.0965	0.016	178	0.70	1560	14	1554	17	3.6	1.3	0.274	1.0	0.7
12A64-42.1	0.000111	0.0806	0.186	45	1.08	1214	18	1171	53	2.3	3.1	0.207	1.6	0.5
12A64-43.1	---	0.0744	0	95	0.44	977	20	1052	36	1.7	2.8	0.164	2.2	0.8
12A64-44.1	---	0.0575	0	352	0.12	526	4			0.7	1.9	0.085	0.9	0.5

Appendix C: Continued.

sample[1]	measured $^{204}Pb/^{206}Pb$	measured $^{207}Pb/^{206}Pb$	%common ^{206}Pb	U (ppm)	Th/U	Age (Ma) $^{206}Pb/^{238}U^{2}$	err[4]	$^{207}Pb/^{206}Pb^{2,3}$	err[4]	$^{207}Pb/^{235}U^{5}$	err[4] (%)	$^{206}Pb/^{238}U^{5}$	err[4] (%)	err. corr.
12A64-45.1	0.000015	0.1135	0.023	204	0.86	1865	16	1852	13	5.2	1.2	0.336	1.0	0.8
12A64-46.1	0.000080	0.1152	0.123	74	0.75	1836	21	1865	22	5.2	1.8	0.330	1.3	0.7
12A64-47.1	---	0.0820	0	161	0.51	1199	11	1245	23	2.3	1.5	0.205	1.0	0.7
12A64-48.1	-0.000332	0.0584	-0.583	70	0.99	555	7			0.8	5.0	0.090	1.4	0.3
12A64-50.1	0.000039	0.0623	0.069	233	1.02	653	6			0.9	1.9	0.107	0.9	0.5
12A64-51.1	0.000099	0.0706	0.171	61	0.44	958	13			1.5	3.1	0.160	1.4	0.5
12A64-52.1	0.000036	0.0708	0.062	82	0.34	1039	12			1.7	2.7	0.175	1.3	0.5
12A64-53.1	-0.000017	0.1173	-0.026	174	0.50	1892	17	1918	13	5.5	1.3	0.341	1.0	0.8
12A64-54.1	-0.000102	0.0530	-0.184	189	2.38	552	6			0.7	3.2	0.089	1.1	0.4
12A64-55.1	-0.000003	0.1836	-0.004	309	0.64	2568	19	2686	6	12.4	1.0	0.489	0.9	0.9
12A64-56.1	0.000043	0.0618	0.075	156	1.44	534	6			0.7	2.7	0.086	1.2	0.4
12A64-57.1	0.000067	0.0616	0.118	217	1.23	615	6			0.8	2.1	0.100	1.0	0.5
12A64-58.1	0.000031	0.0589	0.056	179	0.78	539	5			0.7	2.3	0.087	1.0	0.4
12A64-59.1	0.000088	0.0626	0.155	79	1.16	511	7			0.7	4.1	0.082	1.4	0.3
12A64-60.1	-0.000248	0.0574	-0.439	48	0.28	602	10			0.8	5.8	0.098	1.8	0.3
12A64-61.1	---	0.0602	0	249	0.58	533	5			0.7	2.0	0.086	1.0	0.5
12A64-62.1	0.000033	0.0731	0.056	447	0.23	1015	13	1004	19	1.7	1.7	0.171	1.4	0.8
12A64-63.1	0.000062	0.0621	0.109	191	0.61	678	7			0.9	2.4	0.111	1.1	0.4
12A64-64.1	0.000260	0.0596	0.469	142	1.24	582	6			0.7	3.9	0.094	1.2	0.3
12A64-65.1	-0.000164	0.0600	-0.290	44	1.23	539	9			0.8	5.9	0.087	1.8	0.3
12A64-66.1	---	0.0635	0	313	0.39	634	6			0.9	2.0	0.103	0.9	0.5
12A64-67.1	0.000025	0.0602	0.044	258	0.36	631	6			0.8	2.0	0.103	1.0	0.5
12A64-68.1	---	0.0622	0	231	1.32	632	6			0.9	2.0	0.103	1.0	0.5
12A64-69.1	0.000050	0.0822	0.084	182	0.50	1183	24	1232	46	2.3	3.2	0.201	2.2	0.7
12A64-70.1	0.000075	0.1041	0.118	115	0.60	1651	29	1680	23	4.2	2.3	0.292	2.0	0.8
	Baskahegan Lake Formation (BL) : BL-2 Miramichi Greenfield segment. Greenfield quadrangle, UTM Location 0540624E/4986141N													
14B47-1.1	0.000458	0.0746	0.792	65	0.98	1044	19			1.65	5.9	0.176	2.0	0.3
14B47-2.1	-0.000004	0.0948	-0.007	268	0.30	1488	20	1525	10	3.40	1.6	0.260	1.5	0.9
14B47-3.1	0.000043	0.0608	0.075	282	0.52	610	9			0.82	2.1	0.099	1.5	0.7
14B47-4.1	0.000088	0.1459	0.128	70	0.71	2333	31	2284	15	8.70	1.8	0.436	1.6	0.9
14B47-5.1	0.000043	0.0773	0.072	448	0	1134	15	1113	14	2.04	1.6	0.192	1.5	0.9
14B47-6.1	-0.000053	0.0589	-0.093	130	0.53	558	11			0.74	3.2	0.090	2.0	0.6
14B47-7.1	0.000032	0.0985	0.052	480	0.42	1558	24	1586	8	3.69	1.8	0.273	1.7	1.0
14B47-8.1	-0.000031	0.0618	-0.054	89	0.51	696	10			0.98	2.9	0.114	1.6	0.5
14B47-10.1	0.000053	0.0813	0.088	169	0.38	1214	19	1210	22	2.30	2.1	0.207	1.7	0.8
14B47-11.1	0.000253	0.0629	0.451	104	1.15	637	10			0.85	6.2	0.104	1.6	0.3
14B47-12.1	0.000006	0.1391	0.008	410	0.51	2183	29	2214	9	7.72	1.6	0.403	1.6	1.0
14B47-13.1	-0.000055	0.0671	-0.096	162	0.60	799	11			1.24	2.3	0.132	1.5	0.7
14B47-14.1	0.000422	0.0732	0.732	43	0.53	975	16			1.51	6.9	0.163	1.7	0.3
14B47-15.1	0.000087	0.0873	0.143	66	0.44	1200	58	1339	38	2.43	5.6	0.205	5.3	0.9
14B47-16.1	0.000011	0.0828	0.018	131	0.40	1230	17	1261	18	2.40	1.8	0.210	1.5	0.9
14B47-17.1	-0.000005	0.1801	-0.007	251	0.66	2685	51	2654	6	12.83	2.4	0.517	2.3	1.0
14B47-18.1	---	0.0801	0	141	0.27	1173	16	1198	17	2.20	1.7	0.200	1.5	0.9
14B47-19.1	0.000204	0.1168	0.315	55	0.80	1857	26	1863	32	5.25	2.4	0.334	1.6	0.7
14B47-20.1	-0.000015	0.0610	-0.026	392	0.65	625	9			0.86	1.8	0.102	1.5	0.8
14B47-21.1	-0.000007	0.0587	-0.013	452	0.93	551	10			0.72	2.2	0.089	2.0	0.9
14B47-22.1	0.000600	0.0640	1.082	53	0.54	675	12			0.84	12.9	0.110	1.8	0.1
14B47-23.1	0.000018	0.0623	0.031	339	0.40	613	9			0.85	2.6	0.100	1.5	0.6

Appendix C: Continued.

sample[1]	measured $^{204}Pb/^{206}Pb$	measured $^{207}Pb/^{206}Pb$	%common ^{206}Pb	U (ppm)	Th/U	Age (Ma) $^{206}Pb/^{238}U^{2}$	err[4]	$^{207}Pb/^{206}Pb^{2,3}$	err[4]	$^{207}Pb/^{235}U^{5}$	err[4] (%)	$^{206}Pb/^{238}U^{5}$	err[4] (%)	err. corr.
14B47-24.1	-0.000071	0.0630	-0.125	79	0.59	671	14			0.97	3.8	0.110	2.3	0.6
14B47-25.1	-0.000030	0.0773	-0.050	57	0.51	1058	17	1140	37	1.91	2.5	0.178	1.7	0.7
14B47-26.1*	0.000022	0.1640	0.032	108	0.91	2014	38	2494	10	8.28	2.3	0.367	2.2	1.0
14B47-27.1	0.000016	0.0658	0.028	271	0.64	808	12			1.21	1.9	0.134	1.6	0.9
14B47-28.1	-0.000014	0.0832	-0.023	105	0.66	1204	17	1278	21	2.36	1.9	0.205	1.5	0.8
14B47-29.1	0.000098	0.0684	0.171	70	1.01	798	12			1.22	3.6	0.132	1.6	0.5
14B47-30.1	0.000013	0.0972	0.022	241	0.35	1567	23	1567	30	3.68	2.3	0.275	1.7	0.7
14B47-31.1	0.000410	0.0693	0.719	80	0.57	827	13			1.20	5.9	0.137	1.6	0.3
14B47-32.1	0.000097	0.0882	0.160	41	0.59	1315	20	1356	48	2.71	3.0	0.226	1.7	0.6
14B47-33.1	0.000046	0.0788	0.078	107	0.17	1071	15	1149	30	1.95	2.2	0.181	1.6	0.7
14B47-34.1	-0.000006	0.0809	-0.010	246	0.53	1266	17	1220	13	2.42	1.6	0.217	1.5	0.9
14B47-35.1	0.000025	0.0804	0.042	231	0.59	1244	17	1198	16	2.35	1.7	0.213	1.5	0.9
14B47-36.1	---	0.1243	0	253	0.42	1965	25	2018	7	6.11	1.5	0.356	1.5	1.0
14B47-37.1	0.000019	0.2009	0.025	210	0.14	2697	33	2831	6	14.38	1.6	0.520	1.5	1.0
14B47-38.1	0.000063	0.0755	0.107	1447	0.13	987	13	1057	9	1.70	1.5	0.165	1.5	1.0
14B47-39.1	0.000067	0.0609	0.119	447	0.27	640	12			0.86	2.4	0.104	2.0	0.8
14B47-40.1*	0.000270	0.1309	0.406	523	1.17	1788	23	2061	11	5.61	1.6	0.320	1.5	0.9
14B47-41.1	-0.000037	0.0615	-0.064	161	0.37	634	9			0.88	2.4	0.103	1.5	0.6
14B47-42.1	0.000067	0.0969	0.108	309	0.30	1564	25	1547	13	3.63	1.9	0.275	1.8	0.9
14B47-43.1	0.000039	0.1216	0.060	203	0.79	1868	26	1972	15	5.61	1.8	0.336	1.6	0.9
14B47-44.1	0.000160	0.0768	0.272	146	0.30	1054	15	1055	41	1.83	2.6	0.178	1.6	0.6
14B47-45.1	0.000054	0.0951	0.087	82	0.64	1516	25	1514	24	3.45	2.3	0.265	1.9	0.8
14B47-46.1	0.000018	0.0741	0.030	385	0.86	1025	14	1038	14	1.76	1.6	0.172	1.5	0.9
14B47-47.1	0.000111	0.0617	0.198	337	0.83	610	9			0.82	2.4	0.099	1.5	0.6
14B47-48.1	0.000018	0.0780	0.030	258	0.19	1155	16	1139	15	2.10	1.7	0.196	1.5	0.9
14B47-49.1	0.000023	0.0732	0.040	147	0.35	1032	15	1009	24	1.74	1.9	0.174	1.5	0.8
14B47-50.1	0.000017	0.0946	0.027	132	0.66	1509	21	1514	15	3.43	1.8	0.264	1.6	0.9
14B47-51.1	0.000119	0.0862	0.196	169	0.45	1282	18	1304	26	2.56	2.0	0.220	1.5	0.8
14B47-52.1	-0.000015	0.1158	-0.023	114	0.73	1927	26	1894	12	5.57	1.7	0.348	1.5	0.9
14B47-53.1	0.000171	0.0637	0.303	512	0.76	553	9			0.76	2.6	0.090	1.8	0.7
14B47-54.1	0.000212	0.0626	0.377	93	0.95	639	10			0.86	5.0	0.104	1.6	0.3
14B47-55.1	---	0.1270	0	101	1.20	2064	31	2055	13	6.60	1.9	0.377	1.8	0.9
14B47-56.1	0.000036	0.0953	0.058	213	0.35	1569	21	1523	13	3.60	1.7	0.276	1.5	0.9
14B47-57.1	0.000069	0.0796	0.116	109	0.46	1186	17	1162	31	2.19	2.2	0.202	1.6	0.7
14B47-58.1	-0.000057	0.0600	-0.102	218	0.31	600	10			0.82	2.6	0.097	1.8	0.7
14B47-59.1	-0.000095	0.0673	-0.164	133	0.60	834	12			1.31	2.6	0.138	1.6	0.6
14B47-60.1	-0.000062	0.0640	-0.108	138	0.45	647	9			0.94	2.7	0.105	1.5	0.6
	Bowers Mountain Formation (BM) : BM-1 Miramichi Danforth segment. Dill Hill quadrangle, UTM Location 0582145E/5029072N													
14B34-1.1	-0.000027	0.0841	-0.044	388	0.17	1506	21	1302	43	3.06	2.7	0.263	1.6	0.6
14B34-2.1	0.000114	0.0573	0.205	328	0.84	632	7			0.79	5.8	0.103	1.2	0.2
14B34-3.1	---	0.0823	0	112	0.49	1429	16	1252	51	2.82	2.9	0.248	1.3	0.4
14B34-4.1	-0.000003	0.0664	-0.005	2038	0.08	1005	12			1.54	2.9	0.169	1.2	0.4
14B34-5.1	0.000077	0.0740	0.131	158	0.50	1306	14	1009	97	2.26	5.0	0.225	1.2	0.2
14B34-6.1	---	0.0662	0	202	0.84	1006	11			1.54	1.6	0.169	1.2	0.7
14B34-7.1	-0.000009	0.0782	-0.014	326	0.44	1139	12	1155	17	2.09	1.4	0.193	1.2	0.8
14B34-8.1	---	0.0608	0	50	0.46	486	11			0.66	4.2	0.078	2.4	0.6
14B34-9.1	0.000361	0.0759	0.62	49	0.32	946	14			1.54	7.9	0.158	1.6	0.2
14B34-10.1	0.000027	0.1014	0.043	220	0.39	1573	16	1643	16	3.85	1.5	0.276	1.2	0.8

Appendix C: Continued.

sample[1]	measured $^{204}Pb/^{206}Pb$	measured $^{207}Pb/^{206}Pb$	%common ^{206}Pb	U (ppm)	Th/U	Age (Ma) $^{206}Pb/^{238}U^{2}$	err[4]	$^{207}Pb/^{206}Pb^{2,3}$	err[4]	$^{207}Pb/^{235}U^{5}$	err[4] (%)	$^{206}Pb/^{238}U^{5}$	err[4] (%)	err. corr.
14B34-11.1	0.000110	0.0616	0.195	431	0.99	603	7			0.81	2.5	0.098	1.1	0.5
14B34-12.1	0.000095	0.0906	0.156	92	0.93	1403	17	1408	52	2.99	3.1	0.243	1.4	0.4
14B34-13.1	0.000038	0.0952	0.062	206	0.57	1523	16	1521	37	3.48	2.3	0.267	1.2	0.5
14B34-14.1	-0.000052	0.0607	-0.092	114	0.37	614	8			0.85	3.7	0.100	1.3	0.4
14B34-15.1	0.000133	0.1047	0.211	211	0.74	1594	17	1675	30	3.98	2.0	0.281	1.2	0.6
14B34-16.1	0.000183	0.1811	0.252	17	0.52	2596	44	2642	37	12.23	3.0	0.496	2.1	0.7
14B34-17.1	---	0.0739	0	1055	0.07	1012	11	1039	9	1.73	1.3	0.170	1.2	0.9
14B34-18.1	---	0.0675	0	170	0.72	744	9			1.14	1.9	0.122	1.3	0.7
14B34-19.1	0.000056	0.1032	0.089	439	0.42	1703	17	1668	12	4.27	1.3	0.302	1.1	0.9
14B34-20.1	0.000006	0.0988	0.010	302	0.31	1527	16	1599	14	3.64	1.4	0.267	1.2	0.8
14B34-21.1	0.000205	0.1090	0.322	129	0.52	1671	18	1734	32	4.33	2.2	0.296	1.2	0.6
14B34-22.1	0.000028	0.0747	0.047	1065	0.06	1038	11	1049	12	1.79	1.2	0.175	1.1	0.9
14B34-23.1	0.000018	0.0955	0.029	482	0.32	1435	16	1532	11	3.27	1.4	0.249	1.2	0.9
14B34-24.1	---	0.0639	0	95	0.81	610	8			0.87	2.4	0.099	1.3	0.5
14B34-25.1	0.000017	0.0989	0.028	494	0.52	1518	15	1599	11	3.61	1.3	0.265	1.1	0.9
14B34-26.1	0.000030	0.0974	0.048	859	0.28	1502	15	1565	8	3.51	1.2	0.262	1.1	0.9
14B34-28.1	0.000039	0.1271	0.058	925	0.41	1879	18	2050	6	5.91	1.1	0.338	1.1	1.0
14B34-29.1	0.000060	0.0963	0.096	178	0.49	1457	16	1538	23	3.34	1.7	0.254	1.2	0.7
14B34-30.1	0.000024	0.0966	0.038	414	0.24	1520	22	1552	12	3.53	1.7	0.266	1.6	0.9
14B34-31.1	0.000298	0.0866	0.495	167	0.3	1231	14	1255	56	2.39	3.1	0.210	1.2	0.4
14B34-32.1	-0.000018	0.0646	-0.032	257	2.17	686	8			1.00	3.0	0.112	1.2	0.4
14B34-33.1	0.000116	0.0981	0.186	160	0.32	1565	17	1557	27	3.66	1.9	0.275	1.2	0.7
14B34-34.1	0.000023	0.1521	0.034	246	0.53	2459	33	2366	8	9.72	1.7	0.464	1.6	1.0
14B34-35.1	0.000019	0.0958	0.031	423	0.72	1471	15	1538	12	3.38	1.3	0.256	1.1	0.9
14B34-36.1	---	0.0614	0	544	1.03	581	11			0.80	2.2	0.094	2.0	0.9
14B34-37.1	-0.000012	0.0749	-0.02	781	0.08	1015	10	1069	20	1.76	1.5	0.171	1.1	0.7
14B34-38.1	---	0.1070	0	278	0.53	1770	18	1749	10	4.66	1.3	0.316	1.1	0.9
14B34-39.1	0.000020	0.0738	0.033	808	0.08	1002	10	1027	13	1.70	1.3	0.168	1.1	0.9
14B34-40.1	-0.000012	0.0615	-0.021	463	0.69	611	7			0.85	1.6	0.099	1.1	0.7
14B34-41.1	-0.000005	0.0748	-0.009	1112	0.09	1021	11	1063	9	1.77	1.2	0.172	1.2	0.9
14B34-42.1	0.000059	0.1081	0.092	140	0.52	1713	18	1753	35	4.50	2.3	0.304	1.2	0.5
14B34-43.1	0.000121	0.0959	0.195	312	0.18	1532	16	1512	21	3.49	1.6	0.268	1.2	0.7
14B34-44.1	---	0.0745	0	915	0.09	1054	13	1053	10	1.82	1.4	0.178	1.3	0.9
14B34-45.1	0.000104	0.1940	0.141	53	0.52	2739	34	2765	28	14.07	2.3	0.530	1.5	0.7
14B34-46.1	0.000005	0.0937	0.008	570	0.37	1500	15	1499	8	3.38	1.2	0.262	1.1	0.9
14B34-47.1	0.000132	0.1154	0.204	156	0.60	1800	18	1857	20	5.05	1.6	0.322	1.2	0.7
14B34-48.1	---	0.0744	0	1473	0.10	962	10	1051	7	1.65	1.2	0.161	1.2	1.0
14B34-49.1	0.000013	0.0747	0.022	814	0.09	1042	11	1053	10	1.80	1.3	0.175	1.1	0.9
14B34-50.1	0.000008	0.0985	0.013	333	0.31	1568	17	1593	10	3.74	1.3	0.275	1.2	0.9
14B34-51.1	0.000017	0.0939	0.028	245	0.57	1510	19	1500	13	3.41	1.6	0.264	1.4	0.9
14B34-52.1	0.000071	0.1159	0.109	138	1.41	1886	25	1878	16	5.38	1.8	0.340	1.6	0.9
14B34-53.1	0.000056	0.1091	0.087	393	0.57	1659	18	1772	10	4.39	1.4	0.294	1.2	0.9
14B34-54.1	-0.000011	0.0998	-0.018	499	0.11	1565	15	1623	9	3.79	1.2	0.275	1.1	0.9
14B34-55.1	-0.000033	0.0803	-0.056	164	0.35	1203	21	1215	22	2.28	2.2	0.205	1.9	0.9
14B34-56.1	-0.000015	0.0618	-0.027	471	1.37	658	8			0.92	1.7	0.107	1.2	0.7
14B34-57.1	-0.000031	0.0956	-0.050	92	0.73	1472	16	1548	22	3.40	1.7	0.257	1.2	0.7
14B34-58.1	---	0.0946	0	231	0.46	1489	15	1520	11	3.39	1.3	0.260	1.2	0.9
14B34-59.1	0.000004	0.0977	0.007	632	0.61	1543	20	1579	7	3.64	1.5	0.270	1.5	1.0
14B34-60.1	-0.000010	0.1359	-0.014	100	0.49	2117	22	2176	12	7.29	1.4	0.389	1.2	0.9

Appendix C: Continued.

sample[1]	measured $^{204}Pb/^{206}Pb$	measured $^{207}Pb/^{206}Pb$	%common ^{206}Pb	U (ppm)	Th/U	Age (Ma) $^{206}Pb/^{238}U^{2}$	err[4]	Age (Ma) $^{207}Pb/^{206}Pb^{2,3}$	err[4]	$^{207}Pb/^{235}U^{5}$	err[4] (%)	$^{206}Pb/^{238}U^{5}$	err[4] (%)	err. corr.
ST. CROIX TERRANE														
	Kendall Mountain Formation (KM) : KM-1 Quartz arenite at fault contact with Woodland Fm. Woodland quadrangle, UTM Location 0621322E/5003221N													
12A4A-1.1	0.000008	0.0607	0.014	481	0.51	660	9			0.9	1.7	0.108	1.4	0.8
12A4A-2.1	0.000108	0.0589	0.194	167	0.70	540	5			0.7	2.5	0.087	1.0	0.4
12A4A-3.1	0.000035	0.0743	0.060	201	0.20	1009	9	1034	23	1.7	1.5	0.169	0.9	0.6
12A4A-4.1	0.000012	0.0659	0.021	497	0.56	784	7			1.2	1.3	0.129	1.0	0.8
12A4A-5.1	0.000073	0.0809	0.122	161	0.42	1204	17	1193	23	2.3	1.9	0.205	1.5	0.8
12A4A-6.1	0.000092	0.0714	0.158	86	0.81	954	10			1.5	2.4	0.159	1.2	0.5
12A4A-7.1	---	0.0809	0	45	0.68	1262	19	1218	38	2.4	2.6	0.216	1.7	0.7
12A4A-8.1	0.000063	0.0769	0.106	98	0.20	1195	12	1095	31	2.1	1.9	0.204	1.1	0.6
12A4A-9.1	0.000010	0.0949	0.015	166	0.78	1537	13	1522	16	3.5	1.3	0.269	1.0	0.7
12A4A-10.1	-0.000027	0.0599	-0.047	349	0.74	561	6			0.8	1.8	0.091	1.2	0.7
12A4A-11.1	0.000022	0.0817	0.036	190	0.58	1210	16	1231	20	2.3	1.8	0.206	1.5	0.8
12A4A-12.1	-0.000056	0.0972	-0.089	87	0.50	1483	25	1585	24	3.5	2.2	0.259	1.9	0.8
12A4A-13.1	-0.000029	0.0730	-0.049	165	0.31	1024	9	1023	25	1.7	1.6	0.172	1.0	0.6
12A4A-14.1	---	0.0601	0	178	0.78	667	6			0.9	1.9	0.109	1.0	0.5
12A4A-15.1	---	0.0724	0	93	0.5	958	10			1.6	2.0	0.160	1.1	0.6
12A4A-16.1	0.000113	0.0603	0.202	158	0.81	651	6			0.9	2.5	0.106	1.0	0.4
12A4A-17.1	0.000034	0.0730	0.059	278	0.39	999	8			1.7	1.3	0.168	0.9	0.7
12A4A-18.1	---	0.0723	0	89	0.29	1003	11			1.7	2.0	0.168	1.2	0.6
12A4A-19.1	0.000032	0.0902	0.052	325	0.28	1442	17	1420	13	3.1	1.5	0.251	1.3	0.9
12A4A-20.1	0.000065	0.0666	0.113	239	0.11	809	7			1.2	1.6	0.134	0.9	0.6
12A4A-21.1	0.000035	0.0857	0.057	107	0.36	1339	22	1320	25	2.7	2.2	0.231	1.8	0.8
12A4A-22.1	0.000006	0.0810	0.011	317	0.40	1218	10	1219	15	2.3	1.1	0.208	0.9	0.8
12A4A-23.1	0.000270	0.1009	0.432	122	0.41	1545	15	1571	28	3.6	1.9	0.271	1.1	0.6
12A4A-24.1	-0.000020	0.0600	-0.036	247	0.99	529	5			0.7	1.9	0.086	0.9	0.5
12A4A-25.1	0.000067	0.0692	0.116	120	0.41	928	9			1.5	2.0	0.155	1.1	0.5
12A4A-26.1	---	0.0785	0	96	0.36	1081	12	1158	36	2.0	2.2	0.183	1.2	0.6
12A4A-27.1	-0.000033	0.0625	-0.058	103	0.93	871	40			1.3	5.3	0.145	4.9	0.9
12A4A-28.1	0.000066	0.0671	0.115	291	0.69	789	25			1.2	3.7	0.130	3.4	0.9
12A4A-29.1	0.000015	0.0995	0.024	240	0.36	1736	316	1609	240	4.2	24.4	0.309	20.8	0.8
12A4A-30.1	0.000006	0.0915	0.010	310	0.27	1327	28	1454	16	2.9	2.5	0.228	2.4	0.9
12A4A-31.1	0.000034	0.0729	0.058	138	0.29	1009	52			1.7	5.7	0.169	5.5	1.0
12A4A-32.1	-0.000074	0.0731	-0.126	65	0.31	1025	12	1043	43	1.8	2.5	0.172	1.3	0.5
12A4A-33.1	-0.000018	0.1146	-0.028	86	0.83	1866	37	1877	20	5.3	2.6	0.336	2.3	0.9
12A4A-34.1	-0.000051	0.0613	-0.089	83	0.32	664	14			0.9	3.4	0.108	2.2	0.6
12A4A-35.1	0.000104	0.0629	0.183	103	0.44	710	8			1.0	4.0	0.116	1.1	0.3
12A4A-36.1	0.000110	0.0600	0.196	76	0.62	616	7			0.8	3.9	0.100	1.2	0.3
12A4A-37.1	-0.000013	0.0894	-0.021	136	0.25	1404	13	1416	20	3.0	1.5	0.243	1.0	0.7
12A4A-38.1	---	0.0904	0	149	0.32	1456	13	1433	18	3.2	1.4	0.253	1.0	0.7
12A4A-39.1	0.000014	0.1168	0.022	89	1.07	1878	19	1904	18	5.4	1.5	0.338	1.2	0.8
12A4A-40.1	0.000040	0.0673	0.069	101	0.72	629	7			0.9	2.9	0.102	1.1	0.4
12A4A-41.1	-0.000015	0.1262	-0.022	160	0.52	2029	17	2048	12	6.4	1.2	0.370	1.0	0.8
12A4A-42.1	-0.000081	0.1431	-0.118	61	0.80	2354	28	2276	20	8.8	1.8	0.441	1.4	0.8
12A4A-43.1	0.000011	0.0810	0.018	812	0.19	1232	9	1216	10	2.3	0.9	0.211	0.8	0.8
12A4A-44.1	-0.000062	0.0642	-0.109	109	1.99	817	9			1.2	2.4	0.135	1.1	0.5
12A4A-45.1	-0.000020	0.0860	-0.033	89	1.35	1310	14	1344	26	2.7	1.8	0.225	1.2	0.7
12A4A-46.1	-0.000231	0.0595	-0.406	60	1.06	559	7			0.8	4.4	0.091	1.4	0.3

Appendix C: Continued.

sample[1]	measured $^{204}Pb/^{206}Pb$	measured $^{207}Pb/^{206}Pb$	%common ^{206}Pb	U (ppm)	Th/U	Age (Ma) $^{206}Pb/^{238}U^{2}$	err[4]	$^{207}Pb/^{206}Pb^{2,3}$	err[4]	$^{207}Pb/^{235}U^{5}$	err[4] (%)	$^{206}Pb/^{238}U^{5}$	err[4] (%)	err. corr.
12A4A-47.1	0.000118	0.0612	0.210	145	0.62	618	10			0.8	2.9	0.101	1.6	0.6
12A4A-48.1	-0.000010	0.1358	-0.015	112	0.50	2126	21	2175	13	7.3	1.4	0.391	1.1	0.8
12A4A-49.1	---	0.0965	0	105	0.51	1564	16	1557	36	3.7	2.2	0.275	1.1	0.5
12A4A-50.1	0.000230	0.0698	0.400	200	0.71	796	7			1.2	2.1	0.131	0.9	0.5
12A4A-51.1	0.000026	0.0606	0.045	221	0.82	497	44			0.7	10.1	0.080	9.2	0.9
12A4A-52.1	---	0.0702	0	515	0.35	928	12			1.5	1.6	0.155	1.4	0.9
12A4A-53.1	-0.000007	0.0823	-0.012	272	0.97	1229	22	1255	16	2.4	2.1	0.210	2.0	0.9
12A4A-54.1	0.000006	0.1836	0.009	128	0.39	2726	26	2685	10	13.3	1.3	0.526	1.2	0.9
12A4A-55.1	-0.000061	0.1196	-0.093	80	1.57	1962	21	1962	18	5.9	1.6	0.356	1.2	0.8
12A4A-56.1	-0.000067	0.0709	-0.115	113	0.39	955	11			1.6	2.1	0.160	1.2	0.6
12A4A-57.1	---	0.0566	0	82	1.53	549	6			0.7	3.0	0.089	1.2	0.4
12A4A-58.1	0.000027	0.0603	0.047	157	0.81	631	9			0.8	2.4	0.103	1.5	0.6
12A4A-59.1	0.000039	0.0660	0.068	278	0.43	796	7			1.2	2.4	0.131	1.0	0.4
12A4A-60.1	---	0.0608	0	143	0.27	601	16			0.8	3.4	0.098	2.8	0.8
12A4A-61.1	---	0.0843	0	128	0.43	1356	14	1299	22	2.7	1.6	0.234	1.2	0.7
12A4A-62.1	---	0.0673	0	238	0.75	861	7			1.3	1.4	0.143	0.9	0.6
12A4A-63.1	0.000057	0.0717	0.098	93	0.48	898	27			1.5	3.7	0.149	3.2	0.9
12A4A-64.1	0.000023	0.1246	0.035	274	0.44	1904	15	2018	12	5.9	1.1	0.344	0.9	0.8
12A4A-65.1	0.000055	0.0601	0.098	79	0.81	625	7			0.8	3.1	0.102	1.2	0.4
12A4A-66.1	0.000011	0.1076	0.018	132	0.87	1770	17	1756	16	4.7	1.4	0.316	1.1	0.8
12A4A-67.1	-0.000032	0.0787	-0.053	60	0.45	1267	37	1174	35	2.4	3.6	0.217	3.2	0.9
12A4A-68.1	0.000007	0.2420	0.009	176	0.45	3217	24	3132	6	21.6	1.0	0.647	1.0	0.9
12A4A-69.1	0.000012	0.1075	0.018	104	0.73	1783	17	1754	17	4.7	1.4	0.319	1.1	0.8
12A4A-70.1	0.000017	0.0962	0.028	257	0.66	1572	12	1546	13	3.7	1.1	0.276	0.9	0.8
POST-MIDDLE ORDOVICIAN COVER ROCK UNITS														
FREDERICTON TROUGH AND CORRELATIVES														
Flume Ridge Formation (FR) : FR-1 Eastern facies, Kellyland dam. Kellyland quadrangle, UTM Location 0619272E/5014389N														
FR-1-12-1.1	---	0.0740	0	106	0.33	1066	11	1042	34	1.8	2.0	0.180	1.1	0.6
FR-1-12-2.1	0.000032	0.0583	0.059	614	0.72	430	3			0.6	1.5	0.069	0.7	0.4
FR-1-12-3.1	-0.000018	0.0822	-0.034	289	0.01	1233	17	1256	28	2.4	2.1	0.211	1.5	0.7
FR-1-12-4.1	---	0.0568	0	796	0.53	438	6			0.5	1.8	0.070	1.4	0.8
FR-1-12-5.1	-0.000026	0.0773	-0.048	152	0.33	1053	10	1139	30	1.9	1.8	0.177	1.0	0.6
FR-1-12-6.1	-0.000021	0.0786	-0.039	196	0.83	1210	18	1168	26	2.2	2.1	0.206	1.6	0.8
FR-1-12-7.1	0.000057	0.0746	0.104	137	0.98	1085	18	1036	35	1.9	2.5	0.183	1.8	0.7
FR-1-12-8.1	0.000004	0.0797	0.008	661	0.17	1186	14	1187	11	2.2	1.4	0.202	1.2	0.9
FR-1-12-9.1	0.000012	0.0753	0.023	467	0.20	1071	12	1071	14	1.9	1.4	0.181	1.2	0.9
FR-1-12-10.1	0.000006	0.1133	0.011	294	0.24	1825	31	1852	11	5.1	2.0	0.327	2.0	1.0
FR-1-12-11.1	0.000118	0.0552	0.216	258	0.81	427	8			0.5	3.5	0.068	2.0	0.6
FR-1-12-12.1	0.000238	0.0552	0.435	164	0.65	477	5			0.5	4.4	0.077	1.0	0.2
FR-1-12-13.1	0.000020	0.0571	0.036	1028	0.35	471	3			0.6	1.1	0.076	0.6	0.6
FR-1-12-14.1	0.000020	0.0556	0.036	1009	0.57	433	3			0.5	1.3	0.070	0.6	0.5
FR-1-12-15.1	0.000007	0.0781	0.013	455	0.38	1137	7	1146	15	2.1	1.0	0.193	0.7	0.7
FR-1-12-16.1	0.000251	0.0553	0.459	209	1.12	424	4			0.5	4.6	0.068	1.0	0.2
FR-1-12-17.1	---	0.0855	0	348	0.35	1358	10	1326	26	2.8	1.6	0.234	0.8	0.5
FR-1-12-18.1	0.000028	0.0556	0.051	696	0.99	433	8			0.5	2.3	0.069	1.9	0.8
FR-1-12-19.1	-0.000141	0.0565	-0.257	62	1.01	454	6			0.6	5.3	0.073	1.5	0.3
FR-1-12-20.1	-0.000010	0.0734	-0.019	337	0.35	1023	7	1028	19	1.7	1.2	0.172	0.7	0.6
FR-1-12-21.1	-0.000003	0.1072	-0.006	597	0.27	1679	10	1754	8	4.4	0.8	0.298	0.6	0.8

Appendix C: Continued.

sample[1]	measured $^{204}Pb/^{206}Pb$	measured $^{207}Pb/^{206}Pb$	%common ^{206}Pb	U (ppm)	Th/U	Age (Ma) $^{206}Pb/^{238}U^{2}$	err[4]	$^{207}Pb/^{206}Pb^{2,3}$	err[4]	$^{207}Pb/^{235}U^{5}$	err[4] (%)	$^{206}Pb/^{238}U^{5}$	err[4] (%)	err. corr.
FR-1-12-22.1	0.000008	0.0748	0.014	510	0.60	1050	11	1060	16	1.8	1.4	0.177	1.1	0.8
FR-1-12-23.1	0.000078	0.0816	0.143	319	0.40	1080	9	1208	21	2.0	1.4	0.182	0.9	0.6
FR-1-12-24.1	-0.000006	0.0915	-0.011	434	0.53	1446	9	1459	12	3.2	1.0	0.251	0.7	0.7
FR-1-12-25.1	0.000025	0.0763	0.045	507	0.30	1099	14	1094	15	1.9	1.5	0.186	1.4	0.9
FR-1-12-26.1	0.000015	0.0784	0.027	556	0.08	1160	12	1153	13	2.1	1.3	0.197	1.2	0.9
FR-1-12-27.1	---	0.0916	0	203	0.49	1407	11	1458	17	3.1	1.3	0.244	0.9	0.7
FR-1-12-28.1	0.000028	0.1183	0.051	310	0.38	1892	12	1925	10	5.5	0.9	0.341	0.8	0.8
FR-1-12-29.1	0.000009	0.0770	0.017	357	0.25	1100	7	1119	34	2.0	1.9	0.186	0.7	0.4
FR-1-12-30.1	---	0.0766	0	50	0.84	1103	18	1110	53	2.0	3.2	0.187	1.8	0.6
FR-1-12-31.1	0.000049	0.1024	0.089	237	0.88	1651	14	1656	17	4.1	1.3	0.292	0.9	0.7
FR-1-12-32.1	0.000088	0.0588	0.162	124	0.37	446	5			0.6	3.9	0.072	1.2	0.3
FR-1-12-33.1	-0.000004	0.1003	-0.007	958	0.43	1636	9	1631	7	4.0	0.7	0.289	0.6	0.9
FR-1-12-34.1	0.000009	0.0558	0.016	1137	0.39	430	3			0.5	1.3	0.069	0.8	0.6
FR-1-12-35.1	0.000021	0.1051	0.039	201	0.66	1693	13	1712	15	4.3	1.2	0.300	0.9	0.7
FR-1-12-36.1	---	0.1068	0	248	0.24	1717	13	1746	13	4.5	1.1	0.305	0.8	0.8
FR-1-12-37.1	-0.000054	0.1118	-0.099	99	0.61	1814	21	1840	24	5.0	1.9	0.325	1.3	0.7
FR-1-12-38.1	0.000018	0.0753	0.033	412	0.32	1091	7	1071	18	1.9	1.1	0.184	0.7	0.6
FR-1-12-39.1	0.000028	0.1017	0.051	198	1.19	1637	36	1648	18	4.0	2.7	0.289	2.5	0.9
FR-1-12-40.1	0.000017	0.2015	0.031	83	0.78	2864	31	2837	13	15.5	1.6	0.559	1.3	0.9
FR-1-12-41.1	-0.000011	0.0775	-0.020	362	0.32	1107	16	1139	18	2.0	1.8	0.187	1.5	0.9
FR-1-12-42.1	---	0.0789	0	234	0.40	1138	9	1169	20	2.1	1.3	0.193	0.8	0.6
FR-1-12-43.1	0.000538	0.1113	0.984	1293	0.27	1585	13	1695	19	4.0	1.4	0.279	1.0	0.7
FR-1-12-44.1	-0.000027	0.0956	-0.050	190	0.73	1558	13	1547	18	3.6	1.4	0.273	1.0	0.7
FR-1-12-45.1	---	0.0741	0	1118	0.27	1039	13	1045	9	1.8	1.4	0.175	1.3	0.9
FR-1-12-46.1	---	0.0551	0	180	0.70	450	5			0.5	2.6	0.072	1.1	0.4
FR-1-12-47.1	0.000195	0.0730	0.357	77	0.75	967	12			1.6	3.6	0.162	1.4	0.4
FR-1-12-48.1	-0.000013	0.0916	-0.024	451	0.28	1453	9	1462	13	3.2	1.0	0.253	0.7	0.7
FR-1-12-49.1	0.000285	0.0730	0.521	21	0.00	1056	21			1.7	5.9	0.178	2.1	0.4
FR-1-12-50.1	0.000015	0.0790	0.028	736	1.20	1140	10	1167	13	2.1	1.1	0.193	0.9	0.8
FR-1-12-51.1	0.000010	0.0798	0.018	364	0.52	1200	24	1189	17	2.2	2.4	0.205	2.2	0.9
FR-1-12-52.1	0.000006	0.0857	0.011	772	0.37	1345	15	1329	9	2.7	1.4	0.232	1.3	0.9
FR-1-12-53.1	---	0.0582	0	357	0.51	462	3			0.6	1.7	0.074	0.8	0.4
FR-1-12-54.1	-0.000134	0.0556	-0.246	308	0.35	464	4			0.6	2.6	0.075	0.8	0.3
FR-1-12-55.1	0.000008	0.0914	0.015	613	0.45	1479	26	1453	10	3.2	2.1	0.258	2.0	1.0
FR-1-12-56.1	---	0.0838	0	156	0.37	1269	11	1288	24	2.5	1.6	0.218	1.0	0.6
FR-1-12-57.1	0.000100	0.0745	0.184	83	0.76	1080	13	1017	50	1.8	2.8	0.182	1.3	0.5
FR-1-12-58.1	0.000023	0.0897	0.042	267	0.50	1455	11	1412	39	3.1	2.2	0.253	0.9	0.4
FR-1-12-59.1	0.000024	0.1018	0.043	194	0.83	1662	13	1652	16	4.1	1.3	0.294	0.9	0.7
FR-1-12-60.1	0.000048	0.0783	0.088	337	0.35	1149	8	1137	19	2.1	1.2	0.195	0.7	0.6
	Flume Ridge Formation (FR) : FR-2 Western facies, near fault contact with Miramichi terrane. Tomah Mountain quadrangle, UTM Location 0599839E/5030305N													
FR-2euh-1.1	---	0.0561	-0.616	99	0.58	639	12			0.81	3.8	0.104	2.0	0.5
FR-2euh-2.1	0.000069	0.0600	0.030	123	1.33	595	17			0.79	4.2	0.097	3.0	0.7
FR-2euh-3.1	---	0.0598	-0.048	79	0.66	608	12			0.82	3.5	0.099	2.1	0.6
FR-2euh-4.1	0.000046	0.0578	-0.134	193	1.25	563	9			0.72	2.9	0.091	1.8	0.6
FR-2euh-5.1	-0.000048	0.0563	0.005	210	0.36	461	10			0.58	3.2	0.074	2.2	0.7
FR-2euh-6.1	---	0.0529	-0.462	59	0.87	475	11			0.56	5.0	0.077	2.3	0.5
FR-2euh-7.1	0.000068	0.0592	-0.109	213	0.71	607	10			0.79	2.7	0.099	1.7	0.6
FR-2euh-8.1	0.000025	0.056	-0.034	343	0.89	461	13			0.57	5.2	0.074	3.0	0.6

Appendix C: Continued.

sample[1]	measured $^{204}Pb/^{206}Pb$	measured $^{207}Pb/^{206}Pb$	%common ^{206}Pb	U (ppm)	Th/U	Age (Ma) $^{206}Pb/^{238}U^{2}$	err[4]	$^{207}Pb/^{206}Pb^{2,3}$	err[4]	$^{207}Pb/^{235}U^{5}$	err[4] (%)	$^{206}Pb/^{238}U^{5}$	err[4] (%)	err. corr.
FR-2euh-9.1	-0.000088	0.0558	-0.055	116	0.45	464	9			0.59	4.0	0.075	1.9	0.5
FR-2euh-10.1	---	0.0578	0.245	85	0.70	445	15			0.57	4.8	0.071	3.5	0.7
FR-2euh-11.1	---	0.0558	-0.045	504	0.46	457	7			0.56	2.2	0.073	1.6	0.8
FR-2-1.1	0.000073	0.0589	0.258	148	0.54	486	12			0.63	4.1	0.078	2.6	0.6
FR-2-2.1	0.000072	0.1002	-0.281	113	0.59	1667	28	1610	25	4.04	2.3	0.295	1.9	0.8
FR-2-3.1	---	0.0794	-0.204	165	0.43	1223	20	1183	27	2.29	2.3	0.209	1.8	0.8
FR-2-4.1	0.000107	0.0574	0.243	205	0.64	432	7			0.53	3.5	0.069	1.7	0.5
FR-2-5.1	0.000107	0.0564	0.065	432	1.05	447	9			0.54	3.0	0.072	2.1	0.7
FR-2-6.1	0.000032	0.0999	0.007	166	0.44	1621	26	1615	19	3.92	2.1	0.286	1.8	0.9
FR-2-7.1	---	0.0719	-0.174	101	0.49	1021	32			1.70	3.8	0.172	3.4	0.9
FR-2-8.1	0.000039	0.0964	-0.103	201	0.63	1570	24	1544	18	3.64	2.0	0.276	1.7	0.9
FR-2-9.1	---	0.0579	0.127	346	0.35	488	8		36	0.63	2.4	0.079	1.7	0.7
FR-2-10.1	0.000061	0.0992	0.175	140	0.56	1582	26	1594	22	3.77	2.2	0.278	1.9	0.8
FR-2-11.1	0.000078	0.0722	0.076	251	0.62	974	15			1.60	2.2	0.163	1.7	0.8
FR-2-12.1	0.000039	0.1138	0.291	117	0.16	1824	30	1853	32	5.11	2.6	0.327	1.9	0.7
FR-2-13.1	0.000096	0.0791	0.696	94	0.34	1026	19	1140	51	1.85	3.2	0.173	2.0	0.6
FR-2-14.1	0.000010	0.1848	0.290	146	1.09	2679	40	2695	10	13.12	1.9	0.515	1.8	0.9
FR-2-15.1	0.000154	0.0781	-0.053	123	0.78	1158	20	1094	39	2.06	2.7	0.197	1.9	0.7
FR-2-16.1	0.000120	0.0854	0.848	810	0.61	1160	24	1285	13	2.27	2.3	0.197	2.2	1.0
FR-2-17.1	0.000066	0.0817	0.169	158	0.46	1206	20	1217	27	2.29	2.3	0.206	1.8	0.8
FR-2-18.1	0.000014	0.0894	0.395	239	0.42	1343	22	1408	22	2.85	2.1	0.232	1.8	0.8
FR-2-19.1	0.000073	0.1005	-0.078	76	0.54	1642	30	1614	30	3.98	2.6	0.290	2.1	0.8
FR-2-20.1	0.000139	0.0805	0.420	75	0.24	1123	33	1161	46	2.06	4.0	0.190	3.2	0.8
FR-2-21.1	0.000027	0.0881	0.207	111	0.39	1347	23	1375	26	2.81	2.3	0.232	1.9	0.8
FR-2-22.1	0.000049	0.0632	-0.092	299	0.25	738	12			1.04	2.4	0.121	1.8	0.7
FR-2-23.1	0.000358	0.0713	-0.344	41	0.70	1038	24			1.59	6.1	0.175	2.5	0.4
FR-2-24.1	0.000067	0.0582	0.219	164	0.52	471	8			0.60	3.5	0.076	1.8	0.5
FR-2-25.1	0.000023	0.0615	0.087	327	0.53	632	12			0.87	2.6	0.103	2.1	0.8
FR-2-26.1	---	0.0757	-0.183	113	0.85	1125	21	1087	33	1.99	2.7	0.191	2.1	0.8
FR-2-27.1	---	0.0569	0.056	44	0.55	471	12			0.59	10.1	0.076	2.7	0.3
FR-2-28.1	0.000010	0.1108	0.049	468	0.25	1805	25	1810	10	4.93	1.7	0.323	1.6	0.9
FR-2-29.1	0.000088	0.0550	-0.180	219	0.92	469	8			0.56	3.2	0.075	1.8	0.5
FR-2-30.1	-0.000066	0.0715	-0.328	70	1.15	1047	21			1.76	3.3	0.176	2.1	0.6
FR-2-31.1	0.000026	0.0559	0.008	456	0.86	445	7			0.55	2.3	0.071	1.6	0.7
FR-2-32.1	0.000060	0.0755	-0.025	374	0.48	1085	17	1058	22	1.89	2.0	0.183	1.7	0.8
FR-2-33.1	0.000075	0.0618	0.271	103	0.72	589	11			0.80	3.7	0.096	1.9	0.5
FR-2-34.1	0.000018	0.0892	-0.671	325	0.40	1519	23	1404	28	3.26	2.2	0.266	1.7	0.8
FR-2-35.1	---	0.0560	-0.041	252	0.70	467	11			0.58	3.1	0.075	2.4	0.8
FR-2-36.1	0.000349	0.0984	-0.401	58	0.84	1644	33	1498	47	3.74	3.3	0.290	2.2	0.7
FR-2-37.1	---	0.0771	0.540	10	1.81	1006	44	1123	112	1.80	7.3	0.169	4.7	0.6
FR-2-38.1	---	0.0809	-0.007	227	0.32	1220	19	1218	20	2.32	2.0	0.208	1.7	0.9
FR-2-39.1	-0.000213	0.0751	0.544	23	1.23	954	27	1151	106	1.72	6.1	0.160	3.1	0.5
FR-2-40.1	---	0.0735	-0.014	72	0.42	1031	20	1028	41	1.76	2.9	0.173	2.1	0.7
FR-2-41.1	0.000027	0.0915	0.026	230	0.66	1453	22	1450	18	3.18	2.0	0.253	1.7	0.9
FR-2-42.1	0.000085	0.0602	0.215	91	0.53	548	11			0.72	4.0	0.089	2.0	0.5
FR-2-43.1	0.000074	0.0794	0.377	238	0.35	1104	17	1156	26	2.02	2.2	0.187	1.7	0.8
FR-2-44.1	---	0.0786	0.460	37	0.73	1065	27	1161	58	1.95	4.0	0.180	2.7	0.7
FR-2-45.1	0.000009	0.0568	0.009	1109	0.38	481	7			0.60	1.8	0.077	1.6	0.9
FR-2-46.1	---	0.0734	0.106	131	1.15	1002	18	1026	35	1.70	2.6	0.168	1.9	0.7
FR-2-47.1	0.000792	0.0639	1.029	317	0.27	433	8			0.50	5.4	0.069	2.0	0.4

Appendix C: Continued.

sample[1]	measured $^{204}Pb/^{206}Pb$	measured $^{207}Pb/^{206}Pb$	%common ^{206}Pb	U (ppm)	Th/U	Age (Ma) $^{206}Pb/^{238}U^{2}$	err[4]	$^{207}Pb/^{206}Pb^{2,3}$	err[4]	$^{207}Pb/^{235}U^{5}$	err[4] (%)	$^{206}Pb/^{238}U^{5}$	err[4] (%)	err. corr.
FR-2-48.1	0.000256	0.0602	0.065	81	0.53	590	12			0.75	6.3	0.096	2.2	0.4
FR-2-49.1	0.000120	0.0592	0.488	119	1.25	425	9			0.54	5.0	0.068	2.2	0.4
FR-2-50.1	0.000049	0.0550	-0.159	224	0.64	464	12			0.56	3.7	0.075	2.7	0.7
FR-2-51.1	---	0.0735	-0.103	140	0.51	1050	19	1027	35	1.79	2.6	0.177	1.9	0.7
FR-2-52.1	0.000062	0.0601	0.356	184	0.53	500	9			0.66	3.3	0.081	1.8	0.5
FR-2-53.1	---	0.1064	-0.302	140	0.32	1779	29	1739	18	4.66	2.1	0.318	1.8	0.9
FR-2-54.1	0.000070	0.0583	0.080	364	0.50	516	8			0.66	2.4	0.083	1.6	0.7
FR-2-55.1	---	0.0570	-0.425	75	1.52	617	13			0.79	4.0	0.100	2.2	0.5
FR-2-56.1	0.000046	0.0903	-0.008	123	0.45	1433	50	1419	25	3.08	4.1	0.249	3.9	0.9
FR-2-57.1	0.000037	0.0774	-0.011	242	0.36	1134	18	1119	25	2.04	2.1	0.192	1.7	0.8
FR-2-58.1	0.000055	0.0956	0.127	102	0.76	1519	26	1525	26	3.47	2.4	0.266	1.9	0.8
FR-2-59.1	0.000023	0.0562	-0.024	455	0.77	466	7			0.58	3.5	0.075	1.6	0.5
FR-2-60.1	---	0.1150	-0.431	62	0.78	1931	37	1880	25	5.54	2.6	0.349	2.2	0.8
FR-2-61.1	0.000041	0.0558	-0.090	256	0.71	472	8			0.58	2.8	0.076	1.7	0.6
FR-2-62.1	0.000019	0.1123	-0.413	129	1.87	1887	33	1833	19	5.25	2.3	0.340	2.0	0.9
FR-2-63.1	0.000021	0.0581	-0.056	534	0.88	552	12			0.71	2.6	0.089	2.2	0.8
FR-2-64.1	0.000010	0.1016	-0.282	904	1.90	1693	23	1651	10	4.20	1.7	0.300	1.6	0.9
FR-2-65.1	---	0.0785	-0.032	129	0.81	1167	20	1161	29	2.15	2.4	0.198	1.9	0.8
FR-2-66.1	-0.000024	0.0813	-0.072	136	0.53	1243	22	1237	48	2.39	3.1	0.213	1.9	0.6
FR-2-67.1	0.000061	0.0810	0.038	63	0.43	1212	24	1200	45	2.28	3.2	0.207	2.2	0.7
FR-2-68.1	---	0.1954	3.119	67	0.74	2601	49	2788	18	13.39	2.5	0.497	2.3	0.9
FR-2-69.1	0.000090	0.0776	0.156	252	0.61	1103	132	1104	120	1.96	14.4	0.187	13.1	0.9
FR-2-70.1	0.000141	0.0768	0.003	40	0.72	1113	27	1063	84	1.94	5.0	0.189	2.6	0.5
	Appleton Ridge Formation (AR) : AR-1 Appleton Ridge type locality. Searsmont quadrangle, UTM Location 478363E/4903810N													
MEWFT-2-1.1	0.000042	0.0719	0.071	105	0.41	997	11			1.65	2.2	0.167	1.2	0.6
MEWFT-2-2.1	-0.000012	0.0866	-0.019	267	0.41	1334	14	1354	13	2.75	1.3	0.230	1.1	0.9
MEWFT-2-3.1	-0.000015	0.0742	-0.026	292	0.18	1008	12	1051	17	1.74	1.6	0.169	1.3	0.8
MEWFT-2-4.1	-0.000040	0.0721	-0.069	110	0.51	995	11	1005	62	1.67	3.3	0.167	1.2	0.4
MEWFT-2-5.1	0.000154	0.1039	0.245	589	0.46	1453	17	1656	13	3.55	1.5	0.253	1.3	0.9
MEWFT-2-6.1	0.000073	0.0836	0.122	122	0.4	1194	20	1258	31	2.32	2.4	0.203	1.8	0.7
MEWFT-2-7.1	0.001025	0.0791	1.795	49	0.61	1046	16			1.56	11.0	0.176	1.6	0.1
MEWFT-2-8.1	0.000170	0.0730	0.292	51	0.45	1032	13			1.69	4.5	0.174	1.4	0.3
MEWFT-2-9.1	0.000032	0.0856	0.053	155	0.75	1320	14	1318	21	2.67	1.6	0.227	1.2	0.7
MEWFT-2-10.1	0.000902	0.0716	1.609	25	0.98	973	19			1.31	17.7	0.163	2.1	0.1
MEWFT-2-11.1	0.000109	0.0571	0.196	133	0.79	474	9			0.58	5.3	0.076	1.9	0.4
MEWFT-2-12.1	0.000254	0.0742	0.437	36	0.89	956	21			1.55	6.7	0.160	2.4	0.4
MEWFT-2-13.1	0.000113	0.1219	0.173	183	0.34	1975	20	1961	15	5.95	1.4	0.358	1.2	0.8
MEWFT-2-14.1	0.000064	0.0824	0.107	227	0.47	1158	17	1232	31	2.21	2.3	0.197	1.6	0.7
MEWFT-2-15.1	0.000259	0.0593	0.467	166	0.48	461	7			0.57	6.2	0.074	1.6	0.3
MEWFT-2-16.1	0.000150	0.0783	0.253	58	0.48	996	12	1098	87	1.75	4.6	0.167	1.4	0.3
MEWFT-2-17.1	0.000229	0.0824	0.384	111	0.32	1188	13	1176	72	2.21	3.8	0.202	1.2	0.3
MEWFT-2-18.1	0.000225	0.0765	0.384	87	0.28	1003	22	1020	72	1.70	4.3	0.168	2.4	0.6
MEWFT-2-19.1	---	0.0733	0	127	0.55	998	11	1021	22	1.69	1.6	0.167	1.2	0.7
MEWFT-2-20.1	0.000018	0.0705	0.030	742	0.34	969	12			1.57	1.5	0.162	1.4	0.9
MEWFT-2-21.1	0.000181	0.0745	0.310	45	0.34	999	13			1.66	4.7	0.168	1.4	0.3
MEWFT-2-22.1	0.000019	0.0766	0.033	1506	0.02	912	9	1103	8	1.60	1.1	0.152	1.1	0.9
MEWFT-2-23.1	0.000478	0.0845	0.804	33	0.46	1228	18	1138	136	2.25	7.1	0.210	1.6	0.2
MEWFT-2-24.1	0.000120	0.0575	0.216	552	0.68	466	5			0.58	2.4	0.075	1.1	0.5

Appendix C: Continued.

sample[1]	measured $^{204}Pb/^{206}Pb$	measured $^{207}Pb/^{206}Pb$	%common ^{206}Pb	U (ppm)	Th/U	Age (Ma) $^{206}Pb/^{238}U^{2}$	err[4]	$^{207}Pb/^{206}Pb^{2,3}$	err[4]	$^{207}Pb/^{235}U^{5}$	err[4] (%)	$^{206}Pb/^{238}U^{5}$	err[4] (%)	err. corr.
MEWFT-2-25.1	0.000037	0.0762	0.063	212	0.22	1074	11	1087	23	1.89	1.6	0.181	1.1	0.7
MEWFT-2-26.1	-0.000046	0.0608	-0.081	109	1	453	5			0.62	3.3	0.073	1.2	0.4
MEWFT-2-27.1	-0.000023	0.0583	-0.041	200	0.62	471	6			0.61	2.3	0.076	1.3	0.6
MEWFT-2-28.1	0.000042	0.1031	0.067	56	0.83	1663	19	1670	26	4.16	1.9	0.294	1.3	0.7
MEWFT-2-29.1	0.000034	0.0853	0.056	664	0.2	1260	14	1309	10	2.52	1.3	0.216	1.2	0.9
MEWFT-2-30.1	0.000063	0.0566	0.114	237	0.58	467	5			0.58	2.8	0.075	1.2	0.4
MEWFT-2-31.1	0.000098	0.0735	0.167	62	0.45	1046	13			1.75	3.2	0.176	1.3	0.4
MEWFT-2-32.1	0	0.0582	0	169	0.79	474	5			0.61	2.0	0.076	1.2	0.6
MEWFT-2-33.1	0.000247	0.0739	0.424	81	0.45	980	21			1.59	4.7	0.164	2.3	0.5
MEWFT-2-34.1	---	0.0573	0	450	0.43	463	7			0.59	2.0	0.074	1.7	0.8
MEWFT-2-35.1	0.000138	0.0702	0.239	49	0.35	978	13			1.54	4.5	0.164	1.4	0.3
MEWFT-2-36.1	-0.000036	0.0733	-0.062	169	0.44	1027	11	1036	26	1.76	1.7	0.173	1.2	0.7
MEWFT-2-37.1	0.000040	0.0935	0.065	282	0.18	1449	15	1487	14	3.23	1.4	0.252	1.1	0.8
MEWFT-2-38.1	-0.000010	0.0970	-0.016	395	0.41	1544	23	1570	9	3.63	1.7	0.271	1.7	1.0
MEWFT-2-39.1	0.000026	0.0996	0.042	96	0.43	1632	18	1609	19	3.94	1.6	0.288	1.2	0.8
MEWFT-2-41.1	0.000042	0.0943	0.068	172	0.65	1461	18	1502	18	3.29	1.7	0.254	1.4	0.8
MEWFT-2-42.1	0.000807	0.0576	1.508	80	2.56	472	7			0.48	16.2	0.076	1.5	0.1
MEWFT-2-43.1	0.000004	0.0599	0.007	858	0.57	605	7			0.81	1.4	0.098	1.2	0.9
MEWFT-2-44.1	-0.000080	0.0560	-0.144	182	0.74	467	5			0.59	3.4	0.075	1.2	0.4
MEWFT-2-45.1	0.001180	0.0626	2.206	24	0.5	470	12			0.47	36.6	0.076	2.7	0.1
MEWFT-2-46.1	0.000137	0.0743	0.233	112	0.45	1060	12			1.78	2.7	0.179	1.2	0.4
MEWFT-2-47.1	-0.000032	0.0569	-0.057	281	0.68	473	5			0.60	2.1	0.076	1.1	0.6
MEWFT-2-48.1	0.000144	0.0842	0.239	177	0.25	1251	16	1249	32	2.43	2.1	0.214	1.4	0.6
MEWFT-2-49.1	-0.000009	0.0865	-0.014	182	0.41	1338	14	1352	15	2.76	1.4	0.231	1.2	0.8
MEWFT-2-50.1	0.000089	0.0727	0.153	92	0.47	1018	16			1.68	2.9	0.171	1.7	0.6
MEWFT-2-51.1	0.000028	0.0769	0.047	681	0.23	1023	12	1108	12	1.81	1.4	0.172	1.3	0.9
MEWFT-2-52.1	0.000272	0.0802	0.459	53	0.78	1168	32	1103	86	2.09	5.3	0.199	3.0	0.6
MEWFT-2-53.1	0.000038	0.0640	0.067	345	0.16	635	13			0.91	2.5	0.103	2.1	0.9
MEWFT-2-54.1	0.000249	0.0730	0.429	85	0.62	1017	12			1.64	4.1	0.171	1.3	0.3
MEWFT-2-55.1	0.000355	0.0937	0.580	73	0.77	1441	25	1399	61	3.07	3.7	0.250	2.0	0.5
MEWFT-2-56.1	-0.000007	0.0987	-0.012	657	0.26	1250	21	1601	7	2.92	1.8	0.214	1.8	1.0
MEWFT-2-57.1	0.000193	0.1085	0.303	272	0.69	1679	17	1728	18	4.34	1.5	0.298	1.1	0.8
MEWFT-2-58.1	-0.000157	0.0628	-0.274	90	0.76	465	12			0.67	5.6	0.075	2.7	0.5
MEWFT-2-59.1	-0.000013	0.0576	-0.023	364	0.51	466	5			0.60	1.7	0.075	1.1	0.7
MEWFT-2-60.1	0.000510	0.0949	0.835	353	0.43	1307	16	1377	34	2.72	2.2	0.225	1.3	0.6
CENTRAL MAINE/AROOSTOOK-MATAPEDIA BASIN														
Mayflower Hill Formation (MH) :MH-1 Lower part of formation near contact with Smyrna Mills Fm (Waterville Fm equivalent), Rollins Mountain. East Winn quadrangle, UTM Location 0548340E/5029038N														
MH1-12-1.1	0.000064	0.0555	0.117	311	0.54	439	6			0.5	2.3	0.071	1.3	0.6
MH1-12-2.1	0.000123	0.0576	0.226	1197	0.61	466	3			0.6	1.3	0.075	0.7	0.5
MH1-12-3.1	0.000040	0.0562	0.072	800	1.00	435	4			0.5	1.4	0.070	1.0	0.7
MH1-12-4.1	0.000032	0.0591	0.059	504	0.77	443	5			0.6	1.6	0.071	1.1	0.7
MH1-12-5.1	0.000004	0.0561	0.008	3061	0.77	446	7			0.6	1.8	0.072	1.7	1.0
MH1-12-6.1	0.000007	0.0883	0.014	1377	0.45	1365	12	1387	7	2.9	1.0	0.236	1.0	0.9
MH1-12-7.1	---	0.0574	0	869	1.23	441	6			0.6	1.7	0.071	1.4	0.8
MH1-12-8.1	0.000013	0.0869	0.025	188	0.49	1325	12	1353	19	2.7	1.4	0.228	1.0	0.7
MH1-12-9.1	---	0.0548	0	320	0.75	423	7			0.5	2.4	0.068	1.7	0.7
MH1-12-10.1	0.000009	0.0572	0.017	927	0.88	445	6			0.6	1.9	0.071	1.4	0.8
MH1-12-11.1	0.000033	0.0973	0.060	1180	0.08	1489	12	1563	6	3.5	0.9	0.260	0.9	0.9

Appendix C: Continued.

sample[1]	measured $^{204}Pb/^{206}Pb$	measured $^{207}Pb/^{206}Pb$	%common ^{206}Pb	U (ppm)	Th/U	Age (Ma) $^{206}Pb/^{238}U^{2}$	err[4]	$^{207}Pb/^{206}Pb^{2,3}$	err[4]	$^{207}Pb/^{235}U^{5}$	err[4] (%)	$^{206}Pb/^{238}U^{5}$	err[4] (%)	err. corr.
MH1-12-12.1	---	0.1075	0	895	0.16	1783	18	1758	6	4.7	1.2	0.319	1.2	1.0
MH1-12-13.1	0.000042	0.0572	0.077	658	0.74	432	5			0.5	1.8	0.069	1.2	0.7
MH1-12-14.1	0.000029	0.0903	0.053	182	0.35	1388	12	1424	20	3.0	1.4	0.240	1.0	0.7
MH1-12-15.1	0.000210	0.0997	0.384	253	0.49	1558	18	1563	18	3.6	1.6	0.273	1.3	0.8
MH1-12-16.1	0.000139	0.0724	0.254	768	0.10	775	13			1.2	1.9	0.128	1.7	0.9
MH1-12-17.1*	0.000078	0.1334	0.142	873	0.39	1533	10	2129	7	4.9	0.8	0.268	0.7	0.9
MH1-12-18.1	---	0.0999	0	381	0.69	1607	16	1622	10	3.9	1.3	0.283	1.2	0.9
MH1-12-19.1	0.000006	0.1077	0.011	609	0.30	1711	15	1760	8	4.5	1.1	0.304	1.0	0.9
MH1-12-20.1	0.000425	0.0603	0.778	346	1.16	434	4			0.5	3.8	0.070	0.9	0.2
MH1-12-21.1	0.000018	0.0859	0.033	473	0.80	1342	17	1330	11	2.7	1.5	0.231	1.4	0.9
MH1-12-22.1	0.000020	0.0941	0.036	1192	0.65	1533	15	1505	6	3.5	1.2	0.268	1.1	1.0
MH1-12-23.1	-0.000019	0.0558	-0.035	432	0.83	425	3			0.5	1.7	0.068	0.8	0.5
MH1-12-24.1	0.000008	0.1164	0.014	218	0.92	1825	16	1899	22	5.2	1.5	0.327	1.0	0.6
MH1-12-25.1	0.000067	0.0740	0.122	224	0.63	1026	13	1016	24	1.7	1.8	0.173	1.3	0.7
MH1-12-26.1	0.000011	0.1006	0.020	567	1.07	1597	14	1632	9	3.9	1.1	0.281	1.0	0.9
MH1-12-27.1	---	0.0731	0	257	0.39	1004	7	1017	19	1.7	1.2	0.169	0.8	0.7
MH1-12-28.1	0.000595	0.0845	1.090	110	0.28	1067	11	1096	59	1.9	3.2	0.180	1.1	0.4
MH1-12-29.1	0.000011	0.0941	0.020	865	0.53	1481	18	1507	7	3.3	1.4	0.258	1.3	1.0
MH1-12-30.1	0.000013	0.1001	0.024	443	0.42	1630	11	1622	10	4.0	0.9	0.288	0.8	0.8
MH1-12-31.1	0.000004	0.0811	0.007	635	0.34	1172	8	1223	51	2.2	2.7	0.199	0.7	0.3
MH1-12-32.1	---	0.0734	0	134	1.45	1026	11	1025	54	1.7	2.9	0.173	1.2	0.4
MH1-12-33.1	0.000022	0.0970	0.040	378	0.93	1492	28	1561	12	3.5	2.2	0.260	2.1	1.0
MH1-12-34.1	0.000051	0.1006	0.093	251	0.94	1619	13	1623	15	3.9	1.2	0.285	0.9	0.8
MH1-12-35.1	0.000364	0.0558	0.665	164	0.83	464	4			0.5	4.6	0.075	1.0	0.2
MH1-12-36.1	0.000005	0.1097	0.009	667	0.23	1764	11	1793	13	4.8	1.0	0.315	0.7	0.7
MH1-12-37.1	-0.000006	0.0862	-0.011	408	0.63	1320	25	1345	12	2.7	2.2	0.227	2.1	1.0
MH1-12-38.1	0.000109	0.0539	0.200	257	0.73	437	4			0.5	2.8	0.070	0.9	0.3
MH1-12-39.1	0.000005	0.1078	0.008	1000	0.67	1734	23	1761	5	4.6	1.5	0.309	1.5	1.0
MH1-12-40.1	0.000023	0.1090	0.042	277	0.35	1601	23	1778	31	4.2	2.3	0.282	1.6	0.7
MH1-12-41.1	0.000043	0.0821	0.078	1072	0.03	1024	21	1234	37	1.9	2.9	0.172	2.2	0.8
MH1-12-42.1	0.000008	0.1018	0.015	204	0.55	1618	21	1655	27	4.0	2.1	0.285	1.5	0.7
MH1-12-43.1	-0.000045	0.0878	-0.082	57	0.88	1316	17	1391	36	2.8	2.4	0.226	1.4	0.6
MH1-12-44.1	0.000027	0.0868	0.050	385	0.51	1350	19	1348	14	2.8	1.8	0.233	1.6	0.9
MH1-12-45.1	0.000005	0.1865	0.010	204	0.39	2702	20	2711	7	13.4	1.0	0.521	0.9	0.9
MH1-12-46.1	0.000046	0.0845	0.084	1086	0.39	1225	23	1290	10	2.4	2.1	0.209	2.1	1.0
MH1-12-47.1	0.000007	0.0999	0.012	279	0.93	1622	12	1620	12	3.9	1.0	0.286	0.8	0.8
MH1-12-48.1	-0.000021	0.0875	-0.038	203	0.38	1419	11	1378	17	3.0	1.3	0.246	0.9	0.7
MH1-12-49.1	0.000010	0.0931	0.019	678	0.39	1437	10	1486	9	3.2	0.9	0.250	0.7	0.8
MH1-12-50.1	---	0.0935	0	319	0.95	1544	11	1499	13	3.5	1.1	0.271	0.8	0.8
MH1-12-51.1	0.000012	0.0944	0.022	319	0.43	1464	23	1513	25	3.3	2.2	0.255	1.7	0.8
MH1-12-52.1	0.000025	0.0747	0.047	280	0.29	997	14	1050	22	1.7	1.8	0.167	1.5	0.8
MH1-12-53.1	0.000028	0.0698	0.051	586	0.29	621	4			1.0	1.2	0.101	0.8	0.6
MH1-12-54.1	---	0.0760	0	1198	0.04	1087	13	1094	8	1.9	1.4	0.184	1.3	1.0
MH1-12-55.1	---	0.0676	0	370	0.24	737	8			1.1	1.5	0.121	1.1	0.8
MH1-12-56.1	---	0.1251	0	488	0.62	1983	29	2030	7	6.2	1.7	0.360	1.7	1.0
MH1-12-57.1	0.000007	0.1018	0.013	301	1.03	1661	12	1655	12	4.1	1.1	0.294	0.8	0.8
MH1-12-58.1	0.000043	0.0739	0.079	149	0.35	1020	19	1022	30	1.7	2.5	0.171	2.0	0.8
MH1-12-59.1	0.000263	0.0587	0.482	777	0.67	465	7			0.6	2.4	0.075	1.6	0.7
MH1-12-60.1	0.000020	0.0808	0.037	274	0.25	1200	10	1208	18	2.3	1.3	0.205	0.9	0.7
MH1-12-61.1	0.000020	0.0915	0.037	198	0.48	1525	14	1451	16	3.4	1.3	0.267	1.0	0.8

Appendix C: Continued.

sample[1]	measured $^{204}Pb/^{206}Pb$	measured $^{207}Pb/^{206}Pb$	%common ^{206}Pb	U (ppm)	Th/U	Age (Ma) $^{206}Pb/^{238}U^{2}$	err[4]	$^{207}Pb/^{206}Pb^{2,3}$	err[4]	$^{207}Pb/^{235}U^{5}$	err[4] (%)	$^{206}Pb/^{238}U^{5}$	err[4] (%)	err. corr.
MH1-12-62.1	0.000045	0.0724	0.082	438	0.74	1020	13			1.7	1.6	0.171	1.4	0.8
MH1-12-63.1	0.000027	0.0578	0.049	892	0.73	472	3			0.6	1.3	0.076	0.7	0.6
MH1-12-64.1	0.000031	0.0936	0.057	652	0.18	1543	24	1491	10	3.5	1.8	0.270	1.8	1.0
MH1-12-65.1	---	0.0552	0	735	0.34	449	5			0.5	1.4	0.072	1.1	0.8
MH1-12-66.1	0.000075	0.0557	0.137	703	0.60	434	3			0.5	1.9	0.070	0.8	0.4
MH1-12-67.1	0.000016	0.1021	0.029	243	0.61	1703	13	1658	13	4.2	1.1	0.302	0.9	0.8
MH1-12-68.1	0.000003	0.0894	0.006	1171	0.30	1365	12	1411	6	2.9	1.0	0.236	1.0	0.9
MH1-12-69.1	---	0.1873	0	280	0.66	2720	20	2719	7	13.6	1.0	0.525	0.9	0.9
	Mayflower Hill Formation (MH) : MH-2 Mayflower Hill, base of Mayflower Hill Formation. Waterville quadrangle, UTM Location 447348E; 4932181N													
MGS13-01-1.1	-0.000049	0.0881	0.207	103	0.46	1349	14	1399	28	2.8	1.9	0.233	1.2	0.6
MGS13-01-2.1	0.000401	0.080	1.059	18	1.30	965	41	1048	154	1.7	8.9	0.161	4.6	0.5
MGS13-01-3.1	0.000057	0.0738	-0.277	113	0.59	1096	12	1015	36	1.9	2.1	0.185	1.1	0.5
MGS13-01-4.1	0.000009	0.1141	0.002	204	0.46	1865	15	1863	16	5.3	1.3	0.335	0.9	0.7
MGS13-01-5.1	-0.000010	0.0744	0.069	363	0.66	1037	8	1055	19	1.8	1.2	0.174	0.8	0.7
MGS13-01-6.1	0.000043	0.0823	0.205	61	0.20	1213	16	1239	39	2.3	2.5	0.207	1.4	0.6
MGS13-01-7.1	0.000011	0.0737	-0.056	602	1.44	1045	7	1028	15	1.8	1.0	0.176	0.7	0.7
MGS13-01-8.1	0.000051	0.0711	-0.038	226	0.62	968	8			1.6	1.7	0.162	0.9	0.5
MGS13-01-9.1	0.000017	0.2139	1.175	723	0.41	2881	32	2934	4	16.6	1.4	0.563	1.4	1.0
MGS13-01-10.1	0.000068	0.1011	0.589	217	1.24	1554	12	1627	27	3.8	1.7	0.273	0.9	0.5
MGS13-01-11.1	---	0.0760	0.202	164	0.52	1051	10	1094	27	1.9	1.7	0.177	1.0	0.6
MGS13-01-12.1	0	0.0717	0.234	122	0.52	922	10			1.5	2.0	0.154	1.1	0.5
MGS13-01-13.1	0.000059	0.1927	0.893	41	0.40	2714	153	2760	107	13.9	9.5	0.524	6.9	0.7
MGS13-01-14.1	0.000020	0.0737	-0.009	1327	0.07	1035	6	1026	11	1.8	0.8	0.174	0.7	0.8
MGS13-01-15.1	0.000008	0.0772	-0.127	843	1.19	1151	8	1122	12	2.1	1.0	0.195	0.8	0.8
MGS13-01-16.1	0.000004	0.1011	-0.068	1708	1.18	1654	9	1643	6	4.1	0.7	0.293	0.6	0.9
MGS13-01-17.1	0	0.1916	1.327	235	0.81	2680	20	2756	8	13.6	1.0	0.515	0.9	0.9
MGS13-01-18.1	0.000051	0.0796	0.279	297	0.22	1130	9	1170	22	2.1	1.4	0.192	0.9	0.6
MGS13-01-19.1	0.000205	0.0560	-0.100	151	0.57	482	8			0.6	4.2	0.078	1.7	0.4
MGS13-01-20.1	-0.000116	0.0717	-0.348	64	0.53	1058	14	1025	56	1.8	3.1	0.178	1.5	0.5
MGS13-01-21.1	0.000005	0.0738	0.034	1394	0.15	1029	6	1034	9	1.8	0.8	0.173	0.6	0.8
MGS13-01-22.1	0.000251	0.0761	0.257	43	0.60	1038	17	1000	81	1.7	4.4	0.175	1.7	0.4
MGS13-01-23.1	---	0.0820	0.475	21	0.39	1151	26	1245	70	2.2	4.3	0.196	2.4	0.6
MGS13-01-24.1	0	0.0572	0.217	65	0.85	432	6			0.5	7.8	0.069	1.5	0.2
MGS13-01-25.1	0.000209	0.0688	-0.466	52	1.38	998	14			1.5	4.1	0.167	1.6	0.4
MGS13-01-26.1	0.000011	0.0771	0.129	286	0.37	1096	8	1120	19	2.0	1.3	0.185	0.8	0.7
MGS13-01-27.1	0	0.1135	-0.001	110	0.04	1856	18	1856	18	5.2	1.5	0.334	1.1	0.8
MGS13-01-28.1	0.000020	0.0917	0.117	253	0.91	1442	18	1456	17	3.2	1.6	0.251	1.4	0.8
MGS13-01-29.1	0.000024	0.1047	0.062	244	0.87	1699	13	1703	14	4.3	1.1	0.302	0.9	0.8
MGS13-01-30.1	0	0.0758	0.102	156	0.67	1068	20	1090	32	1.9	2.6	0.180	2.0	0.8
MGS13-01-31.1	---	0.0573	0.243	732	0.53	427	5			0.5	1.7	0.069	1.2	0.7
MGS13-01-32.1	-0.000133	0.0670	-0.902	30	0.37	1051	21			1.7	5.5	0.177	2.2	0.4
MGS13-01-33.1	0.000028	0.1122	-0.041	232	0.58	1839	25	1829	51	5.1	3.2	0.330	1.6	0.5
MGS13-01-34.1	0.000021	0.0887	0.073	154	0.53	1385	14	1392	25	2.9	1.7	0.240	1.1	0.7
MGS13-01-35.1	0	0.0556	-0.132	28	0.44	477	13			0.6	7.4	0.077	2.8	0.4
MGS13-01-36.1	-0.000080	0.0821	-0.286	80	0.58	1303	17	1274	40	2.6	2.5	0.224	1.4	0.6
MGS13-01-37.1	-0.000013	0.0815	0.310	339	0.35	1173	12	1238	20	2.2	1.5	0.200	1.1	0.7
MGS13-01-38.1	0	0.0790	-0.416	63	0.33	1253	23	1172	46	2.3	3.1	0.215	2.0	0.7
MGS13-01-39.1	0.000118	0.0543	-0.269	157	0.70	468	6			0.5	3.8	0.075	1.3	0.3

Appendix C: Continued.

sample[1]	measured $^{204}Pb/^{206}Pb$	measured $^{207}Pb/^{206}Pb$	%common ^{206}Pb	U (ppm)	Th/U	Age (Ma) $^{206}Pb/^{238}U^{2}$	err[4]	$^{207}Pb/^{206}Pb^{2,3}$	err[4]	$^{207}Pb/^{235}U^{5}$	err[4] (%)	$^{206}Pb/^{238}U^{5}$	err[4] (%)	err. corr.
MGS13-01-40.1	0	0.0764	-0.118	378	0.44	1130	22	1106	20	2.0	2.3	0.192	2.1	0.9
MGS13-01-41.1	0.000102	0.0734	-0.006	212	0.72	1025	10			1.7	1.9	0.172	1.0	0.5
MGS13-01-42.1	---	0.0871	-0.025	61	0.32	1367	20	1362	115	2.8	6.2	0.236	1.6	0.3
MGS13-01-43.1	0.000091	0.0946	0.116	91	0.44	1499	40	1494	32	3.4	3.4	0.262	3.0	0.9
MGS13-01-44.1	-0.000026	0.0867	0.131	478	0.40	1332	10	1363	14	2.8	1.1	0.229	0.8	0.7
MGS13-01-45.1	0	0.0877	0.049	361	0.32	1368	11	1377	16	2.9	1.2	0.236	0.9	0.7
MGS13-01-46.1	0.000030	0.1855	-0.007	235	1.55	2703	21	2700	8	13.3	1.1	0.521	1.0	0.9
MGS13-01-47.1	0.000093	0.1246	0.051	67	0.64	2015	27	2005	26	6.2	2.1	0.367	1.5	0.7
MGS13-01-48.1	-0.000044	0.0766	-0.080	85	0.42	1128	14	1126	79	2.0	4.2	0.191	1.4	0.3
MGS13-01-49.1	0.000059	0.1174	0.482	38	0.92	1857	32	1904	35	5.4	2.8	0.334	2.0	0.7
MGS13-01-50.1	-0.000058	0.0797	0.569	74	0.75	1074	15	1211	47	2.0	2.8	0.181	1.5	0.5
MGS13-01-51.1	0.000014	0.1019	-0.077	183	0.80	1669	16	1655	18	4.1	1.5	0.295	1.1	0.7
MGS13-01-52.1	0.000042	0.0731	-0.479	90	0.32	1120	14	1001	50	1.9	2.8	0.190	1.4	0.5
MGS13-01-53.1	0.000073	0.0775	0.138	225	0.42	1104	10	1107	28	2.0	1.7	0.187	1.0	0.6
MGS13-01-54.1	0.000020	0.1123	-0.091	242	0.37	1847	16	1832	14	5.1	1.3	0.332	1.0	0.8
MGS13-01-55.1	---	0.0700	-0.552	60	0.50	1054	16			1.7	3.0	0.178	1.6	0.5
MGS13-01-56.1	---	0.0738	0	84	0.60	1037	24	1037	43	1.8	3.3	0.174	2.5	0.8
MGS13-01-57.1	0.000035	0.0564	-0.012	271	0.35	471	4			0.6	2.4	0.076	0.9	0.4
MGS13-01-58.1	0.000038	0.0749	0.228	398	0.54	1016	9	1052	23	1.8	1.5	0.171	1.0	0.6
MGS13-01-59.1	-0.000029	0.0724	-0.149	206	0.42	1031	31	1009	34	1.7	3.6	0.173	3.2	0.9
MGS13-01-60.1	0.000544	0.0769	0.481	79	0.66	1005	19			1.6	5.6	0.169	2.1	0.4
MGS13-01-61.1	0.000012	0.0869	-0.204	563	1.06	1395	11	1355	14	2.9	1.1	0.242	0.9	0.8
MGS13-01-62.1	0.000044	0.0707	0.029	476	0.29	942	7			1.5	1.4	0.157	0.8	0.6
MGS13-01-63.1	0.000051	0.1041	-0.116	110	0.81	1712	21	1685	25	4.3	1.9	0.304	1.4	0.7
MGS13-01-64.1	0.000021	0.0676	-0.651	269	0.30	1009	65			1.6	7.2	0.169	7.0	1.0
MGS13-01-65.1	0.000072	0.0540	-0.175	165	0.25	429	6			0.5	3.9	0.069	1.4	0.4
MGS13-01-66.1	0.000058	0.0804	0.571	176	0.28	1090	13	1187	34	2.0	2.2	0.184	1.3	0.6
	Mayflower Hill Formation (MH) : MH-3, Howland Dam. Howland quadrangle, UTM Location 0526847E/5009508N													
MH3-12-1.1	---	0.0820	0	229	0.52	1224	11	1245	22	2.4	1.5	0.209	1.0	0.7
MH3-12-2.1	0.000011	0.0824	0.020	265	0.63	1258	9	1252	18	2.4	1.2	0.216	0.8	0.7
MH3-12-3.1	0.000032	0.0630	0.059	707	0.87	690	15			1.0	2.6	0.113	2.3	0.9
MH3-12-4.1	0.003035	0.1110	5.554	177	0.80	1060	13			1.7	16.4	0.179	1.4	0.1
MH3-12-5.1	-0.000039	0.0573	-0.071	222	0.58	470	4			0.6	2.4	0.076	1.0	0.4
MH3-12-6.1	0.000036	0.0783	0.067	105	0.30	1128	12	1141	36	2.1	2.2	0.191	1.2	0.5
MH3-12-7.1	-0.000045	0.0790	-0.082	154	0.35	1127	10	1189	28	2.1	1.7	0.191	1.0	0.6
MH3-12-8.1	-0.000011	0.1043	-0.019	253	0.57	1702	13	1704	15	4.3	1.2	0.302	0.9	0.7
MH3-12-9.1	0.000168	0.0564	0.307	142	0.96	444	9			0.5	4.9	0.071	2.2	0.4
MH3-12-10.1	0.000040	0.0866	0.074	151	0.29	1213	22	1339	25	2.5	2.3	0.207	2.0	0.8
MH3-12-11.1	0.000068	0.0592	0.125	289	0.86	548	6			0.7	2.2	0.089	1.2	0.6
MH3-12-12.1	0.000021	0.1028	0.039	226	0.63	1632	31	1669	16	4.1	2.3	0.288	2.2	0.9
MH3-12-13.1	0.000073	0.0638	0.134	198	0.85	654	12			0.9	3.0	0.107	2.0	0.7
MH3-12-14.1	0.000077	0.0713	0.140	58	0.41	1010	15			1.6	3.4	0.170	1.6	0.5
MH3-12-15.1	-0.000031	0.0748	-0.056	248	0.38	1053	8	1076	23	1.8	1.4	0.177	0.8	0.6
MH3-12-16.1	0.000171	0.0727	0.313	96	0.31	960	19			1.6	3.4	0.161	2.2	0.6
MH3-12-17.1	0.000155	0.0715	0.283	53	0.34	994	14			1.6	3.8	0.167	1.6	0.4
MH3-12-18.1	0.000275	0.0553	0.502	90	0.91	560	11			0.6	6.1	0.091	2.1	0.4
MH3-12-19.1	---	0.0766	0	198	0	1078	15	1110	22	1.9	1.8	0.182	1.5	0.8
MH3-12-20.1	0.000014	0.0867	0.025	222	0.42	1319	12	1351	19	2.7	1.4	0.227	1.0	0.7

Appendix C: Continued.

sample[1]	measured $^{204}Pb/^{206}Pb$	measured $^{207}Pb/^{206}Pb$	%common ^{206}Pb	U (ppm)	Th/U	Age (Ma) $^{206}Pb/^{238}U^{2}$	err[4]	$^{207}Pb/^{206}Pb^{2,3}$	err[4]	$^{207}Pb/^{235}U^{5}$	err[4] (%)	$^{206}Pb/^{238}U^{5}$	err[4] (%)	err. corr.
MH3-12-21.1	0.000035	0.0571	0.063	171	0.67	624	11			0.8	4.0	0.102	1.9	0.5
MH3-12-22.1	---	0.0764	0	55	0.40	1106	17	1105	48	2.0	2.9	0.187	1.7	0.6
MH3-12-23.1	0.000043	0.0601	0.079	298	0.82	625	9			0.8	2.3	0.102	1.5	0.7
MH3-12-24.1	0.001009	0.0559	1.847	49	1.39	485	9			0.4	18.0	0.078	1.9	0.1
MH3-12-25.1	---	0.0849	0	214	0.57	1243	20	1313	19	2.5	2.0	0.213	1.8	0.9
MH3-12-26.1	0.000053	0.0957	0.097	196	0.41	1486	12	1528	19	3.4	1.4	0.259	0.9	0.7
MH3-12-27.1	0.000014	0.0772	0.026	958	0.64	1151	7	1121	11	2.1	0.8	0.196	0.6	0.8
MH3-12-28.1	0.000039	0.0623	0.071	191	0.75	616	6			0.9	2.3	0.100	1.0	0.4
MH3-12-29.1	0.000003	0.0910	0.006	793	0.30	1401	8	1447	18	3.0	1.1	0.243	0.6	0.6
MH3-12-30.1	0.000097	0.0581	0.177	2081	0.31	439	6			0.6	1.6	0.071	1.3	0.8
MH3-12-31.1	-0.000019	0.0843	-0.035	168	0.56	1296	21	1305	24	2.6	2.2	0.223	1.8	0.8
MH3-12-32.1	---	0.0606	0	107	0.90	534	16			0.7	4.1	0.086	3.0	0.8
MH3-12-33.1	0.000495	0.0539	0.905	46	0.55	421	8			0.4	12.8	0.067	1.9	0.1
MH3-12-34.1	---	0.0571	0	273	0.68	485	4			0.6	2.0	0.078	0.8	0.4
MH3-12-35.1	---	0.0792	0	765	0.52	1160	15	1177	11	2.2	1.5	0.197	1.4	0.9
MH3-12-36.1	---	0.1853	0	552	0.67	2682	28	2701	10	13.2	1.4	0.516	1.3	0.9
MH3-12-37.1	0.000115	0.1121	0.210	189	0.69	1663	14	1809	18	4.5	1.4	0.294	0.9	0.7
MH3-12-38.1	0.000079	0.0579	0.145	494	0.54	485	7			0.6	2.1	0.078	1.4	0.7
MH3-12-39.1	0.000054	0.0576	0.098	354	1.41	490	4			0.6	2.1	0.079	0.8	0.4
MH3-12-40.1	0.000031	0.1069	0.057	476	0.44	1668	11	1740	13	4.3	1.0	0.295	0.7	0.7
MH3-12-41.1	0.000036	0.1010	0.066	209	1.00	1601	13	1633	17	3.9	1.3	0.282	0.9	0.7
MH3-12-42.1	-0.000005	0.0726	-0.009	1390	0.25	1000	11	1003	9	1.7	1.3	0.168	1.2	0.9
MH3-12-43.1	0.000068	0.0570	0.124	317	1.00	487	8			0.6	2.8	0.078	1.7	0.6
MH3-12-44.1	0.000032	0.0699	0.059	129	0.42	940	9			1.5	2.1	0.157	1.1	0.5
MH3-12-45.1	-0.000013	0.0908	-0.024	231	0.96	1440	19	1445	18	3.1	1.7	0.250	1.5	0.8
MH3-12-46.1	---	0.0939	0	85	0.57	1452	17	1505	29	3.3	2.0	0.253	1.3	0.7
MH3-12-47.1	0.000065	0.0616	0.118	379	0.74	632	7			0.9	1.9	0.103	1.1	0.6
MH3-12-48.1	0.000006	0.1053	0.012	333	0.35	1753	12	1718	11	4.5	1.0	0.313	0.8	0.8
MH3-12-49.1	0.000497	0.0671	0.909	556	0.68	552	4			0.7	2.5	0.089	0.7	0.3
MH3-12-50.1	-0.000083	0.0565	-0.153	273	0.82	473	5			0.6	2.7	0.076	1.0	0.4
MH3-12-51.1	-0.000034	0.0570	-0.063	314	1.08	464	4			0.6	2.2	0.075	0.9	0.4
MH3-12-52.1	-0.000155	0.0596	-0.283	109	0.81	557	6			0.8	3.9	0.090	1.2	0.3
MH3-12-53.1	0.000175	0.0603	0.319	98	0.46	488	6			0.6	4.5	0.079	1.2	0.3
MH3-12-54.1	0.000012	0.1025	0.021	368	0.43	1661	12	1667	11	4.1	1.0	0.294	0.8	0.8
MH3-12-55.1	---	0.1702	0	126	0.71	2580	24	2560	12	11.6	1.3	0.492	1.1	0.8
MH3-12-56.1	-0.000005	0.0809	-0.009	637	0.28	1232	16	1222	12	2.4	1.5	0.211	1.4	0.9
MH3-12-57.1	-0.000099	0.0760	-0.182	44	0.91	1080	18	1131	66	1.9	3.8	0.182	1.8	0.5
MH3-12-58.1	0.000034	0.1532	0.062	106	2.75	2388	25	2377	18	9.4	1.6	0.448	1.2	0.8
MH3-12-59.1	0.000363	0.0574	0.664	190	1.02	467	5			0.5	5.1	0.075	1.0	0.2
MH3-12-60.1	0.000036	0.0563	0.067	665	0.65	439	8			0.5	2.2	0.071	1.8	0.8
	Vassalboro Group, undifferentiated (VG) : VG-1 Sandstone with uncertain relationships with Waterville Formation. Greenfield quadrangle, UTM Location 0540695E/4994053N													
VG-1-1.1	0.000217	0.0890	1.007	1056	0.40	1217	14	1338	34	2.5	2.2	0.208	1.3	0.6
VG-1-2.1	0.000191	0.0571	0.158	1203	0.06	444	9			0.5	2.6	0.071	2.1	0.8
VG-1-3.1	0.000016	0.0548	-0.150	578	0.60	453	8			0.5	2.2	0.073	1.8	0.8
VG-1-5.1	0.000036	0.1865	0.877	123	1.52	2659	32	2708	11	13.1	1.6	0.511	1.5	0.9
VG-1-4.1	0.000099	0.0957	-0.201	808	0.36	1571	17	1515	10	3.6	1.4	0.276	1.3	0.9
VG-1-6.1	0.000003	0.0739	-0.123	1157	0.02	1066	11	1038	9	1.8	1.2	0.180	1.1	0.9
VG-1-7.1	0.000899	0.0695	1.567	440	0.45	481	10			0.6	4.2	0.078	2.1	0.5

Appendix C: Continued.

sample[1]	measured $^{204}Pb/^{206}Pb$	measured $^{207}Pb/^{206}Pb$	%common ^{206}Pb	U (ppm)	Th/U	Age (Ma) $^{206}Pb/^{238}U^{2}$	err[4]	$^{207}Pb/^{206}Pb^{2,3}$	err[4]	$^{207}Pb/^{235}U^{5}$	err[4] (%)	$^{206}Pb/^{238}U^{5}$	err[4] (%)	err. corr.
VG-1-8.1	0.000175	0.0786	0.531	404	0.32	1048	12	1098	57	1.9	3.1	0.176	1.2	0.4
VG-1-9.1	---	0.0551	0.006	233	0.82	416	5			0.5	2.1	0.067	1.3	0.6
VG-1-10.1	-0.000012	0.1086	-0.183	288	0.53	1801	19	1779	11	4.8	1.3	0.322	1.2	0.9
VG-1-11.1	-0.000090	0.0730	0.062	90	0.27	1002	23	1050	45	1.7	3.3	0.168	2.4	0.7
VG-1-12.1	---	0.0903	0.046	560	0.50	1423	15	1431	10	3.1	1.3	0.247	1.2	0.9
VG-1-13.1	0.000044	0.0941	0.609	144	0.18	1409	21	1498	20	3.1	2.0	0.244	1.7	0.8
VG-1-14.1	0.000071	0.0875	0.542	143	0.33	1272	38	1349	25	2.6	3.6	0.218	3.3	0.9
VG-1-15.1	0.000050	0.0714	0.210	195	0.35	919	11			1.5	1.9	0.153	1.3	0.7
VG-1-16.1	---	0.0607	0.247	376	0.46	556	8			0.8	2.2	0.090	1.5	0.7
VG-1-17.1	0.000070	0.0568	0.023	227	0.70	477	6			0.6	2.7	0.077	1.3	0.5
VG-1-18.1	0.000008	0.1090	0.120	463	0.29	1767	19	1781	9	4.7	1.3	0.315	1.2	0.9
VG-1-19.1	0.000009	0.0722	0.032	1203	0	985	10			1.6	1.7	0.165	1.1	0.7
VG-1-20.1	0.003412	0.1137	5.150	378	0.48	944	12			1.4	7.3	0.158	1.4	0.2
VG-1-21.1	0.002673	0.1003	4.930	569	0.27	605	93			0.8	67.4	0.098	16.1	0.2
VG-1-22.1*	0.000054	0.1846	4.403	312	0.38	2380	25	2689	12	11.3	1.4	0.447	1.2	0.9
VG-1-23.1	0.000063	0.0785	0.515	1399	0.51	1051	26	1137	11	1.9	2.8	0.177	2.7	1.0
VG-1-24.1	0.004323	0.1136	4.760	1099	0.54	1008	24			1.2	24.3	0.169	2.6	0.1
VG-1-25.1	0.000031	0.0880	0.455	1168	0.24	1300	29	1372	11	2.7	2.6	0.223	2.5	1.0
VG-1-26.1	---	0.0554	-0.148	473	0.67	475	5			0.6	1.7	0.076	1.2	0.7
VG-1-27.1	0.000043	0.1103	0.307	501	0.92	1764	39	1795	8	4.8	2.6	0.315	2.5	1.0
VG-1-29.1	---	0.0550	-0.130	324	0.68	454	5			0.6	2.1	0.073	1.2	0.6
VG-1-30.1	---	0.1032	0.023	181	0.62	1679	19	1682	15	4.2	1.5	0.298	1.3	0.8
VG-1-31.1	0.000032	0.0989	0.354	312	0.50	1549	28	1595	14	3.7	2.2	0.272	2.1	0.9
VG-1-32.1	---	0.0728	-0.086	47	0.62	1029	23	1010	48	1.7	3.4	0.173	2.4	0.7
VG-1-33.1	---	0.0986	0.292	125	0.70	1553	18	1597	19	3.7	1.7	0.272	1.3	0.8
VG-1-34.1	---	0.1076	0.031	881	0.67	1755	26	1759	7	4.6	1.7	0.313	1.7	1.0
VG-1-35.1	0.000006	0.0922	-0.423	728	0.21	1539	19	1470	9	3.4	1.5	0.270	1.4	1.0
VG-1-36.1	0.000005	0.1018	-0.033	363	0.83	1661	18	1655	10	4.1	1.3	0.294	1.2	0.9
VG-1-37.1*	0.000170	0.1057	-3.080	112	0.55	2078	44	1687	32	5.4	3.0	0.380	2.5	0.8
VG-1-38.1	0.000114	0.0606	-0.027	44	0.98	632	10			0.8	4.7	0.103	1.7	0.4
VG-1-39.1	0.000024	0.1011	-0.257	185	1.13	1680	25	1638	16	4.1	1.9	0.298	1.7	0.9
VG-1-42.1	---	0.0567	0.061	277	0.09	461	6			0.6	2.2	0.074	1.3	0.6
VG-1-43.1	0.000026	0.0725	-0.147	133	0.55	1034	13			1.7	2.1	0.174	1.4	0.7
VG-1-44.1	---	0.0597	0.015	750	0.90	588	11			0.8	2.0	0.095	1.9	0.9
VG-1-45.1	0.000199	0.0572	0.158	6054	1.60	450	7			0.5	2.6	0.072	1.5	0.6
VG-1-46.1	0.000039	0.0986	0.451	617	0.63	1527	40	1587	9	3.6	2.9	0.267	2.9	1.0
VG-1-48.1	0.000539	0.0707	0.957	137	0.85	701	9			1.0	5.4	0.115	1.4	0.3
VG-1-49.1	-0.000589	0.0580	0.114	14	0.32	499	13			0.7	14.6	0.080	2.8	0.2
VG-1-51.1*	0.000955	0.0953	2.913	574	0.53	968	25	1240	30	1.8	3.2	0.162	2.8	0.9
VG-1-52.1	0.000029	0.0927	-0.024	303	0.50	1485	20	1474	14	3.3	1.7	0.259	1.5	0.9
VG-1-53.1	0.000015	0.0849	-0.265	404	0.80	1362	24	1310	14	2.7	2.1	0.235	2.0	0.9
VG-1-54.1	0.000038	0.0574	0.073	415	0.05	483	6			0.6	2.0	0.078	1.2	0.6
VG-1-56.1	0.000491	0.0664	1.243	1976	0.20	468	10			0.6	2.6	0.075	2.1	0.8
VG-1-57.1	---	0.0734	-0.011	329	0.42	1027	12	1024	17	1.7	1.5	0.173	1.2	0.8
VG-1-58.1	0.000005	0.0774	-0.074	542	0.27	1147	17	1130	13	2.1	1.7	0.195	1.6	0.9
VG-1-59.1	0.000010	0.0898	0.359	645	0.48	1360	23	1419	9	2.9	1.9	0.235	1.9	1.0
VG-1-60.1	0.000042	0.0746	0.133	85	0.64	1028	15	1041	41	1.8	2.6	0.173	1.6	0.6
VG-1-61.1	0.000024	0.0926	-0.046	99	0.92	1487	34	1474	50	3.3	3.6	0.260	2.5	0.7
VG-1-28.1	-0.000011	0.0548	-0.071	737	0.56	427	6			0.5	1.9	0.068	1.5	0.8
VG-1-41.1	0.000022	0.0769	-0.092	248	0.27	1137	25	1111	27	2.0	2.8	0.193	2.4	0.9

Appendix C: Continued.

sample[1]	measured $^{204}Pb/^{206}Pb$	measured $^{207}Pb/^{206}Pb$	%common ^{206}Pb	U (ppm)	Th/U	Age (Ma) $^{206}Pb/^{238}U^{2}$	err[4]	$^{207}Pb/^{206}Pb^{2,3}$	err[4]	$^{207}Pb/^{235}U^{5}$	err[4] (%)	$^{206}Pb/^{238}U^{5}$	err[4] (%)	err. corr.
VG-1-47.1	0.000134	0.1012	-0.055	1047	0.57	1651	24	1613	8	4.0	1.7	0.292	1.7	1.0
VG-1-50.1	---	0.0513	-0.501	145	1.25	425	8			0.5	4.0	0.068	1.9	0.5
VG-1-63.1*	0.000009	0.0870	1.518	673	0.33	1063	54	1357	47	2.1	6.1	0.179	5.6	0.9
VG-1-64.1	0.000348	0.0777	0.265	1013	0.55	1079	27	1007	41	1.8	3.4	0.182	2.7	0.8
VG-1-65.1	0.000168	0.0552	-0.102	394	0.29	452	9			0.5	3.0	0.073	2.0	0.7
VG-1-66.1	0.000119	0.0586	-0.127	319	0.42	589	7			0.8	2.3	0.096	1.3	0.6
	Hutchins Corner Formation (HC) : HC-1 Lower part of Hutchins Corner Formation. Unity quadrangle, UTM location 476531E/4930780N													
MGS13-03-1.1	0.000281	0.0966	0.249	89	0.69	1514	21	1481	38	3.4	2.5	0.265	1.5	0.6
MGS13-03-2.1	0.000596	0.0570	-0.634	32	0.25	670	14			0.7	12.2	0.110	2.1	0.2
MGS13-03-3.1	---	0.0780	-0.065	171	0.38	1161	11	1148	26	2.1	1.7	0.197	1.0	0.6
MGS13-03-4.1	0.000008	0.0756	-0.032	471	1.18	1092	8	1082	16	1.9	1.1	0.185	0.8	0.7
MGS13-03-5.1	0.000054	0.1965	1.104	115	0.37	2736	26	2792	21	14.3	1.7	0.529	1.2	0.7
MGS13-03-6.1	0	0.0742	0.123	1122	0.18	1019	6	1046	27	1.8	1.5	0.171	0.7	0.5
MGS13-03-7.1	0.000047	0.0793	0.317	219	0.19	1114	10	1162	24	2.0	1.6	0.189	0.9	0.6
MGS13-03-8.1	-0.000020	0.1016	0.418	234	0.96	1592	13	1658	15	3.9	1.2	0.280	0.9	0.7
MGS13-03-9.1	0.000132	0.0951	0.153	161	0.51	1503	14	1493	25	3.4	1.7	0.263	1.1	0.6
MGS13-03-10.1	0.000081	0.0814	0.158	103	0.39	1198	13	1202	34	2.3	2.1	0.204	1.2	0.6
MGS13-03-11.1	-0.000014	0.0863	0.025	211	0.45	1340	12	1349	20	2.8	1.4	0.231	1.0	0.7
MGS13-03-12.1	0.000088	0.0712	-0.031	216	0.96	970	9			1.6	1.8	0.162	1.0	0.5
MGS13-03-13.1	0	0.0779	-0.049	229	0.19	1154	10	1144	22	2.1	1.4	0.196	0.9	0.6
MGS13-03-14.1	-0.000031	0.0809	0.239	111	0.38	1173	13	1230	33	2.2	2.1	0.200	1.2	0.6
MGS13-03-15.1	0.000009	0.1127	0.130	233	0.28	1828	15	1842	16	5.1	1.3	0.328	0.9	0.7
MGS13-03-16.1	0.000565	0.0718	0.132	42	1.53	941	16			1.4	6.5	0.157	1.8	0.3
MGS13-03-17.1	0.000014	0.0846	0.191	245	0.16	1271	11	1302	21	2.5	1.4	0.218	0.9	0.7
MGS13-03-18.1	0.000030	0.0791	-0.064	110	0.55	1187	13	1164	33	2.2	2.0	0.202	1.2	0.6
MGS13-03-19.1	0.000030	0.0752	0.030	369	0.45	1067	8	1062	20	1.9	1.3	0.180	0.8	0.6
MGS13-03-20.1	0	0.0782	0.195	129	0.40	1111	12	1151	29	2.0	1.9	0.188	1.1	0.6
MGS13-03-21.1	---	0.0759	0.259	83	0.39	1035	13	1091	40	1.8	2.4	0.174	1.3	0.6
MGS13-03-22.1	0.001791	0.0730	-0.021	15	0.99	991	29			1.1	23.5	0.166	3.1	0.1
MGS13-03-23.1	-0.000017	0.0713	0.107	256	0.40	940	8			1.5	1.5	0.157	0.9	0.6
MGS13-03-24.1	0.000048	0.0771	-0.192	142	0.43	1163	13	1107	31	2.1	2.0	0.198	1.3	0.6
MGS13-03-25.1	0.000009	0.0788	0.001	1808	0.58	1167	11	1164	8	2.2	1.1	0.199	1.1	0.9
MGS13-03-26.1	0	0.0749	-0.042	260	0.54	1075	9	1067	22	1.9	1.4	0.182	0.9	0.6
MGS13-03-27.1	-0.000067	0.2191	-2.669	32	0.38	3074	48	2979	18	18.5	2.3	0.611	2.0	0.9
MGS13-03-28.1	0.000029	0.0827	0.345	203	0.29	1194	12	1252	27	2.3	1.7	0.204	1.1	0.6
MGS13-03-29.1	0.000021	0.0714	0.056	184	0.26	957	9			1.6	1.7	0.160	1.0	0.6
MGS13-03-30.1	0.000013	0.0577	0.171	563	0.51	465	3			0.6	1.4	0.075	0.7	0.5
MGS13-03-31.1	0.000194	0.0571	0.098	348	0.61	463	4			0.6	2.7	0.074	0.9	0.3
MGS13-03-32.1	0	0.0553	-0.127	178	0.35	465	4			0.6	2.6	0.075	1.0	0.4
MGS13-03-33.1	0.000064	0.0931	0.059	142	1.45	1480	32	1472	26	3.3	2.8	0.258	2.4	0.9
MGS13-03-34.1	0.000066	0.0724	-0.258	194	0.36	1053	11			1.7	1.9	0.177	1.1	0.6
MGS13-03-35.1	0.000054	0.0734	-0.034	321	0.36	1031	8	1003	22	1.7	1.4	0.173	0.8	0.6
MGS13-03-36.1	0.000169	0.0894	0.207	43	0.65	1373	21	1360	50	2.8	3.1	0.237	1.7	0.5
MGS13-03-37.1	-0.000014	0.0733	-0.024	257	0.35	1028	8	1028	27	1.8	1.6	0.173	0.9	0.5
MGS13-03-38.1	0	0.0950	0.614	54	0.37	1429	20	1529	34	3.3	2.3	0.248	1.5	0.6
MGS13-03-39.1	0.000121	0.0768	0.406	143	0.49	1026	10	1069	36	1.8	2.1	0.172	1.0	0.5
MGS13-03-40.1	0.000017	0.0888	0.076	325	0.38	1386	10	1394	16	2.9	1.2	0.240	0.8	0.7
MGS13-03-41.1	0.000020	0.0801	0.258	151	0.34	1148	11	1193	27	2.1	1.7	0.195	1.0	0.6

Appendix C: Continued.

sample[1]	measured $^{204}Pb/^{206}Pb$	measured $^{207}Pb/^{206}Pb$	%common ^{206}Pb	U (ppm)	Th/U	Age (Ma) $^{206}Pb/^{238}U^{2}$	err[4]	$^{207}Pb/^{206}Pb^{2,3}$	err[4]	$^{207}Pb/^{235}U^{5}$	err[4] (%)	$^{206}Pb/^{238}U^{5}$	err[4] (%)	err. corr.
MGS13-03-42.1	0	0.0558	-0.076	85	0.48	468	6			0.6	3.4	0.075	1.2	0.4
MGS13-03-43.1	0.000055	0.0771	0.161	116	0.82	1090	11	1104	34	1.9	2.0	0.184	1.1	0.5
MGS13-03-44.1	0	0.0612	-0.064	272	0.57	666	5			0.9	1.7	0.109	0.9	0.5
MGS13-03-46.1	0	0.0597	-0.073	95	0.48	613	7			0.8	2.8	0.100	1.2	0.4
MGS13-03-47.1	0.000036	0.1117	-0.451	412	0.39	1881	13	1819	10	5.2	0.9	0.339	0.8	0.8
MGS13-03-48.1	0.000032	0.1055	-0.386	184	0.46	1773	15	1715	27	4.6	1.8	0.317	1.0	0.5
MGS13-03-49.1	0.000064	0.0809	-0.036	367	0.35	1224	22	1196	18	2.3	2.2	0.209	2.0	0.9
MGS13-03-50.1	0.000041	0.0929	-0.16	55	0.38	1510	36	1473	35	3.4	3.2	0.264	2.7	0.8
MGS13-03-51.1	0	0.1117	-0.049	202	0.54	1834	15	1828	13	5.1	1.2	0.329	0.9	0.8
MGS13-03-52.1	0.000083	0.0788	-0.052	69	0.57	1177	15	1138	43	2.1	2.5	0.200	1.3	0.5
MGS13-03-53.1	0.000197	0.0839	0.093	69	0.88	1269	16	1224	47	2.4	2.7	0.218	1.4	0.5
MGS13-03-54.1	0.000055	0.0603	0.223	236	0.58	550	5			0.7	2.2	0.089	0.9	0.4
MGS13-03-55.1	0.000086	0.0775	0.433	86	0.40	1042	13	1104	52	1.8	2.9	0.175	1.3	0.5
MGS13-03-56.1	0.000027	0.0924	0.172	790	0.42	1447	9	1468	9	3.2	0.8	0.252	0.7	0.8
MGS13-03-57.1	0.000371	0.0716	-0.374	29	0.65	1052	20			1.6	6.3	0.177	2.1	0.3
MGS13-03-58.1	0.000016	0.0765	0.224	224	0.40	1059	9	1101	24	1.9	1.5	0.179	0.9	0.6
MGS13-03-59.1	-0.000068	0.0553	-0.015	452	0.62	431	3			0.5	1.8	0.069	0.8	0.4
MGS13-03-60.1	0.000063	0.0733	-0.060	334	0.25	1034	8			1.7	1.4	0.174	0.8	0.6
MGS13-03-61.1	0.001208	0.1020	1.276	84	0.61	1438	20	1316	82	2.9	4.5	0.250	1.5	0.3
MGS13-03-62.1	0.000067	0.0988	-0.450	92	0.69	1666	21	1585	31	4.0	2.2	0.295	1.4	0.7
MGS13-03-63.1	0.000072	0.0578	0.168	320	0.16	471	4			0.6	2.5	0.076	0.9	0.4
MGS13-03-64.1	0.000292	0.1017	0.058	36	1.28	1641	31	1581	58	3.9	3.8	0.290	2.1	0.6
MGS13-03-65.1	0.000093	0.0909	-0.083	135	0.58	1456	16	1417	29	3.1	1.9	0.253	1.2	0.6
MGS13-03-66.1	0.000036	0.1789	1.946	196	0.87	2512	22	2639	28	11.7	2.0	0.476	1.1	0.5
Madrid Formation (MA) : MA-1 Mattawamkeag quadrangle, UTM Location 0551778E/5043667N														
Ma1-12-1.1	0.000020	0.2086	0.037	270	0.35	2843	22	2893	7	15.93	1.1	0.554	1.0	0.9
Ma1-12-2.1	0.000043	0.1026	0.079	178	0.76	1617	15	1661	19	4.01	1.5	0.285	1.1	0.7
Ma1-12-3.1	---	0.1324	0	123	0.68	2146	22	2130	16	7.21	1.5	0.395	1.2	0.8
Ma1-12-4.1	0.000048	0.0764	0.088	163	0.4	1063	11	1088	31	1.87	1.9	0.179	1.1	0.6
Ma1-12-5.1	0.000021	0.1228	0.038	254	0.55	1978	23	1993	11	6.07	1.5	0.359	1.3	0.9
Ma1-12-6.1	0.000009	0.0751	0.017	382	0.54	1083	9	1067	18	1.89	1.2	0.183	0.9	0.7
Ma1-12-7.1	0.000069	0.0747	0.126	114	0.63	1050	13	1033	39	1.80	2.3	0.177	1.3	0.6
Ma1-12-8.1	0.000010	0.0785	0.018	383	0.2	1122	9	1155	17	2.05	1.2	0.190	0.9	0.7
Ma1-12-9.1	0.000035	0.2016	0.065	191	1.07	2716	23	2835	8	14.53	1.2	0.524	1.0	0.9
Ma1-12-10.1	0.000014	0.0568	0.026	678	0.87	461	4			0.58	1.5	0.074	0.8	0.6
Ma1-12-11.1	0.000079	0.0756	0.144	98	0.93	1076	13	1054	42	1.87	2.4	0.182	1.3	0.5
Ma1-12-12.1	-0.000019	0.0945	-0.036	270	0.55	1493	13	1524	16	3.41	1.3	0.261	0.9	0.8
Ma1-12-13.1	0.000026	0.0710	0.048	257	0.27	941	8			1.53	1.4	0.157	0.9	0.6
Ma1-12-14.1	0.000005	0.1857	0.008	218	0.68	2714	21	2704	7	13.40	1.0	0.524	0.9	0.9
Ma1-12-15.1	0	0.0565	0	171	0.4	434	4			0.54	2.5	0.070	1.0	0.4
Ma1-12-16.1	0.000019	0.0881	0.034	286	0.46	1343	18	1378	16	2.81	1.7	0.232	1.5	0.9
Ma1-12-17.1	0.000014	0.1884	0.025	348	1.08	2748	21	2727	7	13.79	1.0	0.532	0.9	0.9
Ma1-12-18.1	0.000015	0.1837	0.028	186	0.85	2660	23	2684	9	12.92	1.2	0.511	1.1	0.9
Ma1-12-19.1	0	0.0998	0	162	0.3	1647	17	1621	20	4.01	1.6	0.291	1.2	0.7
Ma1-12-20.1	0.000059	0.0903	0.108	249	0.61	1407	20	1415	19	3.01	1.9	0.244	1.6	0.8
Ma1-12-21.1	0.000629	0.0761	1.151	13	0.26	1122	35			1.76	11.7	0.190	3.4	0.3
Ma1-12-22.1	0.000017	0.0726	0.032	229	0.32	1035	9			1.74	1.6	0.174	1.0	0.6
Ma1-12-23.1	---	0.0990	0	121	0.47	1526	16	1606	20	3.65	1.6	0.267	1.2	0.7
Ma1-12-24.1	---	0.0745	0	116	0.38	1058	12	1055	34	1.83	2.1	0.178	1.2	0.6

Appendix C: Continued.

sample[1]	measured $^{204}Pb/^{206}Pb$	measured $^{207}Pb/^{206}Pb$	%common ^{206}Pb	U (ppm)	Th/U	Age (Ma) $^{206}Pb/^{238}U^{2}$	err[4]	$^{207}Pb/^{206}Pb^{2,3}$	err[4]	$^{207}Pb/^{235}U^{5}$	err[4] (%)	$^{206}Pb/^{238}U^{5}$	err[4] (%)	err. corr.
Ma1-12-25.1	0.000037	0.0996	0.067	122	0.53	1678	17	1607	21	4.06	1.6	0.297	1.2	0.7
Ma1-12-26.1*	0.000049	0.1157	0.089	731	0.28	1330	19	1880	7	3.63	1.6	0.229	1.6	1.0
Ma1-12-27.1	0.000024	0.0716	0.044	214	0.44	930	9			1.52	1.8	0.155	1.0	0.6
Ma1-12-28.1	0	0.0680	0	103	0.52	906	12			1.42	2.4	0.151	1.4	0.6
Ma1-12-29.1	-0.000005	0.0761	-0.008	669	0.02	1114	8	1099	12	1.98	1.0	0.189	0.8	0.8
Ma1-12-30.1	0.000077	0.0565	0.140	506	0.58	458	4			0.56	1.9	0.074	0.8	0.4
Ma1-12-31.1	0.000064	0.0737	0.118	64	0.53	997	14	1009	54	1.68	3.1	0.167	1.5	0.5
Ma1-12-32.1	0.000063	0.0712	0.115	137	1.44	943	10			1.53	2.2	0.157	1.2	0.5
Ma1-12-33.1	0.000027	0.0709	0.049	332	0.37	921	8			1.49	1.4	0.154	0.9	0.6
Ma1-12-34.1	0.000008	0.0777	0.015	745	0.25	1126	8	1136	12	2.04	1.0	0.191	0.8	0.8
Ma1-12-35.1	0.000049	0.0556	0.089	430	0.54	464	4			0.57	2.0	0.075	0.9	0.4
Ma1-12-36.1	0.000342	0.0583	0.626	111	0.84	470	6			0.56	5.9	0.076	1.3	0.2
Ma1-12-37.1	0.000030	0.0712	0.055	350	0.28	920	7			1.50	1.3	0.153	0.9	0.7
Ma1-12-38.1	-0.000060	0.0574	-0.110	307	0.23	472	7			0.61	2.8	0.076	1.6	0.6
Ma1-12-39.1	0.000588	0.0889	1.076	24	0.86	1287	29	1210	124	2.45	6.8	0.221	2.5	0.4
Ma1-12-40.1	0.000005	0.0860	0.010	1140	0.28	1310	10	1337	7	2.67	0.9	0.225	0.9	0.9
Ma1-12-41.1	0.000016	0.2003	0.029	148	0.87	2849	25	2827	9	15.34	1.2	0.556	1.1	0.9
Ma1-12-42.1	0.000133	0.1009	0.243	138	0.39	1595	20	1606	26	3.83	2.0	0.281	1.4	0.7
Ma1-12-43.1	0.000108	0.0727	0.197	121	0.38	978	11			1.61	2.5	0.164	1.2	0.5
Ma1-12-44.1	---	0.1011	0	237	0.56	1644	14	1644	13	4.05	1.2	0.290	0.9	0.8
Ma1-12-45.1	---	0.0743	0	125	0.29	953	10	1051	31	1.63	1.9	0.159	1.1	0.6
Ma1-12-46.1	0.000003	0.0730	0.006	1242	0.25	999	7	1013	10	1.69	0.9	0.168	0.7	0.8
Ma1-12-47.1*	0.000024	0.1756	0.043	174	1.02	2217	21	2609	113	9.92	6.8	0.410	1.1	0.2
Ma1-12-48.1	0.000094	0.0566	0.171	186	0.84	469	5			0.57	3.0	0.075	1.0	0.3
Ma1-12-49.1	---	0.0756	0	118	0.57	1063	11	1085	31	1.87	1.9	0.179	1.2	0.6
Ma1-12-50.1	0.000018	0.1875	0.033	306	0.78	2688	36	2719	6	13.36	1.7	0.517	1.6	1.0
Ma1-12-51.1	0.000013	0.0718	0.023	337	0.51	958	8			1.58	1.4	0.160	0.9	0.7
Ma1-12-52.1	---	0.0788	0	258	0.61	1178	18	1166	20	2.18	2.0	0.201	1.7	0.9
Ma1-12-53.1	0.000173	0.0738	0.317	49	0.7	972	15			1.60	4.1	0.163	1.7	0.4
Ma1-12-54.1	---	0.0735	0	401	0.39	1048	9	1026	16	1.79	1.2	0.176	0.9	0.7
Ma1-12-55.1	0.000066	0.0812	0.12	299	0.58	1217	10	1203	20	2.30	1.4	0.208	0.9	0.7
Ma1-12-56.1	-0.000024	0.0763	-0.044	135	0.39	1173	14	1111	34	2.11	2.1	0.200	1.3	0.6
Ma1-12-57.1	---	0.0954	0	136	0.46	1556	16	1536	20	3.59	1.6	0.273	1.1	0.7
Ma1-12-58.1	0.000309	0.0685	0.565	28	0.87	1049	22			1.56	6.7	0.177	2.3	0.3
Ma1-12-59.1	0.000022	0.0708	0.040	304	0.3	946	16			1.54	2.1	0.158	1.9	0.9
Ma1-12-60.1	0.000033	0.1012	0.059	281	0.37	1611	16	1638	16	3.94	1.4	0.284	1.1	0.8
Ma1-12-61.1	0.000076	0.0562	0.140	1401	0.52	501	4			0.61	1.4	0.081	0.9	0.7
Ma1-12-62.1	0.000198	0.0588	0.363	202	0.63	473	5			0.59	3.7	0.076	1.1	0.3
Ma1-12-63.1	0.000259	0.0559	0.475	180	0.67	467	5			0.54	3.9	0.075	1.0	0.3
Ma1-12-64.1	0.000206	0.1020	0.377	1201	0.08	1619	11	1608	13	3.90	1.0	0.286	0.7	0.7
Ma1-12-65.1	0.000103	0.0723	0.189	71	0.52	941	13			1.53	2.9	0.157	1.4	0.5
Ma1-12-66.1	0.000084	0.0556	0.153	550	0.35	447	5			0.54	2.0	0.072	1.2	0.6
Ma1-12-67.1	0.000006	0.0556	0.012	1204	0.51	450	3			0.55	1.1	0.072	0.8	0.7
Ma1-12-68.1	0.000020	0.0771	0.036	148	0.39	1027	10	1115	26	1.83	1.7	0.173	1.0	0.6
Ma1-12-69.1	0.000027	0.0628	0.049	335	0.53	734	6			1.04	1.5	0.121	0.9	0.6
Ma1-12-70.1	0.000038	0.0573	0.070	517	0.44	472	4			0.59	1.5	0.076	0.8	0.5
Ma1-12-71.1	---	0.0567	0	180	0.62	398	4			0.50	2.9	0.064	1.1	0.4
Ma1-12-72.1	0	0.0568	0	701	0.63	460	3			0.58	1.4	0.074	0.8	0.6
Ma1-12-73.1	0.000147	0.0589	0.269	982	0.07	471	5			0.59	1.7	0.076	1.1	0.6
Ma1-12-74.1	0.000061	0.0570	0.111	618	0.98	470	8			0.58	2.2	0.076	1.7	0.7

Appendix C: Continued.

sample[1]	measured $^{204}Pb/^{206}Pb$	measured $^{207}Pb/^{206}Pb$	%common ^{206}Pb	U (ppm)	Th/U	Age (Ma) $^{206}Pb/^{238}U^{2}$	err[4]	Age (Ma) $^{207}Pb/^{206}Pb^{2,3}$	err[4]	$^{207}Pb/^{235}U^{5}$	err[4] (%)	$^{206}Pb/^{238}U^{5}$	err[4] (%)	err. corr.
Ma1-12-75.1	0.000030	0.0558	0.055	692	1.27	432	5			0.53	1.9	0.069	1.3	0.7
Ma1-12-76.1	0	0.0575	0	876	0.27	474	4			0.60	1.2	0.076	0.8	0.7
Madrid Formation (MA) : MA-2 Alder Brook quadrangle, UTM Location 0575363E/50687765N														
UNSS-1-12-1.1	0.000087	0.1017	0.160	171	0.38	1611	14	1633	18	3.9	1.4	0.284	1.0	0.7
UNSS-1-12-2.1	0.000019	0.0885	0.035	925	0.81	1366	11	1387	9	2.9	1.0	0.236	0.9	0.9
UNSS-1-12-3.1	---	0.1032	0	199	0.75	1643	13	1683	15	4.1	1.2	0.290	0.9	0.8
UNSS-1-12-4.1	0.000083	0.0817	0.151	32	1.17	1316	23	1210	57	2.5	3.5	0.226	1.9	0.6
UNSS-1-12-5.1	0.000028	0.0747	0.050	209	0.38	991	9	1050	23	1.7	1.5	0.166	1.0	0.6
UNSS-1-12-6.1	0.000011	0.0916	0.021	402	0.28	1412	19	1455	12	3.1	1.6	0.245	1.5	0.9
UNSS-1-12-7.1	-0.000030	0.0695	-0.055	263	0.32	890	7			1.4	1.5	0.148	0.9	0.6
UNSS-1-12-8.1	0.000011	0.0861	0.020	205	0.64	1308	22	1337	17	2.7	2.1	0.225	1.9	0.9
UNSS-1-12-9.1	-0.000011	0.0933	-0.020	177	0.27	1531	13	1497	50	3.5	2.8	0.268	0.9	0.3
UNSS-1-12-10.1	0.000011	0.0727	0.021	2892	0.05	950	5	1002	14	1.6	0.9	0.159	0.6	0.7
UNSS-1-12-11.1	-0.000113	0.0704	-0.206	34	3.96	984	17			1.6	4.2	0.165	1.9	0.4
UNSS-1-12-12.1	-0.000072	0.0580	-0.132	219	0.82	452	4			0.6	2.4	0.073	1.0	0.4
UNSS-1-12-13.1	0.000012	0.0744	0.021	756	0.31	1049	16	1047	10	1.8	1.7	0.177	1.7	1.0
UNSS-1-12-14.1	0.000013	0.0734	0.023	243	1.27	962	7	1019	21	1.6	1.3	0.161	0.8	0.6
UNSS-1-12-15.1	0.000030	0.1083	0.055	1334	1.13	1759	22	1764	5	4.7	1.4	0.314	1.4	1.0
UNSS-1-12-16.1	0.000050	0.0729	0.092	153	0.66	995	9			1.7	1.9	0.167	1.0	0.5
UNSS-1-12-17.1	-0.000014	0.0564	-0.025	469	0.76	471	3			0.6	1.4	0.076	0.7	0.5
UNSS-1-12-18.1	0.000008	0.0774	0.015	1008	0.17	1063	19	1128	8	1.9	2.0	0.179	1.9	1.0
UNSS-1-12-19.1	0.000006	0.1881	0.011	235	0.59	2648	20	2725	8	13.2	1.1	0.508	0.9	0.9
UNSS-1-12-20.1	0.000035	0.0915	0.064	140	0.35	1405	28	1446	22	3.1	2.5	0.243	2.3	0.9
UNSS-1-12-21.1	0.000024	0.0739	0.044	243	0.19	1004	16	1031	21	1.7	2.0	0.168	1.7	0.9
UNSS-1-12-22.1	0.000014	0.0750	0.026	369	0.58	1041	14	1064	16	1.8	1.7	0.175	1.5	0.9
UNSS-1-12-23.1	0	0.0995	0	216	0.97	1580	14	1614	14	3.8	1.2	0.278	1.0	0.8
UNSS-1-12-24.1	0.000488	0.0636	0.892	602	0.62	469	7			0.6	2.8	0.075	1.5	0.6
UNSS-1-12-25.1	0.000023	0.1011	0.042	265	0.73	1620	12	1639	13	4.0	1.1	0.286	0.8	0.8
UNSS-1-12-26.1	0	0.0758	0	233	0.61	1053	15	1091	19	1.9	1.8	0.177	1.5	0.8
UNSS-1-12-27.1	0.000028	0.0847	0.051	91	0.5	1220	23	1300	29	2.4	2.5	0.208	2.1	0.8
UNSS-1-12-28.1	0.000047	0.0578	0.085	172	0.82	443	4			0.6	4.3	0.071	1.0	0.2
UNSS-1-12-29.1	0.000020	0.0574	0.037	314	0.76	474	4			0.6	1.7	0.076	0.8	0.5
UNSS-1-12-30.1	---	0.1867	0	208	0.65	2734	23	2713	8	13.6	1.1	0.528	1.0	0.9
UNSS-1-12-31.1	-0.000020	0.0745	-0.036	166	0.42	1033	10	1063	26	1.8	1.7	0.174	1.1	0.6
UNSS-1-12-32.1	0.000009	0.0884	0.017	927	0.27	1283	17	1388	8	2.7	1.5	0.220	1.5	1.0
UNSS-1-12-33.1	0.000027	0.0554	0.050	590	0.64	426	5			0.5	1.8	0.068	1.2	0.7
UNSS-1-12-34.1	0.000154	0.0570	0.282	198	1.11	440	4			0.5	3.5	0.071	1.0	0.3
UNSS-1-12-35.1	0.000009	0.1035	0.016	251	0.8	1730	14	1685	14	4.4	1.2	0.308	0.9	0.8
UNSS-1-12-36.1	0.000059	0.0550	0.108	378	0.91	454	10			0.5	3.1	0.073	2.3	0.7
UNSS-1-12-37.1	0.000028	0.0923	0.050	233	0.17	1511	12	1465	16	3.3	1.2	0.264	0.9	0.7
UNSS-1-12-38.1	0.000028	0.1026	0.052	343	1.76	1665	13	1665	15	4.2	1.2	0.295	0.9	0.8
UNSS-1-12-39.1	-0.000005	0.1006	-0.009	438	0.61	1609	11	1637	10	3.9	0.9	0.283	0.8	0.8
UNSS-1-12-40.1	-0.000045	0.0550	-0.082	320	0.44	431	4			0.5	2.6	0.069	0.9	0.4
UNSS-1-12-41.1	0.000018	0.1024	0.033	158	0.85	1721	17	1664	20	4.3	1.6	0.306	1.1	0.7
UNSS-1-12-42.1	-0.000008	0.1895	-0.014	231	0.86	2759	23	2738	9	14.0	1.2	0.534	1.0	0.9
UNSS-1-12-43.1	0.000010	0.1703	0.019	174	1.34	2502	23	2560	11	11.1	1.3	0.474	1.1	0.9
UNSS-1-12-44.1	0.000061	0.0979	0.111	102	0.78	1487	17	1569	61	3.5	3.5	0.259	1.3	0.4
UNSS-1-12-45.1	0.000076	0.0555	0.139	323	0.34	442	5			0.5	2.4	0.071	1.2	0.5
UNSS-1-12-46.1	0.000018	0.1018	0.033	166	0.62	1634	16	1653	20	4.0	1.5	0.288	1.1	0.7

Appendix C: Continued.

sample[1]	measured $^{204}Pb/^{206}Pb$	measured $^{207}Pb/^{206}Pb$	%common ^{206}Pb	U (ppm)	Th/U	Age (Ma) $^{206}Pb/^{238}U^{2}$	err[4]	$^{207}Pb/^{206}Pb^{2,3}$	err[4]	$^{207}Pb/^{235}U^{5}$	err[4] (%)	$^{206}Pb/^{238}U^{5}$	err[4] (%)	err. corr.
UNSS-1-12-47.1	0.000017	0.1874	0.031	68	1.07	2711	30	2717	13	13.5	1.6	0.523	1.4	0.9
UNSS-1-12-48.1	-0.00012	0.0557	-0.220	136	0.09	488	5			0.6	3.4	0.079	1.1	0.3
UNSS-1-12-49.1	-0.000019	0.1957	-0.034	135	0.81	2794	25	2793	10	14.7	1.3	0.543	1.1	0.9
UNSS-1-12-50.1	---	0.0863	0	80	0.64	1351	18	1346	35	2.8	2.3	0.233	1.5	0.6
UNSS-1-12-51.1	0.000015	0.0860	0.027	484	0.5	1340	10	1334	14	2.7	1.1	0.231	0.8	0.7
UNSS-1-12-52.1	-0.000012	0.1156	-0.022	306	0.2	1909	14	1892	11	5.5	1.0	0.345	0.8	0.8
UNSS-1-12-53.1	0.000029	0.0881	0.054	123	0.53	1359	15	1375	29	2.8	1.9	0.235	1.2	0.6
UNSS-1-12-54.1	-0.000008	0.1873	-0.014	154	0.66	2784	23	2719	9	14.0	1.2	0.540	1.0	0.9
UNSS-1-12-55.1	0	0.1015	0	140	0.67	1631	16	1652	19	4.0	1.5	0.288	1.1	0.7
UNSS-1-12-56.1	-0.000004	0.0996	-0.008	478	0.07	1626	14	1618	9	3.9	1.1	0.287	1.0	0.9
UNSS-1-12-57.1	0.000066	0.1052	0.121	105	0.77	1653	18	1702	23	4.2	1.7	0.292	1.2	0.7
UNSS-1-12-58.1	---	0.0724	0	108	0.76	1060	12			1.8	2.2	0.179	1.2	0.6
UNSS-1-12-59.1	0.000021	0.1080	0.039	459	0.13	1697	18	1762	10	4.5	1.3	0.301	1.2	0.9
UNSS-1-12-60.1	-0.000007	0.0731	-0.013	457	0.72	1020	10	1018	15	1.7	1.3	0.171	1.1	0.8

Notes: [1] All detrital zircon samples analyzed on USGS/Stanford SHRIMP-RG, Stanford University; [2] $^{206}Pb/^{238}U$ and $^{207}Pb/^{206}Pb$ ages corrected for common Pb using the ^{204}Pb-correction method. Decay constants from Steiger and Jäger (1977); [3] Not listed for ages <1.0 Ga; [4] 1-sigma errors; [5] Radiogenic ratios, corrected for common Pb using the ^{204}Pb-correction method, based on the Stacey and Kramers (1975) model.

Appendix D. SHRIMP U-Th-Pb data for zircons from igneous rocks of eastern and east-central Maine. Location coordinates in UTM metres, (Zone 19, NAD27).

sample[1]	measured $^{204}Pb/^{206}Pb$	measured $^{207}Pb/^{206}Pb$	%common ^{206}Pb	U (ppm)	Th/U	in Ma $^{206}Pb/^{238}U^{2}$	err[3]	$^{207}Pb/^{206}Pb^{2,4}$	err[3]	$^{207}Pb/^{235}U$	err[3] (%)	$^{206}Pb/^{238}U$	err[3] (%)
	KMV-1 Kendall Mountain Formation tuff near base of formation. Woodland quadrangle, UTM Location 0623730E/5001066N												
KMV1-25.1	0.000013	0.0758	0.023	1633	0.55	998	8	1083	6	6.0	0.9	0.076	0.28
KMV1-1.1	0.001140	0.0744	2.048	345	0.78	474	5			13.1	1.1	0.058	3.27
KMV1-2.1	-0.000010	0.0562	-0.017	422	1.04	479	5			13.0	1.0	0.056	0.93
KMV1-3.1	0.000172	0.0585	0.310	133	0.79	472	7			13.2	1.5	0.056	2.43
KMV1-4.1	-0.000021	0.0576	-0.038	514	1.45	475	6			13.1	1.4	0.058	0.82
KMV1-5.1	0.000028	0.0589	0.050	452	1.26	470	9			13.2	1.9	0.058	0.96
KMV1-6.1	0.000003	0.0770	0.006	526	0.22	1077	9	1120	9	5.5	0.9	0.077	0.46
KMV1-7.1	0	0.0568	0	260	0.80	473	7			13.1	1.4	0.057	1.12
KMV1-8.1	0.000213	0.0599	0.382	363	0.75	472	8			13.2	1.7	0.057	1.49
KMV1-9.1	0.000023	0.0570	0.041	313	0.90	482	7			12.9	1.5	0.057	1.06
KMV1-10.1	0.000154	0.0582	0.278	278	0.71	469	5			13.2	1.1	0.056	2.47
KMV1-11.1	0.000051	0.0560	0.091	230	0.68	475	6			13.1	1.3	0.055	1.43
KMV1-12.1	0.000018	0.0799	0.030	166	0.27	1147	25	1187	17	5.1	2.4	0.080	0.84
KMV1-13.1	0.000002	0.0758	0.004	814	0.34	1096	18	1087	16	5.4	1.7	0.076	0.79
KMV1-14.1	0.000043	0.0579	0.078	272	1.15	469	7			13.3	1.6	0.057	1.30
KMV1-15.1	0.000136	0.0832	0.228	66	0.32	1170	19	1227	43	5.0	1.8	0.081	2.18
KMV1-16.1	0	0.0586	0	249	0.79	474	7			13.1	1.5	0.059	1.16
KMV1-17.1	0.000004	0.075	0.006	903	0.08	1055	11	1067	7	5.6	1.1	0.075	0.35
KMV1-18.1	0	0.0764	0	447	0.30	1076	14	1106	16	5.5	1.5	0.076	0.80
KMV1-19.1	-0.000007	0.0572	-0.012	586	1.35	480	6			12.9	1.2	0.057	0.78
KMV1-20.1	-0.000141	0.0564	-0.253	118	0.57	476	8			13.0	1.8	0.058	2.43
KMV1-21.1	0.000013	0.0573	0.023	295	0.88	483	4			12.9	1.0	0.057	1.09
KMV1-22.1	0.000017	0.0574	0.031	270	0.76	484	6			12.8	1.3	0.057	1.26
	OS-1 Olamon Stream Formation. Greenfield quadrangle, UTM Location 0545193E/4983992N												
13A78-1.1	0.000780	0.0577	1.402	55	0.63	462	9			13.4	2.1	0.046	16.0
13A78-2.1	0.000281	0.0597	0.495	70	2.2	662	10			9.2	1.7	0.056	6.6
13A78-3.1	0.000799	0.0553	1.437	56	0.61	460	8			13.5	1.8	0.043	16.8
13A78-4.1	-0.000059	0.0572	-0.107	55	0.61	471	7			13.2	1.6	0.058	5.3
13A78-5.1	0.000430	0.0579	0.772	57	0.64	462	10			13.5	2.3	0.052	10.0
13A78-6.1	-0.000145	0.0577	-0.261	68	0.63	460	16			13.5	3.5	0.060	5.8
13A78-7.1	-0.000101	0.0593	-0.181	64	0.63	481	8			12.9	1.6	0.061	4.3
13A78-8.1	0.000209	0.0584	0.375	71	0.67	459	7			13.5	1.6	0.055	6.6
13A78-9.1	0.000045	0.0563	0.081	71	0.65	473	8			13.1	1.8	0.056	3.3
13A78-10.1	0.000284	0.0574	0.510	81	1.1	483	8			12.8	1.8	0.053	7.5
13A78-11.1	0.000052	0.0574	0.093	61	0.63	469	10			13.3	2.1	0.057	3.7
13A78-12.1	0.000388	0.0599	0.692	102	0.77	549	11			11.3	2.2	0.054	8.6
13A78-13.1	0.000086	0.0575	0.155	74	0.68	472	9			13.2	1.9	0.056	4.1
13A78-14.1	-0.000152	0.0560	-0.274	62	0.63	460	10			13.5	2.3	0.058	5.3
13A78-15.1	-0.000156	0.0581	-0.280	64	0.63	468	10			13.3	2.3	0.060	6.2
13A78-16.1	-0.000050	0.0587	-0.090	73	0.65	461	7			13.5	1.6	0.059	3.4
13A78-17.1	0.000213	0.0572	0.381	82	0.75	497	15			12.5	3.2	0.054	6.9
	PM Pocomoonshine gabbro-diorite, near northern margin. Princeton quadrangle, UTM Location 0612829E/5002319N												
Poco1-13-1.1	0.000173	0.0560	0.092	262	0.3	421	3			14.8	0.8	0.053	3.6
Poco1-13-2.1	0.000014	0.0563	0.121	482	0.45	425	3			14.7	0.7	0.056	1.3

Appendix D. Continued.

sample[1]	measured $^{204}Pb/^{206}Pb$	measured $^{207}Pb/^{206}Pb$	%common ^{206}Pb	U (ppm)	Th/U	in Ma $^{206}Pb/^{238}U$[2]	err[3]	$^{207}Pb/^{206}Pb$[2,4]	err[3]	$^{207}Pb/^{235}U$	err[3] (%)	$^{206}Pb/^{238}U$	err[3] (%)
Poco1-13-3.1	0.000089	0.0556	0.064	231	0.34	415	3			15.0	0.8	0.054	2.4
Poco1-13-4.1	0.000067	0.0552	-0.002	336	0.41	422	3			14.8	0.8	0.054	2.0
Poco1-13-5.1	0	0.0575	0.275	526	0.3	425	5			14.7	1.3	0.058	1.2
Poco1-13-6.1	0.000113	0.0548	-0.062	370	0.4	423	3			14.8	0.7	0.053	2.0
Poco1-13-7.1	0.000061	0.0548	-0.064	234	0.31	425	3			14.7	0.8	0.054	2.2
Poco1-13-8.1	-0.000018	0.0560	0.099	417	0.37	422	5			14.8	1.1	0.056	1.5
Poco1-13-9.1	0.000065	0.0562	0.115	439	0.33	421	5			14.8	1.2	0.055	1.6
Poco1-13-10.1	0.000053	0.0564	0.151	424	0.31	421	3			14.8	0.7	0.056	1.6
Poco1-13-11.1	0.000068	0.0545	-0.081	212	0.35	417	7			14.9	1.7	0.054	2.4
Poco1-13-12.1	0.000151	0.0551	-0.039	191	0.36	429	10			14.5	2.4	0.053	4.5
Poco1-13-13.1	-0.000020	0.0543	-0.125	342	0.47	423	3			14.8	0.7	0.055	1.6
Poco1-13-14.1	0.000029	0.0539	-0.172	245	0.33	425	5			14.7	1.3	0.054	2.0
Poco1-13-15.1	0.000060	0.0580	0.350	236	0.35	420	6			14.8	1.5	0.057	2.1
Poco1-13-16.1	0.000074	0.0548	-0.055	474	0.45	423	5			14.7	1.2	0.054	1.6
Poco1-13-17.1	0	0.0557	0.052	290	0.46	423	3			14.8	0.8	0.056	1.6
Poco1-13-18.1	0.000080	0.0533	-0.242	254	0.46	421	3			14.8	0.8	0.052	2.2

Notes: [1] All detrital zircon samples analyzed on USGS/Stanford SHRIMP-RG, Stanford University; [2] $^{206}Pb/^{238}U$ and $^{207}Pb/^{206}Pb$ ages corrected for common Pb using the ^{204}Pb-correction method. Decay constants from Steiger and Jäger (1977); [3] 1-sigma errors; [4] Listed only for ages >1.0 Ga.